ESTIMATING SOIL CARBON SEQUESTRATION IN GHANA

By

JAWOO KOO

A DISSERTATION PRESENTED TO THE GRADUATE SCHOOL
OF THE UNIVERSITY OF FLORIDA IN PARTIAL FULFILLMENT
OF THE REQUIREMENTS FOR THE DEGREE OF
DOCTOR OF PHILOSOPHY

UNIVERSITY OF FLORIDA

2007

For my late father, Chiwhe Koo, who would have been the happiest to see this work.
For my late *super* friend, McNair Bostick, who was a big part of my life in the past five years.

ACKNOWLEDGMENTS

This dissertation would not have been completed without the support and help of a number of people to whom I wish to express my sincere appreciation. First I wish to express my deepest gratitude to Dr. James W. Jones for his great help. In every step of the past five years, I was so grateful to work with him and have him as my advisor. Indeed, he was more than an advisor to me. We have been through good and bad times together ever since I started my graduate studies in Gainesville. He was always there when I was stuck and needed help, and he always guided me in the right direction. Discussions with him were always fruitful, with many inspiring exciting new ideas. I thank him for everything that I learned from him, inside and outside of my life at the McNair Bostick Simulation Lab.

I would like to thank my committee members for their great support and help. Dr. Kenneth J. Boote always kindly advised me to keep the good scientific background knowledge in my study. His experiences and expertise over many related disciplines, including plant physiology, soil science, and crop modeling, helped to keep many parts of my research work on track. Dr. Wendy D. Graham was a big part in my research on geostatistics and the implementation of a data assimilation method. Her insightful comments and questions always led me to new inspirations. Dr. Johannes M. Scholberg was always friendly and helpful throughout my studies to advise basic ideas behind my research topic and carefully revise draft chapters. His teaching on plant and soil nutrition and its lab sessions were helpful to design *in situ* measurement protocols correctly. Dr. Jane Southworth introduced me into the area of remote sensing and related science. I especially thank her for excellent teaching and encouragement that helped me to expand this dissertation to incorporate spatial datasets based on GIS and remote sensing. I always felt that I was lucky to have all of these great committee members. I sincerely wish to continue our relationship beyond my graduation, academically and personally.

I thank my research collaborators in West Africa: Dr. Jesse B. Naab (Savannah Agricultural Research Institute, Wa, Ghana), Prof. S.G.K. Adiku (University of Ghana, Accra, Ghana), P.C.S. Traore (ICRISAT-Mali, Bamako, Mali). Their friendly help in conducting *in situ* measurements in Ghana made the characterization of the study area possible.

I thank to two of my colleagues who spent many days and nights working together on the soil carbon sequestration research project in West Africa: W. McNair Bostick and Valerie K Walen. Especially, I would like to thank McNair for his knowledgeable comments, inspirational discussion, thoughtful care, and friendly encouragement. I will always miss him.

Finally, but most importantly, I thank all of my loving family. My mother, sister, and brother in South Korea, late father in heaven, lovely wife (and my best friend) Soonho, and precious daughter Bonny. I thank all of them for their endless support, care, and cheering for my five-year-long studies.

TABLE OF CONTENTS

LIST OF TABLES

LIST OF FIGURES

Abstract of Dissertation Presented to the Graduate School
of the University of Florida in Partial Fulfillment of the
Requirements for the Degree of Doctor of Philosophy

ESTIMATING SOIL CARBON SEQUESTRATION IN GHANA

By

Jawoo Koo

May 2007

Chair: James W. Jones
Major: Agricultural and Biological Engineering

Soil carbon sequestration is often referred to as a win-win strategy for developing countries to improve food security while mitigating atmospheric CO_2 increase. However, to accept the soil carbon sequestration as a mechanism for reducing atmospheric CO_2 levels, its regional potential should be assessed, and a reliable soil carbon monitoring system needs to be developed. Based on *in situ* measurements and cropping systems survey in the study area located in Northern Ghana in 2004 and 2006, smallholders' cropping systems in 132 fields were characterized and simulated for 20 years using the DSSAT-Century model. Soil carbon sequestration potential under the adoption of recommended management practices (e.g., no-till practice, fertilization of cereals, and retention of crop residues in the field) was assessed. The potential soil carbon sequestration rate was estimated as a tradable amount when regionally aggregated. To reduce estimation variability in soil carbon measurements, the potential of using a data assimilation method that assimilates measurements with simulated outputs was studied. Using an ensemble Kalman filter with simulated cropping systems, this approach reduced uncertainty in soil carbon measurements by 60% in a single-field study. The ensemble Kalman filter was also used to spatially assimilate soil carbon measurements and aggregate estimations over landscape. Compared with a geostatistical interpolation method, the data assimilation method showed

superior estimation accuracy with less uncertainty. Overall, results of this study showed a potential of soil carbon sequestration in the study area and the potential of using a data assimilation method to develop a reliable soil carbon monitoring system.

CHAPTER 1
INTRODUCTION

All organic materials are made of the element *carbon*. The amount of carbon contained in soil organic matter is estimated to be three times as much as in the world's living vegetation (Brady and Weil, 2002). As a result, soil organic matter plays a critical role in the global carbon balance, which is a major factor that influences global warming. It is estimated that the historical depletion of soil organic carbon due to land-use conversion and soil cultivation is responsible for about one third of carbon dioxide (CO_2) emission to the atmosphere (FAO, 2004; Lal, 2003). Since factors determining global soil carbon input and output are influenced by human-induced land management or disturbance, it is believed that a large proportion of the lost carbon from soils can be re-sequestered into soils by adopting appropriate management practices in agriculture, and thus help mitigate global warming (Lal, 2003).

Soil carbon sequestration is often referred to as a win-win strategy for developing countries to increase agricultural productivity and improve food security. Lal (2006) reported strong positive effects of soil organic carbon on soil quality, agronomic/biomass productivity, and advancing global food security. Especially for degraded soils in dryland agricultural areas, soil carbon sequestration can improve crop production as well as prevent soil erosion and desertification (FAO, 2004).

Dryland agricultural environments in West Africa can be characterized by water deficiency and high temperature. These two conditions contribute to degrade soil quality and deplete soil organic matter in dryland cropping systems in cropping systems over time. Water deficiency constrains crop productivity, which provides the input source of soil organic carbon (Farage et al., 2003). High temperature exponentially decreases the magnitude of soil organic matter pools, and consequently most agricultural soils in West Africa have less than 1% of soil organic carbon

(Bationo et al., 2007; Lal, 2002). However, due to the degree of depletion in soil carbon pools, there may be more potential to sequester carbon in the dryland soils than in other areas (Scurlock and Hall, 1998).

Cropping field management practices that influence soil carbon stocks include practices involved in land preparation (e.g., tillage), crop production (e.g., nutrient input from inorganic fertilizer applications), and residue management (e.g., amount of crop residue left after harvest). Based on current cropping field management practices in dryland cropping systems in West Africa that mostly extract nutrients from native soil organic matter pools, many studies have shown alternative management practices, such as no-till practice, inorganic N-fertilization, and retention of a majority of crop residues in the field, that would potentially increase soil carbon stocks (e.g., IPCC, 2006; Lal, 2004b).

Estimating soil carbon sequestration potential is a complicated process, as it requires knowledge of how land will be managed and how much carbon will be sequestered under different management practices. Therefore, the estimated potentials are often based on a number of assumptions and a limited number of scenarios (Conant, 2002). Soil carbon sequestration potential in agricultural lands has been assessed with cropping system-specific data from long-term field trials (e.g., Ghosh et al., 2006). Alternatively, crop systems models can be used to assess the potential of soil carbon sequestration under different cropping field management scenarios.

Crop systems models have been used as powerful analytical tools to understand environmental influences on the dynamics in the cropping system (Ferreyra, 2003). The use of crop systems models can help estimate soil carbon and its changes under different weather, soil, and management practices (Jones et al., 2002; Parton et al., 1988; Parton and Rasmussen, 1994).

However, as the performance of a biophysical model is often limited to the environmental conditions where the model was developed and tested, adjustments in the model structure and/or parameters are necessary when a crop systems model is used in a new study area with different environmental conditions. In that case, analyzing characteristics of the study area needs to be done first, to provide baseline information to initialize the model and build the model input data. In an agricultural study, the characterization of a study area provides information on each component of the cropping system, including crops (e.g., species, cultivar, and temporal cropping sequence), soil properties (e.g., soil water properties, soil organic matter content, slope, and soil texture), climate (e.g., seasonal climate variability), and management (e.g., preparing land, planting, applying fertilizer, harvesting, and managing residue).

Crop systems models are site-specific, and they are often designed to be used in a small scale within a management unit with homogenous field management practices. In a field-level study, *in situ* measurements can provide most field characteristics in the management unit, and its soil carbon sequestration potential may be assessed based on measurements. However, for policy makers, a regional estimate of the soil carbon sequestration potential is important to strategize land use for the future (Falloon et al., 1998). In a region where diverse smallholder farming systems coexist and their processes take place at multiple different sites, such as in dryland cropping systems in West Africa, a different approach may be needed. High-resolution remote sensing imagery can be used to monitor regional vegetation status, such as classifying land-use/land-cover, crop species coverage, and estimating crop biomass productivity, thus provide information on the crop biomass production, which is the fundamental source of soil organic carbon, in a regional scale.

To monitor soil carbon changes, a reliable soil carbon monitoring system needs to be developed (Antle and Uehara, 2002). Carbon content in a soil sample is commonly measured using the Walkley-Black process (1934), but the measurement variability may be several times higher than the annual soil carbon change (Jones et al., 2004). In previous theoretical studies, a data assimilation method showed the potential of reducing the soil carbon estimation variability using a simple soil carbon model (Jones et al., 2004; Jones et al., 2007). A data assimilation method combines measurements of the current state of a system with predictions made by a mathematical model to produce an estimate of the current state of the system (Daley, 1991).

Research question. How to reliably estimate soil carbon sequestration using limited and uncertain *in situ* measurements.

Objective 1: Characterize the study area

Objective 2: Assess the soil carbon sequestration potential in the study area

Objective 3: Develop a data assimilation framework in at the field level, and at the regional level

CHAPTER 2
CHARACTERIZATION OF STUDY AREA IN GHANA

Introduction

Modeling biophysical systems helps improve our understanding of these systems and also facilitates making projections of model states. The characterization of a study area in a biophysical modeling project is an important preliminary step.

Crop models have been used as powerful analytical tools to understand environmental influences on the dynamics in the cropping system (Ferreyra, 2003). However, the performance of a biophysical model may be poor if the environmental conditions or production systems greatly differ from those used during model development and evaluation. Therefore, when one attempts to use the model in a new environment in which the model was not tested, adjustments in the model structure and/or parameters may be necessary, depending on the characteristics of the study area. Analyzing the characteristics of the study area is also critical to enhance our understanding of local cropping systems to provide baseline information for model initialization and to generate model input data.

In agricultural studies, the characterization of a study area provides information on each component of the cropping system, including crops (e.g., species, cultivar, and temporal cropping sequence), soil properties (e.g., soil water properties, soil organic matter content, slope, and soil texture), climate (e.g., seasonal climate variability), and management (e.g., preparing land, planting, applying fertilizer, harvesting, and managing residue). Specifically for the soil carbon sequestration project, it is necessary to characterize components of cropping systems that might affect soil carbon dynamics in the study area, such as soil properties and management practices, as well as general characteristics of the study area.

In general, soil organic matter (SOM) affects many soil properties and processes (e.g., Amato and Ladd, 1992; Hassink et al., 1997; Hassink, 1997). Close correlations are thus expected between soil organic carbon content and other soil properties. Given the high variability in soil carbon measurements, correlations among those components may be used to develop more accurate soil carbon estimates. For example, sandy soils are generally lower in organic matter than are clay and silty soils (e.g., Burke et al., 1989; Nichols, 1984). This is related to a lower production capacity that results in lower organic carbon addition rates (e.g., Chikowo et al., 2004), improved aeration that enhances SOM decomposition (e.g., Schjonning et al., 1999), and lack of SOM encapsulation (e.g., Baldock and Skjemstad, 2000).

Soil carbon sequestration has been proposed as an option to mitigate adverse impacts of atmospheric CO_2 increase (Reichle et al., 1999) as well as to increase SOM and agricultural productivity in developing countries with SOM-depleted soils (Lal, 2004a; Lal, 2003). To monitor soil carbon changes, development of a reliable soil carbon accounting system is necessary (Antle and Uehara, 2002). Carbon content in a soil sample is commonly measured using Walkley-Black process (1934), but inherent variability in measurements may be several times higher than the annual soil carbon change (Jones et al., 2004). Use of a data assimilation method that combines model estimates and measurements may help reduce the variability in soil carbon measurements (e.g., Gelb, 1974; Maybeck, 1979; Welch and Bishop, 2003). The overall goal of this dissertation is to develop a method to estimate and spatially aggregate soil carbon sequestration using a data assimilation approach for data sets with limited and uncertain observations. However, to initialize the model in the data assimilation framework and develop model input datasets, first requires an initial characterization of the study area.

Materials and Methods

Study Site and in Situ Measurements

The study site was located south of Wa in the Upper West Region of Ghana (Latitude: 10.02, Longitude: -2.38) (Figure 2-1). In July 2004 and April 2006, *in situ* soil samples and farm management surveys were obtained in four villages in the area: Nakor, Kparisaga, Kumfabiala, and Bamahu. A total of 132 farmers' fields were identified (Figure 2-2) within an area of about 18 km^2 (6 km in North-South and 3 km in East-West direction). In each field, a composite soil sample consisting of 5-6 subsamples to 20 cm depth was taken in 2004 and 2006, and soil organic carbon contents and soil texture were analyzed by Savannah Agricultural Research Institute. Other information collected at each sampled field included field boundary, cropping history, residue management, and fertilizer application. The survey forms used in 2004 and 2006 are included in Appendix. A database of 132 fields was created to organize all of these data for subsequent analyses.

Climate and Vegetation

The climate of the area is classified as a dry winter region (Aw) since rainfall is typically low during the winter season (Osei and Aryeetey-Attoh, 1997). The major native vegetation types are savannah grassland where herbaceous plants and grasses dominate (Osei and Aryeetey-Attoh, 1997). Analysis of 50 years of daily weather data from 1953 to 2004 (J. B. Naab, Savannah Agricultural Research Institute, personal communication, October 2005) showed that the annual average rainfall was 1042 mm, which was distributed with a skewed bell shape curve peak in August (Figure 2-3). Average monthly rainfall was highest in August (200 mm) and lowest in January (40 mm). There was one rainy season that generally starts in April and ends in October. Irrigation is not available in the study area, thus most crop cultivation takes place during the rainy season. The dry (winter) season starts in November and lasts until March of the

following year. No crop can be cultivated during the dry period without supplemental irrigation, which is not common in the area (J. B. Naab, Savannah Agricultural Research Institute, personal communication, February 2006).

Soil Properties

Local soil properties of the area were analyzed based on two datasets. First, detailed soil characteristics measured at a soil pit located in the Nakor Village to 1 m depth with seven layers (0-5, 5-15, 15-30, 30-45, 45-60, 60-90, and 90-100 cm) (Table 2-1) by J. B. Naab (Savannah Agricultural Research Institute, personal communication, December 2005) were used to describe the general soil properties in the area. Second, the analysis of soil organic carbon content (SOC) and soil texture from *in situ* soil samples collected from 132 fields in 2004 and 2006 was used to analyze the soil quality of the fields and the SOC measurement variability. In each field, composite soil samples (with 5-6 subsamples each) were obtained from the top 20 cm depth. The Walkley-Black (1934) and hydrometer methods were used to analyze soil carbon content and texture in each sample. Using the correlation between SOC and sand content, the feasibility of estimating SOC based on soil texture was tested. Out of 264 data points from two years of soil analysis in 132 fields, 176 data points (i.e., 2/3 of the dataset) were randomly selected and used to develop the linear regression model, and the other 88 data points (i.e., 1/3 of the dataset) were used to validate the model.

Slope Inclination

Based on a digital elevation model of the study area obtained from the Shuttle Radar Topography Mission (SRTM) Database with three arc second (90 m) spatial resolution (USGS, 2004), the percentage slope of each pixel was calculated using the ERDAS IMAGINE 8.7 (Leica Geosystems GIS & Mapping LLC, 2003), which uses the quadratic surface method (Zevenbergen and Thorne, 1987). The calculated slope in the study area was created as a raster

data layer. A vector layer containing field boundaries was overlaid on the slope data, and the average slope within each field boundary was calculated for each field. Descriptive statistics of the slope of 132 fields were calculated and used to characterize the slope of fields in the study area.

Cropping History

Depending on surveyed farmers' memories of cropping history and the length of cultivation in each field, the surveyed cropping history in each field ranged from 2 to 18 years. However, five years of cropping sequence data were obtained from the survey with farmers in most fields. Thus, the cropping history of last five years (2001 - 2005) was analyzed for all of the 132 surveyed fields. There were 16 gaps in the five-year cropping history data due to farmers' incomplete answers (2003: 1 field, 2002: 4 fields, and 2001: 11 fields); they were recorded as fallow, assuming those fields were not cultivated during those years.

Results

Soil Properties

The predominant soil order in the study area is Alfisol (J. B. Naab, Savannah Agricultural Research Institute, personal communication, August 2006). In general, Alfisols are known as productive soils in regions with sufficient rainfall (Brady and Weil, 2002). However, Alfisols may not be ideal for agricultural production in dryland systems due to their low water holding capacity, relatively high erosion and runoff potential, high susceptibility to crust formation, presence of compaction zones, and high gravel content (El-Swaify et al., 1984).

The soil analysis at the soil pit showed the texture is sandy in most layers (Table 2-1). The deepest layer between 90 and 100 cm contained about 50% gravel. Bulk density ranged between 1.56 and 1.67 Mg m^{-3} over seven layers (Table 2-1) and averaged 1.63 Mg m^{-3} in the top 20 cm layer. The pH of the soil showed slight acidity ranging from 6.17 to 6.29. Soil organic carbon

content (SOC) was relatively low, ranging from 0.22 g kg^{-1} to 0.34 g kg^{-1} over the layers, and averaged 0.30 g kg-1 in the top 20 cm layer. As most soil nitrogen exists in the soil organic matter, the total soil nitrogen content was also low, ranging from 0.03 to 0.06 g kg^{-1}.

For the 132 composite soil samples taken from farmers' fields in the study area (Figure 2-2), the average SOC value was 0.53 g kg^{-1} in 2004 (standard deviation was 0.26 g kg-1, and coefficient of variation was 48%) and 0.50 g kg^{-1} in 2006 (standard deviation was 0.20 g kg^{-1}, and coefficient of variation was 40%) (Table 2-2). However, percentile charts showed that the SOC measurements were positively skewed in both years (Figure 2-4), thus their arithmetic mean values may not appropriately represent the true characteristics of SOC in the area. Normality of the SOC measurements was also rejected for both the 2004 and 2006 datasets when the Shapiro-Wilk test was applied at $\alpha = 0.05$. The difference between the SOC measurements in the 2004 and 2006 datasets was tested with a nonparametric Wilcoxon signed-rank test due to the non-normality in the two datasets, and the test result showed no significant difference at $\alpha = 0.05$. The median value of the SOC measurements was 0.45 g kg^{-1} in 2004 and 0.44 g kg^{-1} in 2006 (Table 2-2). On a mass basis, the median SOC values were equal to 14.7 t ha^{-1} and 14.3 t ha^{-1}, respectively, based on the bulk density of 1.63 g cm^{-3} for the top 20 cm soil depth measured in the soil pit (J. B. Naab, Savannah Agricultural Research Institute, personal communication, December 2005).

To estimate the SOC measurement variability, SOC of each soil sample in 2006 was analyzed three times. For each soil sample, the measurement standard deviation value was calculated from the triplicate measurement. The average value of the 132 standard deviation values was 0.04 g kg^{-1} (Table 2-3). The percentile chart of the standard deviation values also showed positive skewness (Figure 2-5), and the median standard deviation value was 0.03 g kg^{-1}

(Table 2-3). Given the positive skewness also shown in the SOC measurement (Figure 2-4), this result implied that the SOC measurement variance may be heteroscedastic, thus the standard deviation is correlated with the magnitude of SOC. The correlation analysis between the magnitude of SOC and measurement standard deviations confirmed the heteroscedastic nature of the SOC measurement (Figure 2-6). The SOC measurement standard deviation showed an increasing trend as the magnitude of SOC increased. The correlation coefficient was 0.60, which was significant at $P<0.01$.

Based on the SOC measurement standard deviation, the SOC measurement variability in the lab can be estimated. Considering the positive skewness in the SOC measurements and their standard deviations, the coefficient of variation for the SOC measurement in the lab was calculated as 12% of measured values with the average median value of SOC measurements between 2004 and 2006 measurements (0.45 g kg^{-1}) and the median SOC measurement standard deviation in 2006 (0.05 g kg^{-1}). This value, 12% of measured values, was within the range of the coefficient of variation values of 3-18% reported by W. M. Bostick (Graduate student, University of Florida, personal communication, June 2005) from a long-term SOC measurement dataset under various management systems in Burkina Faso. On a mass basis, the SOC measurement coefficient of variation value of 12% is approximately 1,738 kg ha^{-1}, assuming a bulk density of 1.63 g cm^{-3}.

The soil texture analysis showed that the average proportion of silt and clay content in the 132 fields was 24% in 2004 and 26% in 2006. The percentile chart showed that most of the fields have low silt and clay content, and the distribution was positively skewed (Figure 2-7). Median values for the silt and clay content were 20% in 2004 and 22% in 2006. Since the same fields were visited in 2004 and 2006, the increased silt and clay content between those years by 2% is

due to sampling and measurement errors, as the soil texture does not change noticeably within a short time period (Brady and Weil, 2002). The correlation matrix showed that the SOC was positively correlated with silt and clay content with significance ($P<0.01$); the correlation coefficients were 0.81 in 2004 and 0.88 in 2006 (Table 2-4). When the SOC content was linearly regressed with the silt and clay content, it was shown that soil texture explained 66% and 77% of the SOC variability in 2004 and 2006, respectively (Figure 2-8). These significant correlations implied that soil texture could be used to estimate SOC when the measurement of SOC is not available in these communities and for fields under cultivation. To estimate uncertainty of this method, the SOC measurement data in 2004 and 2006 were combined, randomly ordered, and split into two parts so that 67% of the data were used for the linear model development and the other 33% of data to be used for the model validation. The linear model was developed as:

$$SOC(\%) = 0.0132 \times (Silt + Clay) + 0.1793 \quad (2\text{-}1)$$

where *Silt+Clay* is the silt and clay content in percentage (Figure 2-9A). For the model development dataset, this model yielded an RMSE of 0.13 g kg^{-1} with a coefficient of variation of 25% of measured SOC values (Figure 2-9B). When the model was used for the validation dataset (Figure 2-10A), the estimated SOC also had an RMSE for prediction (RMSEP) of 0.13 g kg^{-1}. Dividing the RMSEP by the average SOC in the validation dataset, the coefficient of variation was calculated as 25%. This value was about two times higher than the coefficient of variation calculated from the SOC measurements made in the laboratory. That is, the estimated SOC based on soil texture without measurement was about two times more uncertain than the SOC measurement in this study.

Slope Inclination

The overall landscape of the area was relatively flat with an average slope of 1.1 % with a standard deviation of 0.8 %. Using a percentile-based quantification, the median slope was 1.0 %, where the minimum and maximum values were 0.0 % and 3.0 %, respectively. It was also shown that 75% of the fields had slopes of 1.75 or lower (Figure 2-11).

Correlations between SOC and slope were not significant ($P<0.10$), 0.05 in 2004 and 0.01 in 2006 (Table 2-5). The relatively flat landscape may be the reason for the weak correlation between SOC and slope.

Fertilizer

Fertilizer application was not common in the area. Based on surveyed farmers it appears that maize was the only crop that may be fertilized but out of the 132 fields in this study, only one maize field was fertilized with 1 bag of N-P-K fertilizer, applied once four weeks after planting. Although all maize farmers were aware of the fact that their maize production would be poor without applying fertilizers, they indicated that fertilizer prices were cost-prohibitive.

Residue Management

Crop residues (e.g., maize stems, sorghum stalks, and peanut stems) were left in the field after harvest. However, due to the dry winter seasons (Figure 2-3), residue material remains dry and very slowly decomposes until the next cropping season starts (J. B. Naab, Savannah Agriculture Research Institute, personal communication, July 2004) (Figure 2-12A). Part of the residues is typically removed by grazing livestock and termites. When the rainy season approaches during the following spring, the main practice of preparing land is controlled fire. Farmers cut crop residues (Figure 2-12B), collect them in several spots in the field (Figure 2-12C), and burn them (Figure 2-12D). Although the ashes may contribute to soil fertility, carbon compounds in crop residue that could have been potentially incorporated into the soil to increase

the soil organic matter are lost by burning crop residues (Brye et al., 2006; Prasad et al., 1999). After the aboveground residues are burned, roots are also typically dug and removed (Figure 2-12E) to prepare the land for planting the next crop (Figure 2-12F).

Tillage

After clearing the land, fields are tilled. Most fields are manually tilled using hand-hoes (Figure 2-13) while few fields are tilled with tractors. Out of the 132 fields in the survey, there were only five fields (4%) where tractors were used in 2006.

Cropping History

As a snapshot of cropping in the study area, five years of cropping history data were combined, and the number of fields with each crop type was counted. When more than one crop was cultivated in a given field in one season as an intercropping practice, the fraction of the field was counted for each crop. For example, if millet and peanut were intercropped in a given field, 0.5 was counted for each of millet and peanut. The counted number of fields for each crop was then proportionally presented as shown in Figure 2-14. Ten different crops were cultivated in the study area during the five-year period. Sorghum (27%) and peanut (22%) were the two most commonly grown crop, as they were cultivated in almost 50% of fields. There were four cereal crops (maize, sorghum, millet, and rice), four legume crops (peanut, cowpea, bambara nut, and soybean), and two tuber crops (yam and cassava) and these groups accounted for 61%, 30%, and 9% of the cropping area, respectively.

The data used for Figure 2-14 were rearranged for each of the three crop types (i.e., cereals, legumes, and tubers) to generate a more detailed snapshot of cropping systems for each crop type (Figure 2-15). For cereal crops, sorghum was cultivated most (47%) while the number of maize fields cultivated (26%) was about half of the number of sorghum fields. For legume crops, peanut was the most cultivated crop (in about 70% of the fields with legumes). Tuber crops were

not cultivated as widely as cereals or legumes. Yam was the most cultivated tuber crop (in about 80% of the fields with tuber crops).

To analyze changes in the cropping trend, the counted number of fields in Figure 2-14 was presented on a yearly basis (Figure 2-16A). Fallow was included in the analysis to see the transitions between cultivations and fallow. Although there was no obvious trend among different crops, the proportion of fallow decreased from about 50% in 2001 to 16% in 2005 and it appears that millet acreage tended to increase over the years. When the crops were grouped into the three crop types (Figure 2-16B), it was clearly shown that the cultivation of cereal crops was increasing while the percentage fallow fields decreased. Tuber crops were cultivated in each year (between 4% and 12% of the fields).

The sequence of crops in the 132 fields was analyzed to characterize a typical cropping system in the study area. Although cropping sequence differed greatly, the most popular cropping sequence in general was alternating cereal crops with fallow (cereals-fallow), which was practiced in 57 fields (43%). Cereal crops were continuously cultivated for about four years, then fields were left fallow for about four years. In some cases (11 fields, or 8%), legumes were cultivated between cereals and fallow (cereals-legumes-fallow) with typically about two years of cereals followed by two years of legumes alternated with four years of fallow.

The cropping history showed that intercropping was commonly practiced. Out of 132 fields, 96 fields (73%) were intercropped in at least one year during the five-year period. The most common form of intercropping was using a mixture of cereals and legumes (e.g., maize and peanut) which was practiced in 54 fields (41%). Surveyed farmers believed that intercropping reduced the risk of crop failures.

To analyze correlations between the SOC and cropping history, the number of years that a specific crop was cultivated in each field was counted and correlated with the SOC during 2004 and 2006 for all of the ten crops (Table 2-6) and/or three crop types (Table 2-7). The correlation matrix showed that overall correlations between the SOC and cropping history were not always significant, although the SOC in both years were positively correlated with maize, rice, and peanut and negatively correlated with other crops (Table 2-6). In general, correlations were positive with cereal crops and negative with legumes and tubers (Table 2-7). The positive correlations with cereal crops may be due to their relatively larger amounts of residue biomass production than legumes and tubers or sowing of cereals on the areas with productive soils (e.g., high SOC content). Correlations between the SOC and the number of fallow years were very small (correlation coefficients were not significant: 0.00 in 2004 and 0.08 in 2006). In contrast, it was noted that correlations between SOC and rice cropping were the most significant (correlation coefficient with significances at $P<0.01$: 0.65 in 2004, 0.59 in 2006) (Table 2-6). However, such correlation may not suggest a causality relationship between cropping history and SOC levels, as rice cultivations were mostly observed in lowland areas, which are typically flooded during rainy seasons. The lowland areas may have a lower SOM mineralization rates, which would result in higher SOC (Sahrawat et al., 2005).

Discussion

Different characteristics of the study area in Wa, Ghana, were analyzed in 132 farmers' fields located over the landscape. The purposes of these analyses were for initializing a cropping systems model and building the model input datasets in subsequent chapters.

In the absence of inorganic fertilizer applications, most farmers relied on the native soil fertility. However, overall quality of soils in the area is not ideal for low-input agricultural production. Brady and Weil (2002) listed the factors of an agricultural system that lead to losses

of soil organic matter, and this study showed that many of such factors occurred in the study area, including intensive tillage, residue removal, high temperature, low soil moisture, fire, and low plant productivity. Low levels of SOC may thus be related to continuous cultivation alternated with an ineffective (overly short) fallow. Soil texture was mostly sandy, which has poor water and nutrient retention capacities. In addition, residue burning practices also greatly increases SOM losses. Shifting cultivation to new land was becoming more limited due to rapidly increasing population pressure (J. B. Naab, Savannah Agricultural Research Institute, personal communication, April 2006). In order to sustain the cropping system under this low-input management condition, strategies that can effectively increase soil organic matter, such as no-till agriculture (Lal et al., 2004) and increased use of supplemental irrigation and/or fertilizers, should be considered.

Correlation analysis showed good potential for estimating the soil organic carbon content by using soil texture analysis. This approach may be useful, especially where SOC measurements are not readily available. However, the estimation variability was too high to have practical significance for assessing soil carbon sequestration.

Table 2-1 Soil properties of the soil pit in Nakor, Ghana

Depth (cm)	Sand (%)	Silt (%)	Clay (%)	Gravel (%)	Bulk Density (g cm3^{-1})	Acidity (pH)	Organic C (g kg-1)	Total N (g kg-1)	Available P by Bray method (mg kg[soil]$^{-1}$)	Available K by Bray method (mg kg[soil]$^{-1}$)
0-5	87.36	9.72	2.92	1.58	1.56	6.18	0.34	0.06	31.39	25.30
5-15	88.36	6.72	4.92	1.81	1.67	6.17	0.31	0.04	22.32	23.92
15-30	84.48	8.88	6.64	5.28	1.60	6.29	0.23	0.04	19.53	22.54
30-45	84.48	8.88	6.64	16.23	1.61	6.21	0.25	0.04	18.83	22.08
45-60	86.88	4.48	8.64	4.40	1.60	6.20	0.25	0.04	18.13	22.08
60-90	85.78	4.53	9.66	10.27	1.63	6.17	0.22	0.04	13.95	21.16
90-100	84.48	6.88	8.64	48.41	1.66	6.26	0.23	0.03	11.16	18.40

Table 2-2 Descriptive statistical analysis of the SOC measurements in 132 fields in Wa, Ghana, during 2004 and 2006.

Year	Number of samples	Min (g kg^{-1})	Max (g kg^{-1})	Average (g kg^{-1})	Standard Deviation (g kg^{-1})	Normality ($\alpha = 0.05$)	Median (g kg^{-1})
2004	132	0.23	1.61	0.53	0.26	Normality rejected	0.45
2006	132	0.31	1.33	0.50	0.20	Normality rejected	0.44

Table 2-3 Descriptive statistical analysis of the standard deviation of the SOC measurement in 132 fields in Wa, Ghana, in 2006

Year	Number of samples	Min (g kg^{-1})	Max (g kg^{-1})	Average (g kg^{-1})	Standard Deviation (g kg^{-1})	Normality ($\alpha = 0.05$)	Median (g kg^{-1})
2006	132	0.0025	0.19	0.04	0.03	Normality rejected	0.03

Table 2-4 Correlation matrix between the SOC and soil texture during 2004 and 2006 (n=132).

	SOC 2004	SOC 2006	Silt & Clay 2004	Silt & Clay 2006
SOC 2004	--			
SOC 2006	0.83 ***	--		
Silt & Clay 2004	0.81 ***	0.84 ***	--	
Silt & Clay 2006	0.72 ***	0.88 ***	0.92 ***	--

(Note: *** represents significance at α=0.01.)

Table 2-5 Correlation matrix with the SOC measured in 2004 and 2006 and the slope inclination in the 132 fields in the study area (n=132, α=0.05).

	SOC 2004	SOC 2006	Slope inclination
SOC 2004	--		
SOC 2006	0.83 ***	--	
Slope inclination	0.05 ns	0.01 ns	--

(Note: ns and *** represent non-significance and significance at α=0.01, respectively.)

Table 2-6 Correlation matrix with the SOC measured in 2004 and 2006 and the cropping history (number of years that specific crop species was cultivated) in the 132 fields in the study area for five-year period (2001-2005) (n=132, α=0.05)[1].

	SOC 2004	SOC 2006	Maize	Fallow	Peanut	Sorghum	Millet	Rice	Cowpea	Bambara	Soybean
SOC 2004	--										
SOC 2006	0.83 ***	--									
Maize	0.41 ***	0.38 ***	--								
Fallow	0.00 ns	0.08 ns	-0.31 ***	--							
Peanut	-0.36 ***	-0.33 ***	-0.37 ***	-0.16 *	--						
Sorghum	-0.23 ***	-0.27 ***	-0.30 ***	-0.33 ***	-0.09 ns	--					
Millet	-0.15 *	-0.19 **	-0.28 ***	-0.04 ns	0.03 ns	-0.06 ns	--				
Rice	0.65 ***	0.59 ***	0.58 ***	-0.27 ***	-0.33 ***	-0.25 ***	-0.27 ***	--			
Cowpea	-0.18 **	-0.19 **	-0.26 ***	-0.16 *	-0.17 *	0.26 ***	0.10 ns	-0.21 **	--		
Bambara	-0.20 **	-0.20 **	-0.20 **	-0.13 ns	-0.01 ns	0.00 ns	0.08 ns	-0.20 **	0.02 ns	--	
Soybean	-0.09 ns	-0.05 ns	-0.11 ns	-0.09 ns	0.00 ns	-0.07 ns	0.00 ns	-0.08 ns	-0.10 ns	-0.10 ns	--

(Note: ns, *, **, and *** represent non-significance, significance at α=0.1, significance at α=0.05, and significance at α=0.01, respectively.)

Table 2-7 Correlation matrix with the SOC measured in 2004 and 2006 and the cropping history (number of years that specific crop type was cultivated) in the 132 fields in the study area for five-year period (2001-2005) (n=132, α=0.05)[1].

	SOC 2004	SOC 2006	Cereals	Legumes	Tubers	Fallow
SOC 2004	--					
SOC 2006	0.83 ***	--				
Cereals	0.40 ***	0.31 ***	--			
Legumes	-0.40 ***	-0.38 ***	-0.52 ***	--		
Tubers	-0.22 **	-0.20 **	-0.29 ***	-0.06 ns	--	
Fallow	0.00 ns	0.08 ns	-0.58 ***	-0.22 **	-0.16 *	--

Figure 2-1 Location of study site, Wa, Ghana, in West Africa (Latitude: 10.02, Longitude: -2.38). Satellite image and the country boundary was generated by Google Earth™ Mapping Service (http://earth.google.com).

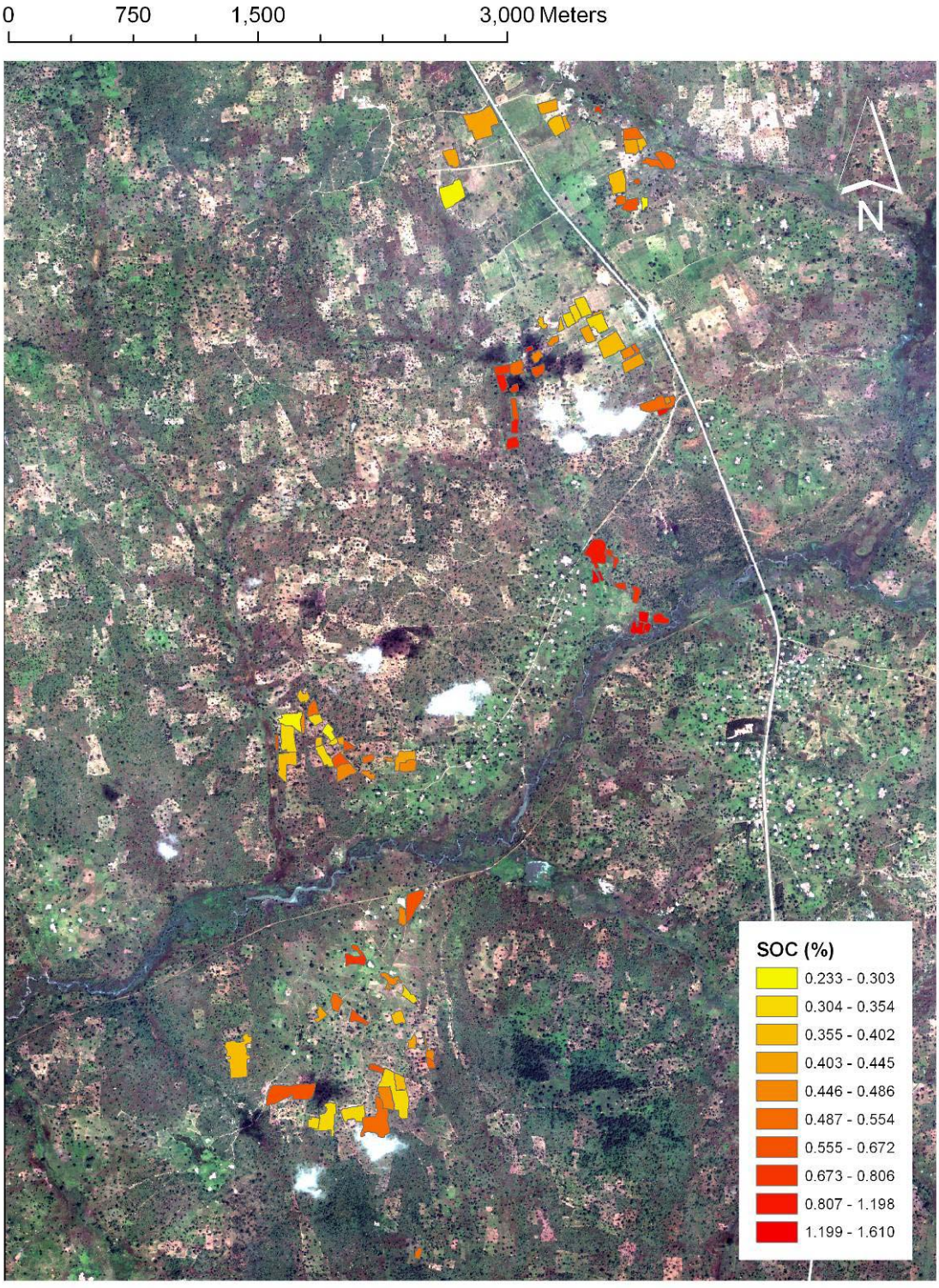

Figure 2-2 Field boundaries and measured soil organic carbon content percentage (SOC%) in farmers' field at a study site south of Wa, Ghana, overlaid on the QuickBird remote sensing image.

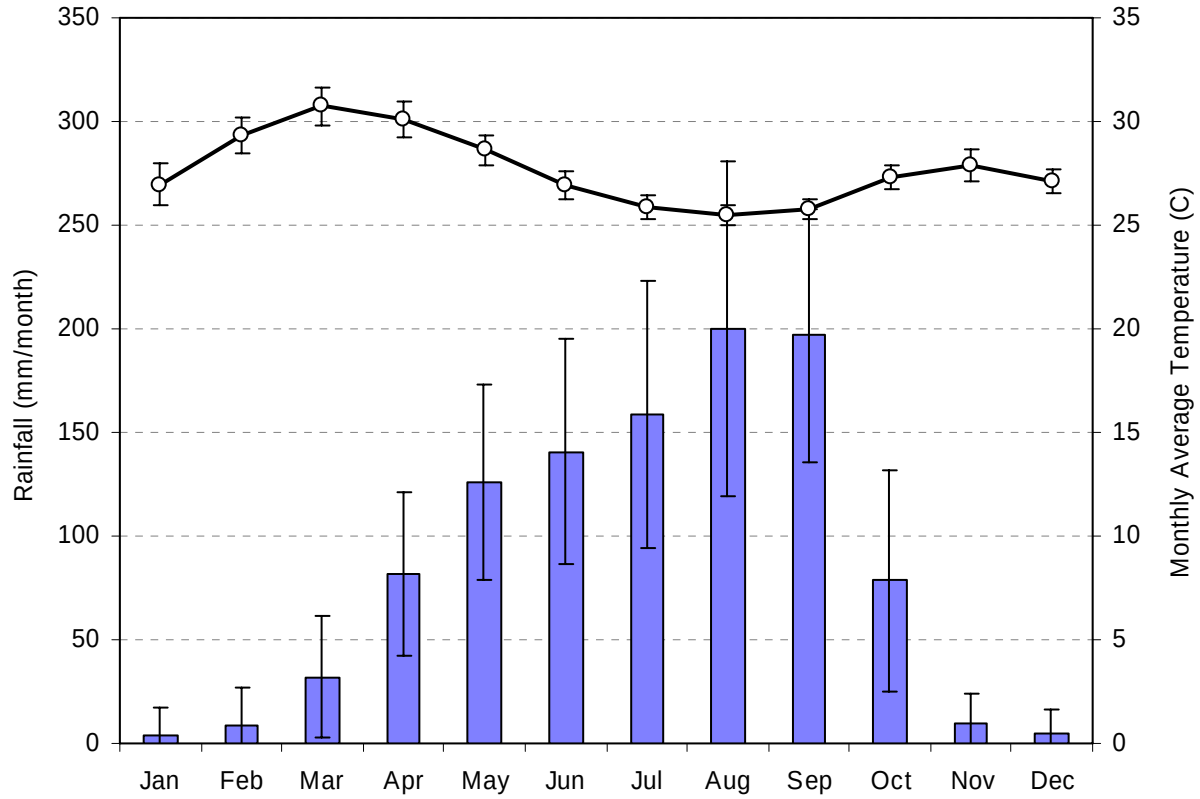

Figure 2-3 Averaged monthly rainfall and average temperature in Wa, Ghana (1953-2004), bars indicate standard errors (n=51).

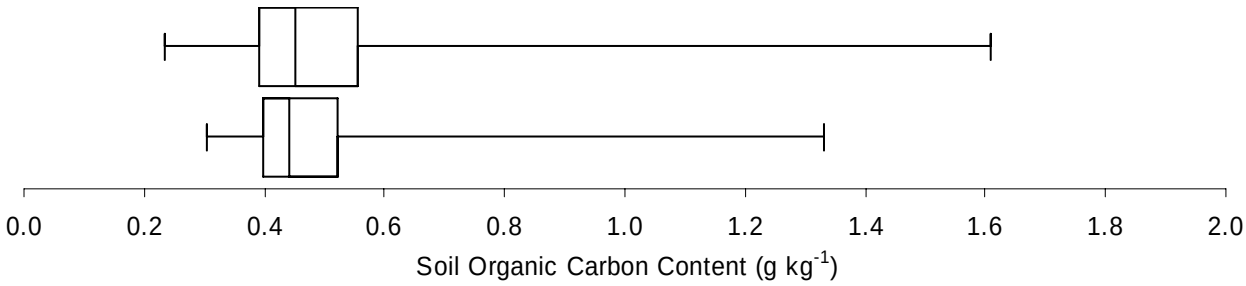

Figure 2-4 Percentile charts of the SOC measured in 132 farmers' fields in Wa, Ghana, in 2004 and 2006.

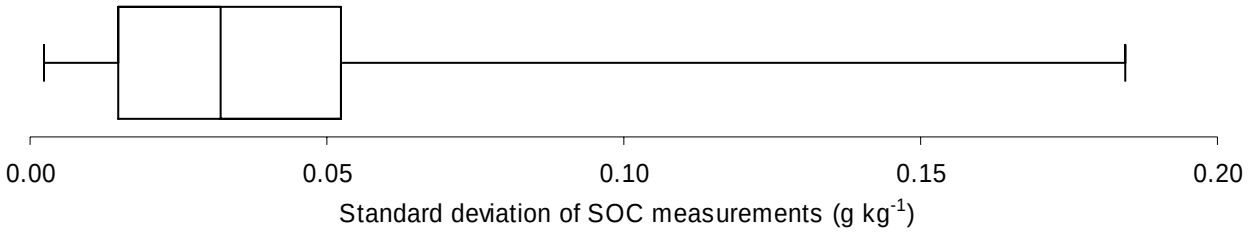

Figure 2-5 Percentile chart of the standard deviation from triplicate SOC measurements in 132 farmers' fields in Wa, Ghana, in 2006.

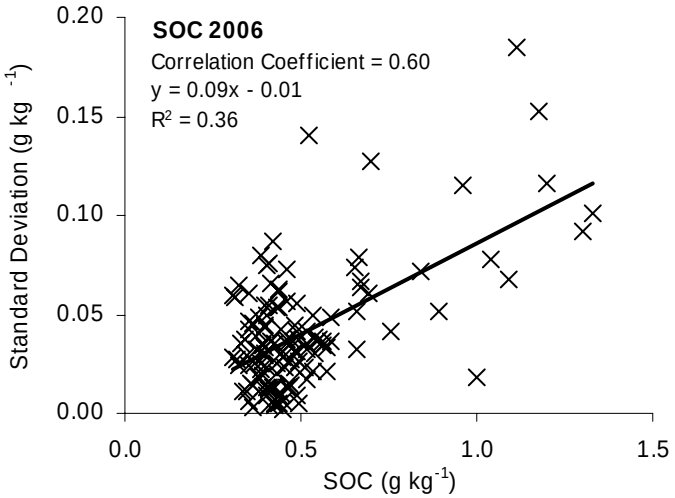

Figure 2-6 Soil organic carbon (SOC) content and corresponding standard deviation values from three replications of 132 composite soil samples in Wa, Ghana, in 2006 with a significant correlation ($P<0.01$).

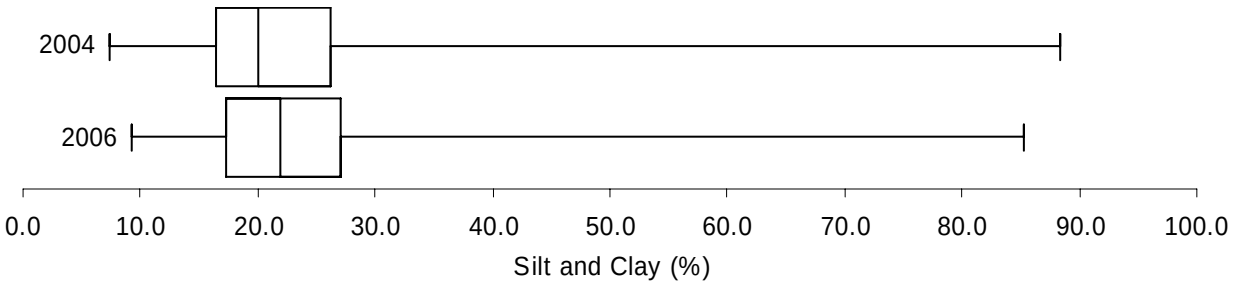

Figure 2-7 Percentile chart of the proportion of silt and clay content measured in 132 fields in Wa, Ghana, in 2004 and 2006. Vertical bars indicate minimum, 25% percentile, median, 75% percentile, and maximum values (from left to right).

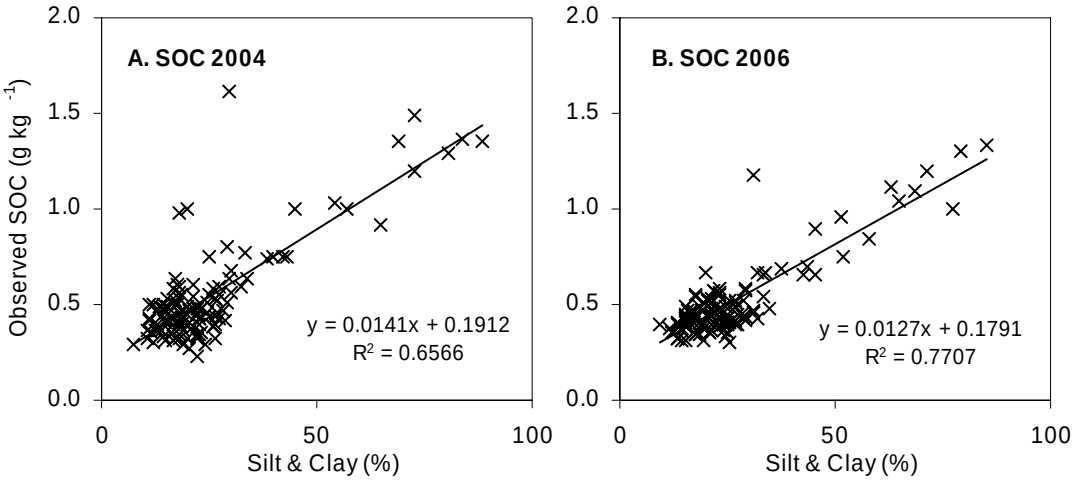

Figure 2-8 Linear regression of the SOC measured in 2004 and 2006 with silt and clay contents

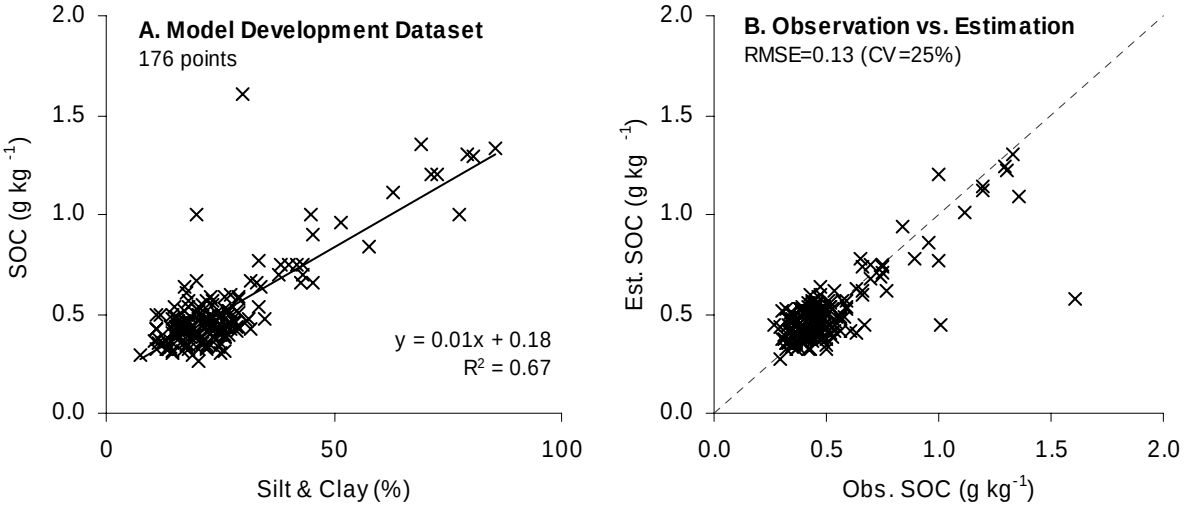

Figure 2-9 A) Linear regression between soil organic carbon (SOC) content and silt and clay content with the randomly selected subset of the 2004 and 2006 measurement data. B) Outline of observed versus predicted SOC values based on the linear model.

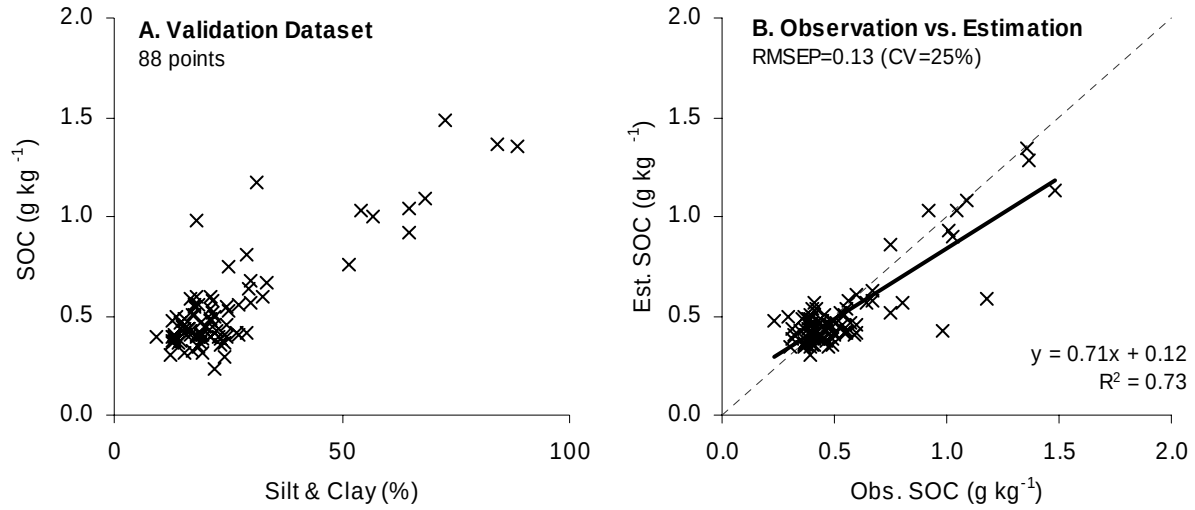

Figure 2-10 Validation of the linear model that estimates SOC from silt and clay content using a subset of dataset that were not used in the model development: A) Estimated SOC from silt and clay content, B) Observation versus estimation of SOC.

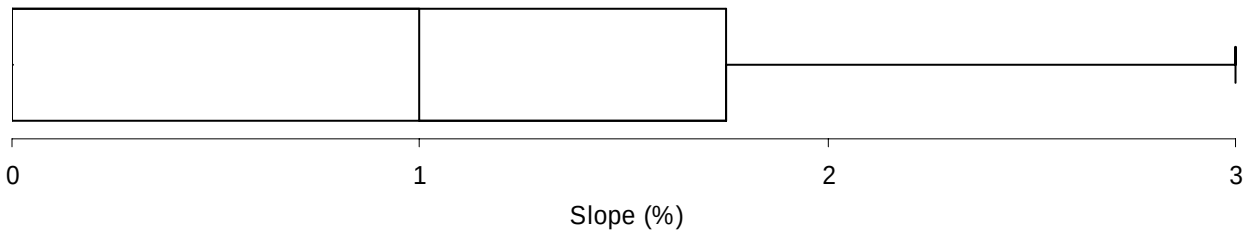

Figure 2-11 Percentile chart of the slope of 132 farmers' fields calculated from the SRTM (Shuttle Radar Topography Mission) DEM database

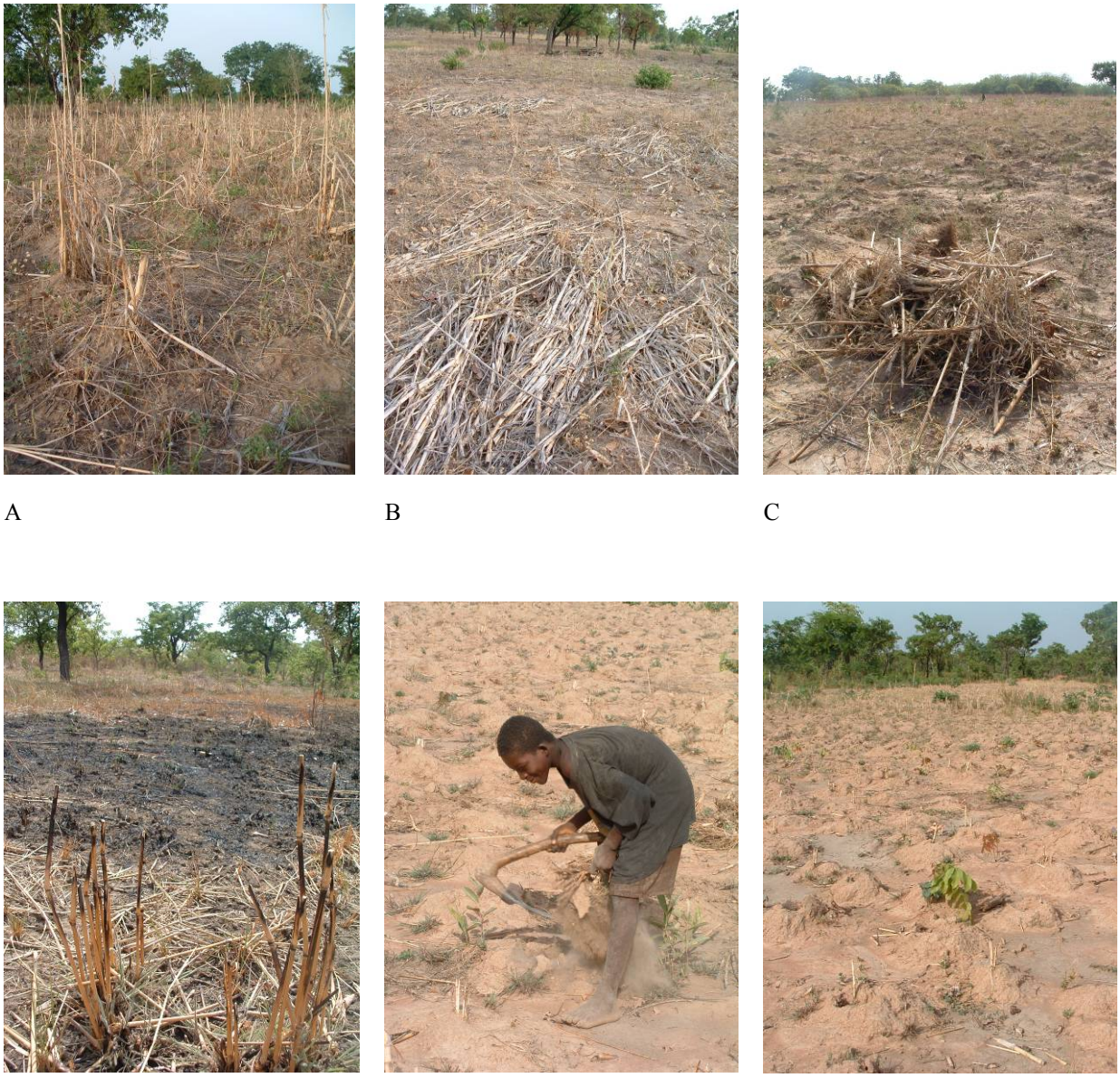

Figure 2-12 Sorghum fields showing the residue removal and burning typical in this region. A) Residue left in the field. B) Residue cutting. C) Residue collection. D) Residue burning. E) Root removal. F) Residue removal.

Figure 2-13 Field after tillage with hand hoe.

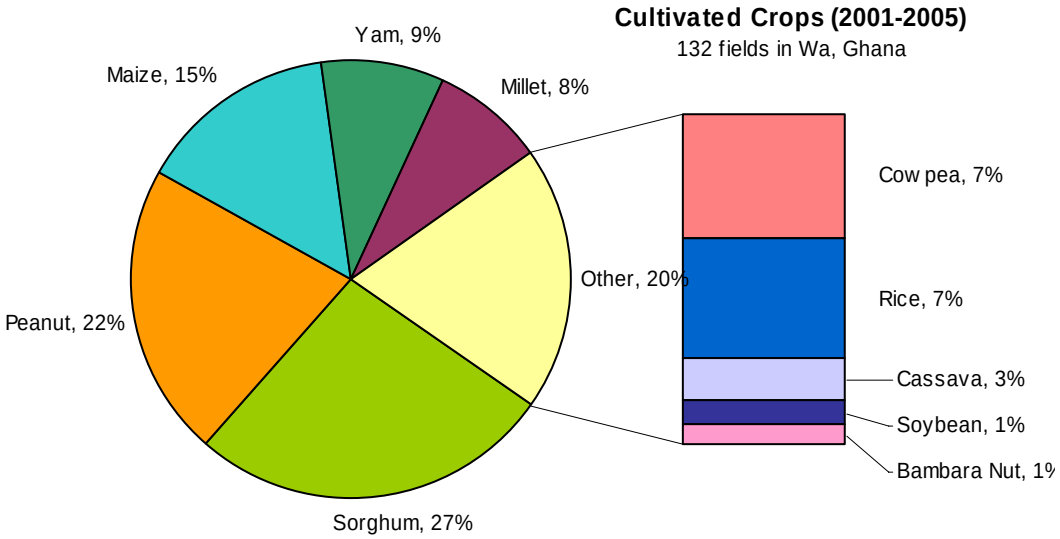

Figure 2-14 Proportion of land allocation to different crops cultivated in the study area for 2001-2005

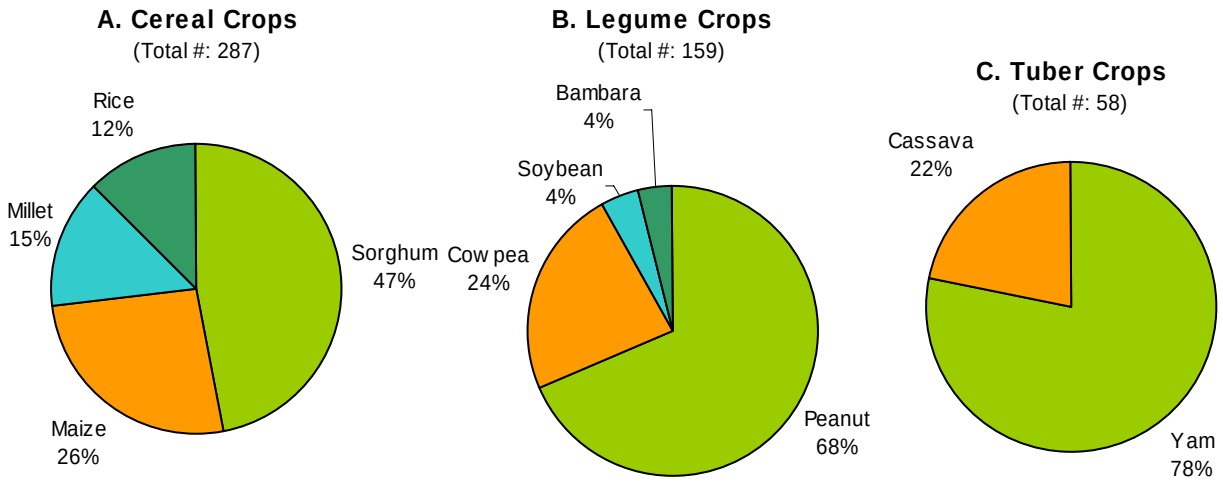

Figure 2-15 Proportion of three different types of cultivated crops in 132 farmers' fields for 1996-2005

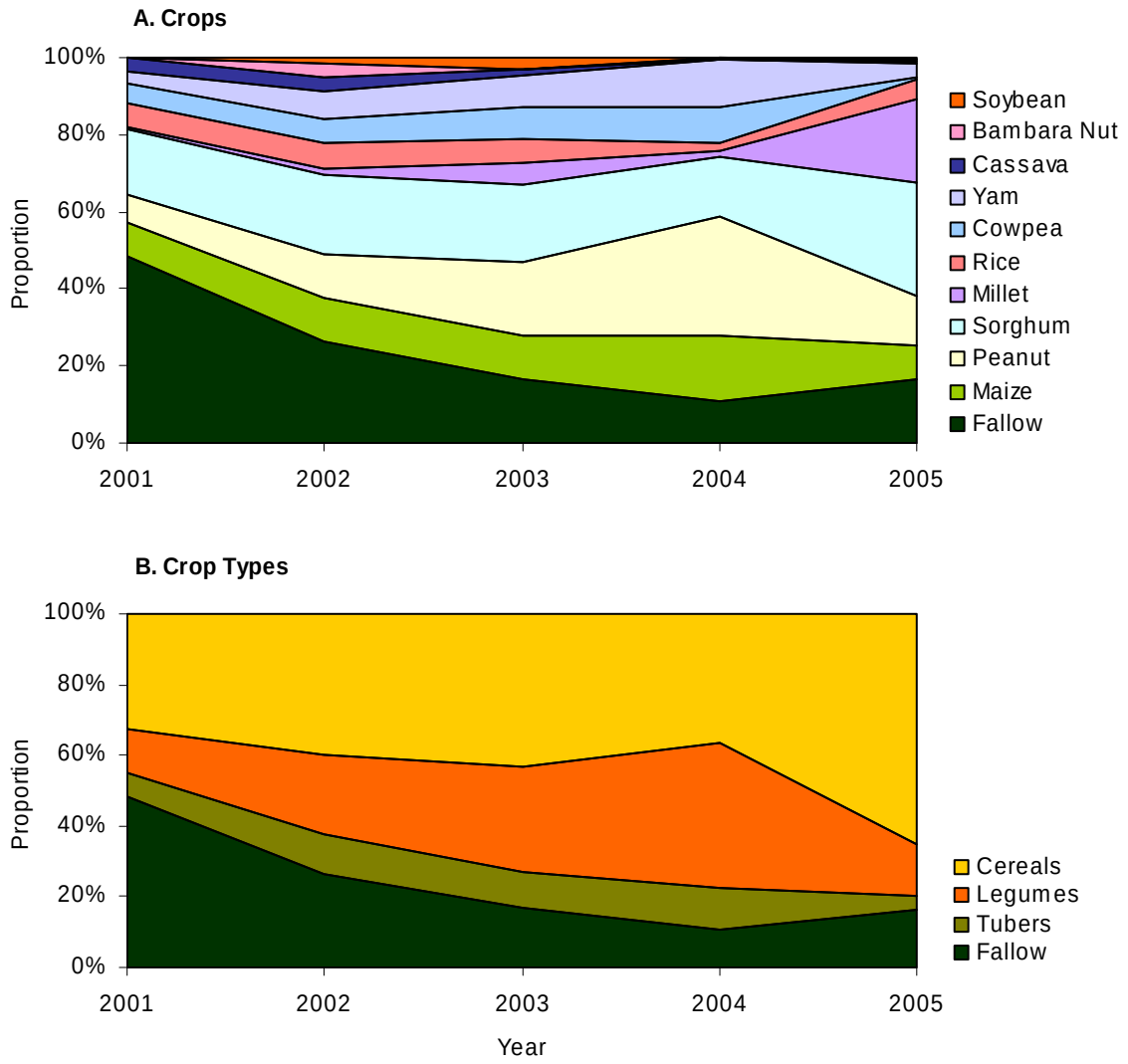

Figure 2-16 Proportions of land allocation to different types of crops cultivated in 132 farmers' fields in Wa, Ghana, during 2001-2005

CHAPTER 3
CARBON SEQUESTRATION POTENTIAL IN SMALLHOLDER AGRICULTURAL SYSTEMS IN NORTHERN GHANA

Introduction

All organic materials contain carbon and the soil carbon pool in soil organic matter is estimated to be about three times larger than that of the global above-ground vegetation (Brady and Weil, 2002). As a result, soil organic matter (SOM) plays a critical buffering role in the global carbon balance, and thus also is a major factor influencing global warming. It is estimated that the historical depletion of soil organic carbon due to land-use conversion and soil cultivation is responsible for about one third of carbon dioxide (CO_2) emission to the atmosphere (FAO, 2004; Lal, 2003). Since factors determining global soil carbon input and output are influenced by human-induced land management or disturbance, it is believed that a large proportion of the lost carbon can be re-sequestered into soils by adopting appropriate agricultural management practices which can help mitigate global warming (Lal, 2003). Moreover, soil carbon sequestration is often referred to as a win-win strategy for developing countries since, in addition to enhancing global well-being, it will also improve local agricultural productivity and food security. Lal (2006) reported strong positive effects of soil organic carbon on soil quality, crop productivity, and global food security. Especially for degraded soils in dryland agricultural areas in West Africa, soil carbon sequestration can play an important role to improve crop production as well as prevent soil erosion and desertification (FAO, 2004).

Dryland Agriculture

Dryland agricultural environments in West Africa can be characterized by two conditions that degrade soil quality and deplete soil organic matter: water deficits and high temperature. Water stress constrains crop productivity, which in turn drives soil organic carbon accumulation (Farage et al., 2003). Decomposition of SOM, on the other hand, increases exponentially with

temperature, and consequently most agricultural soils in some parts of West Africa have less than 1% of soil organic carbon (Bationo et al., 2007; Lal, 2002). However, these soils also offer a unique yet currently unexploited potential to sequester soil carbon (Scurlock and Hall, 1998).

Recommended Management Practices

Farm management practices that influence soil carbon stocks include land preparation (e.g., tillage), crop production (e.g., nutrient input from inorganic fertilizer applications), crop rotation (e.g. use of green manures and fallow periods), and residue management (e.g., amount of crop residue left after harvest). In contrast to current farm management practices that extract nutrients from native SOM pools, some studies provide evidence that appropriate use of following alternative management practices could increase soil carbon stocks (e.g., IPCC, 2006; Lal, 2004b).

Conservational tillage

In agricultural soils, conventional tillage practices decrease organic carbon stock by destructing soil aggregates, accelerating plant residue decomposition, and promoting erosion (Hussain et al., 1999; Reicosky, 1997). Carbon-depleted soils can sequester additional organic carbon via use of conservational tillage farming practices (e.g., reduced tillage or no-till) that reduce soil disturbance and by including cover crops in rotation schemes which may increased carbon addition rates (Lal, 2004b). Conservational tillage practices tend to be most effective in dryland agricultural systems (Batjes and Sombroek, 1997). However, there are known problems that may potentially deter the adoption of conservational tillage practices, especially in developing countries. Weeds, plant diseases, and pest pressure may increase, as crop residues may provide places where weed seedlings, plant pathogens, or insects can survive during winter seasons. In addition, when fertilizers are applied on the soil surface, plant nitrogen uptake efficiency in the undisturbed soils is lower than in disturbed ones. When no fertilizers are applied,

the mineralization rate of soil-native nitrogen may be lower in undisturbed soils than in tilled, thus aerated ones.

Inorganic fertilization

Increased crop biomass production by fertilization offers opportunity to sequester more soil organic carbon as well as to increase crop productivity over time (Halvorson et al., 1999; Lal, 2004b). Twomlow and Tabo (2006) reported that even a small dose of fertilizer, as little as 20 kg[N]/ha, increased sorghum and millet yields by 44% and 120%, respectively, in Sub-Saharan African countries. However, currently most farmers in dryland agricultural systems can not afford to purchase fertilizers (Farage et al., 2003). Moreover, farmers in drought-prone West African countries often perceive that their farming practices are too risky to justify the fertilizer investment (J.M. Antle, Montana State University, personal communication, June 2006). Thus, mining residual soil nutrients (extractive farming practices) prevails in West Africa and farmers thus mainly rely on the native soil fertility. In the study area in northern Ghana, only one maize field out of 132 surveyed fields, was fertilized in 2005 (see Chapter 2). In addition to this, on a global scale the positive impacts of applying inorganic fertilizers on enhancing local soil carbon sequestration may be off-set by the fossil fuel cost associated with the production and transportation cost of inorganic fertilizer (e.g., Schlesinger, 2000).

Bush fallows

Between cropping seasons, fallow lands play an important role to preserve vegetation cover so that soil erosion and land degradation in farm fields can be minimized (Bationo and Buerkert, 2001; Cherr et al., 2006; Franke et al., 2004; Hauser et al., 2006). In West Africa, bush fallows are included in crop rotation schemes to replenish depleted soil fertility due to continuous cropping (see Chapter 2). However, the benefit of rotating bush fallows with crops will depend on the quantity of crop residues that may be added to the soil and their effectiveness

in recycling and/or adding crop nutrients. If crop productivity is poor, and only negligible amounts of crop residues are added to the soils, bush fallows can help increase organic matter input relative to continuous cropping. Otherwise, if continuous crop cultivations can sustain good productivity by adopting recommended management practices, elimination of fallows may be more beneficial for soil carbon sequestration (Hutchinson et al., 2007; Manlay et al., 2002).

Crop residue

The ultimate source of soil organic carbon is atmospheric CO_2 captured by plants. Therefore, to increase the amount of soil organic carbon, plant biomass productivity should be increased. However, low soil fertility with depleted soil organic matter commonly constrains crop production in dryland agriculture in West Africa (Schlecht et al., 2006). Thus, low fertility is an important factor that constraints the input source for soil carbon sequestration in dryland agriculture (Bationo and Buerkert, 2001). In addition, failure to return crop residues under continuous cropping systems will reduce soil organic carbon (Sainju et al., 2006; Wang et al., 2005). Currently in West Africa, large proportions of crop residues are not added to soils but burned or removed to use in household for feeding livestock or cooking (Lal, 2004b). In general, about 20% of crop biomass is estimated to be added to the soil organic matter pool in the tropics (Batjes and Sombroek, 1997), and about 15% of the incorporated crop residues is estimated to convert to the relatively stable soil organic carbon pool (Lal, 1997).

Assessing Soil Carbon Sequestration Potential

Estimating soil carbon sequestration potential is a complicated process, as it requires knowledge of how land will be managed and how much carbon will be sequestered under different management practices. Therefore, estimated soil carbon sequestration potentials are typically based on a number of assumptions and evaluated for a limited number of scenarios (Conant, 2002). Soil carbon sequestration potential for agricultural lands with specific cropping

systems has been assessed with data from long-term field trials (e.g., Ghosh et al., 2006) or simulation results (e.g., Tschakert et al., 2004). Such studies provided estimates for specific cropping systems and management scenarios. However, a regional estimate of the soil carbon sequestration potential is also important, especially for policy makers to develop land use strategies. Linking simulation models with Geographical Information Systems (GIS) allowed assessment of soil carbon sequestration potential on a regional scale (e.g., Falloon et al., 1998), but those models may not suitably account for variations in crop production factors and management practices in smaller scales (Schlecht et al., 2006). In dryland cropping systems in West Africa, diverse smallholder farming systems coexist and processes take place at different spatial scales. In this case, a different approach would be needed to take into account inherent variability of cropping systems components at different scales since these greatly impact overall regional soil organic carbon dynamics.

Objective

The objective of this study is to estimate aggregate regional soil carbon sequestration potential for area with predominant smallholders' cropping systems in northern Ghana using DSSAT-CENTURY cropping systems model and scenario analyses. Based on smallholder farmers' current farm management practices, scenarios describing the adoption of recommended management practices were defined and used to simulate cropping systems for estimating soil carbon sequestration potential at field and regional scales.

Materials and Methods

Study Area

The study area of about 18 km^2 was located south of Wa, in the Upper Western Region of Ghana (Latitude: 9.89 and 10.12, Longitude: -2.58 and -2.50) (Figure 2-2 in Chapter 2). The main source of household income in the area is cereal-based cropping with an average farm size

of about 1 ha (Braimoh and Vlek, 2004). The climate is classified as a dry winter (Aw) type (Osei and Aryeetey-Attoh, 1997). Between 1953 and 2004 annual rainfall averaged about 1000 mm. There is one rainy season which generally starts in April and ends in October. Rainfall distribution is skewed and is greatest (200 mm) in August and lowest (40 mm) in January (J.B. Naab, Savannah Agricultural Research Institute, personal communication, October 2005) (Figure 2-3 in Chapter 2).

The study area consisted of 132 fields managed by smallholder farmers (see Chapter 2). As measured field area was not available, the area of each field was assumed to be 1 ha, which was the average field area in northern Ghana reported by Braimoh and Vlek (2004). Soil analysis of the upper 20 cm of the soil profile using composite samples taken from 132 fields in the study area in 2006 showed depleted soil organic carbon content (median value of 0.44% carbon on a mass basis) (Figure 2-4 in Chapter 2) and mostly sandy soil texture (median sand-sized particle content of 78%) (Figure 2-7 in Chapter 2). The majority of soils are classified as Alfisols (J.B. Naab, Savannah Agricultural Research Institute, personal communication, August 2006).

Simulation Model and Input Data

The DSSAT-CENTURY model

Gijsman et al. (2002) modified the DSSAT (Decision Support System for Agrotechnology Transfer) cropping system model (Jones et al., 2003) by incorporating a soil organic matter-residue module from the CENTURY model (Parton et al., 1988; Parton and Rasmussen, 1994). The combined model, DSSAT-CENTURY, was designed to be more suitable for simulating low-input cropping systems and conducting long-term sustainability analyses (Gijsman et al., 2002). This study used the DSSAT-CENTURY model to simulate crop growth and soil organic carbon dynamics under low-input cropping systems in the study area.

Simulation time-period

The simulation time period was set at 20 years with 2006 being the initial year. Soil organic carbon content and texture measurements in 2006 were used as the initial soil properties in each field.

Daily weather data

Daily weather data for input to the DSSAT-CENTURY model (i.e., minimum and maximum temperature, solar radiation, and rainfall) were stochastically generated using the *Weatherman* 4.0.2.0 (Hoogenboom et al., 2006) program based on parameters estimated from 8 years of daily weather measurements from Wa, Ghana (J.B. Naab, Savannah Agricultural Research Institute, personal communication, March 2004).

Soil data

For each of 132 fields, a soil profile was generated using the *SBuild* (Hoogenboom et al., 2006) program based on the soil organic carbon and soil texture measured at 20 cm depth in 2006. Each soil profile included estimated soil properties related to water holding characteristics (e.g., lower limit, drained upper limit, saturated upper limit, and saturated hydraulic conductivity), root growth factor, bulk density, and soil pH in each of seven soil layers to 1 m depth (layer depth: 5, 15, 30, 45, 60, 90, and 100 cm).

The DSSAT-CENTURY model needs the initial fractions for three soil organic matter pools (i.e., SOM1: microbial, SOM2: intermediate, and SOM3: stable) for each soil layer. As no measurements were available to estimate these soil organic matter pool fractions, estimates were made based on assumptions that: 1) the overall soil organic matter dynamics is not sensitive to the initial fraction of SOM1 (microbial pool), which was assumed as 1% in all fields, 2) the initial fraction of SOM3 at the beginning of cultivation (i.e., when native vegetation was cleared and converted to cropping system) in each field was identical, and 3) the present fraction of

SOM3 in each field followed an exponentially decreasing trend since the beginning of cultivation.

Bostick et al. (2007) analyzed results from a long-term cultivation and soil carbon dynamics experiment conducted in Burkina Faso and reported that, after ten-years of continuous sorghum cultivation without applying fertilizer, soil organic carbon decreased from 0.55% to 0.32%. Using a two-pool (labile and stable) soil organic matter model, they estimated that the fraction of stable pool (i.e., SOM3 in DSSAT-CENTURY) increased from about 58% to 98% over the ten-year period.

Assuming that the labile pool (SOM1) accounts for 1%, the result of Bostick et al. (2007) was reconstructed as shown in Figures 3-1A (changes in soil organic carbon) and 3-2B (changes in soil organic matter pool fraction). Based on the proximity of the two study sites (Wa, Ghana and Farako-Bâ, Burkina Faso) and the similarity in respective climates, it was assumed that 1) SOM3 fraction when the cultivation began in each field was same as the initial value used by Bostick et al. (2007) for the stable pool (i.e., 0.57 at 1992 in Figure 3-1), 2) SOM1 fraction is 1% of the labile pool estimated by Bostick et al. (2007), and 3) continuous cultivation reduces SOM2 and increases SOM3 fractions at the same rate that Bostick et al. (2007) reported. A nonlinear regression was fitted to the data reported by Bostick et al. (2007) which expresses SOM3 fraction as a function of the number of cultivated years since fallow (Figure 3-2). Then, the number of cropping years of the most recent cultivation for the 132 surveyed farmers' fields (Figure 3-3A) was used to estimate the initial SOM3 pool fraction (Figure 3-3B) in each field. This resulted in a distribution of SOM3 fractions among fields as well as a distribution of soil carbon levels measured in the fields.

Nitrogen in rainfall

Atmospheric-borne nitrogen was assumed to be added to soils at the beginning of the rainy season every year. Based on the typical annual rate of 5 to 8 kg[N] ha^{-1} reported in non-industrial temperate regions (Brady and Weil, 2002), 5 kg[N] ha^{-1} was assumed to be added to soils in each cropping season by split application of 1 kg[N] ha^{-1} five times with four-day interval on 1, 5, 9, 13, and 17 days after planting.

Simulating manure applications

Compounds fields near houses may receive domestic animal manure applications in the study area. The manure application was assumed to be applied within 50 m from farmers' houses (J.B. Naab, Savannah Agricultural Research Institute, personal communication, October 2006). Therefore, cow manure application was simulated for a field whose centroid was within 50 m distance from farmers' houses. The centroid coordinates of farmers' fields were calculated using the measured field boundary (see Chapter 2) and a GIS software package, ESRI ArcMap 9.0 (http://www.esri.com). Farmers' houses in the study area were located using a high-resolution remote sensing image (see Chapter 2).

Simulating tillage

The impact of crop cultivation and its disturbances on soil organic matter dynamics may be simulated by enhancing organic matter decomposition rates (Metherell et al., 1993). Based on the CENTURY 4.0 model, the DSSAT-CENTURY model simulates the impact of tillage on soil organic matters by accelerating decomposition processes by 60% for 30 days to the soil depth defined by user (A. J. Gijsman, University of Florida, personal communication, March 2007). In this study, manual tillage using hand-hoes at 20 cm depth was simulated, based on surveyed smallholder farmers' current practices (Chapter 2).

Genetic coefficients

Growth of four different crops, including three cereals (i.e., sorghum, maize, and millet) and one legume (i.e., peanut), and bush fallow were simulated for the different cropping system scenarios. Genetic coefficients of simulated cultivars for sorghum, millet, and peanut were estimated from the literature as follows.

- **Sorghum:** Folliard et al. (2004) reported a new method to simulate sorghum response to daylength during the photoperiod inductive phase. The proposed new method, threshold-hyperbolic modeling approach, and the published genetic coefficients for the photoperiod-sensitive local cultivar in Mali, CSM388, were used in this study.

- **Millet:** Photoperiod sensitivity of a local millet cultivar was assumed to be similar to the one of sorghum. Genetic coefficients and the photoperiod sensitivity of a local millet cultivar, Sanioba-B, were calibrated by P.C.S. Traoré (ICRISAT-Mali, personal communication, November 2006) and used in this study.

- **Peanut:** The Chinese cultivar was used to simulate peanut production in the study area. Genetic coefficients of the Chinese cultivar were calibrated by Naab et al. (2004) to analyze yield gap in the Wa study area. Damages to peanut production due to plant leafspot disease epidemics were not simulated, thus dry matter production may be overpredicted.

For maize, growth of the Obatanpa cultivar was simulated. A survey of farmers showed that Obatanpa was the most commonly grown cultivar in the study area. Obatanpa is a tropically adapted, intermediate maturing, and open-pollinating cultivar with increased level of lysine and tryptophan (Badu-Apraku et al., 2006). Grain yield of Obatanpa was reported as about 5 t ha^{-1} (Asiedu et al., 2000; Dankyi et al., 2005). However, on-station maize cultivation experiment in the study area in 2004 and 2005 showed that the average grain yield of Obatanpa ranged from about 0.2 to 4 t ha^{-1}, depending on the level of nitrogen and phosphorus fertilizations (J.B. Naab, Savannah Agricultural Research Institute, personal communication, April 2006).

The DSSAT-Maize model requires following six genetic coefficients to be calibrated for a new maize cultivar (Tsuji et al., 1994):

1. P1: Degree days (base temperature = 8 C) from seedling emergence to the end of the juvenile phase when tassels are observed.

2. P2: Extent to which development is delayed for each hour increase in photoperiod above the longest photoperiod at which development proceeds at a maximum rate, 12.5 hours.

3. P5: Thermal time from silking to physiological maturity (base temperature = 8 C).

4. G2: Maximum possible number of kernels per plant.

5. G3: Kernel filling rate during the linear grain filling stage and under optimum conditions (mg/day).

6. PHINT: Phylochron interval; the interval in thermal time (degree days) between successive leaf tip appearances.

However, calibrated genetic coefficients of Obatanpa were not available from literatures, thus values of these coefficients were estimated from maize growth analysis data obtained from on-station experiments conducted in the study area to study the maize growth response to nitrogen and phosphorus fertilizations in 2004 and 2005 (J. B. Naab, Savannah Agricultural Research Institute, personal communication, April 2006). The 2004 dataset was used to calibrate genetic coefficients, and the 2005 dataset was used to validate them. Harvest maturity date was set as 110 days after planting (Asiedu et al., 2000). The calibration process was based on a previous study published by Jagtap et al. (1993).

1. The number of leaves per plant was assumed as 15, based on the reported leaf number of Obatanpa by Asiedu et al. (2000).

2. The photo-sensitivity parameter (P2) was set as 0.0, as day lengths in the study area, whose latitude is about +10 degree, are close to 12 hours throughout the year (Jagtap et al., 1993).

3. The phylochron interval (PHINT) was adjusted so that the simulated leaf number to be close to 15.

4. The value of P1 was adjusted so that the simulated 75% silking date was close to 62 days after planting. The measured 50% silking date was 60 days, thus 2 days were added to take into account the 25% increase to 75% (J.B. Naab, Savannah Agricultural Research Institute, personal communication, March 2007).

5. The values of PHINT and P1 were simultaneously fine-tuned to match the leaf number of 15 and the simulated 75% silking date to be 62 days after planting.

6. The value of P5 was calculated by summing degree days from the measured 50% silking date until harvest maturity date with a base temperature of 8C (Jagtap et al., 1993).

7. The value of G2, the maximum possible number of kernels per plant, was not available in the measurement. Considering the typical value of G2 ranges between 500 and 600 (J. Lizaso, University of Florida, personal communication, February 2006), the value of G2 was assumed as 550.

8. The value of G3, the kernel filling rate under optimum water and N fertility conditions, was adjusted so that the simulated grain yield without soil water and nitrogen stress was about 5 t ha^{-1}, as reported by Badu-Apraku et al. (2006).

The calibrated values of the genetic coefficients were as shown in Table 3-1. Observed and simulated phenology data correlated well for both emergence and silking dates (Figure 3-4). Observed and simulated grain yield also showed good agreement for treatments with and without fertilizations (RMSE: 345 kg ha^{-1}, CV: 17%) (Figure 3-5).

For simulating bush fallow, V. K. Walen (Graduate student, University of Florida, personal communication, November 2006) modified the bahiagrass model in DSSAT-CENTURY to represent the mixed bush fallow vegetation observed in Ghana. The modifications included allowing plants to persistently grow and develop for multiple years without harvest, developing a substantial root stock over the years, and increasing tolerance to drought and low nitrogen. The modified bahiagrass model was used in this study to simulate bush fallows in cropping sequences.

Cropping sequences

To estimate crop biomass production dynamics and subsequent carbon input to the soil organic matter pools, a projected cropping sequence in each field was created for the simulation time period. Assuming future cropping sequences will reflect the surveyed cropping history (see Chapter 2), a one-step transition probability matrix of crop types was calculated from the surveyed cropping history (Table 3-2) and used to stochastically create cropping sequences for

all fields using the Markov Chain Monte Carlo (MCMC) method (Figure 3-6). This stochastic method was used to mimic the spontaneous nature of smallholder farmers' crop selection in each season based on several factors, including market price in a previous season, seed variability, and rainfall onset date. Values in the transition probability matrix represent the probability that a particular crop in the sequence (in columns) follows a particular crop that is found in a field (in rows). For example, the probability that sorghum follows sorghum is 0.54 and the probability that fallow peanut follows sorghum is 0.27 (Table 3-2). The scenarios used in this study were based on current cropping sequences and did not include new relative frequencies of the cropping sequences. Cropping sequences in the area may change considerably in reality if prices change and yield increases occur in staple crops under fertilizer, residue, and tillage practice alternatives considered in the study. For example, peanut price in the study area was high in 2003, and that caused increased peanut cultivation in 2004 (J. B. Naab, Savannah Agricultural Research Institute, personal communication, March 2007) (Figure 2-16). In addition, with higher yields of maize and sorghum, farmers may choose to plant more of these crops in their rotations or leave more land fallow, both of which would influence production and soil carbon changes. The Tradeoff Analysis Model (Stoorvogel and Antle, 2001) or other farm- or region-level models could be used to explore changes to cropping sequences, but that was beyond the scope of the current study.

Scenario Analyses

Five scenarios were chosen to study the impact of adopting different management practices that potentially influence crop growth and soil carbon dynamics (e.g., tillage, fertilization, and residue removal) (Table 3-3). First, the business-as-usual (BAU) scenario was implemented to reflect farmers' current field management practices, including tilling the field before planting with hand-hoes to a soil depth of 20 cm depth, no fertilization, and removal of most crop

residues after harvest. The residue removal rate for the BAU scenario was defined as 100, 75, and 100% for cereals, legumes, and bush fallow, respectively, based on the surveyed smallholder farmers' residue management practices in the study area (see Chapter 2) (J. B. Naab, Savannah Agricultural Research Institute, personal communication, March 2007). When bush fallow was continued for more than one season, residue was removed only in the last season. Then, based on the BAU scenario, three additional scenarios were generated by changing each of the management treatments, such as tillage (i.e., NTL for no-till), fertilization (i.e., FRT for fertilization on cereal crops, see Table 3-3 for details), and residue retention (i.e., RSD for conserving crop residues with only 25% residue removal instead of 75-100% being removed). The NTL scenario also conserved crop residues with only 25% removal. Finally, an "ideal" scenario based on a set of recommended management practices (RMP) proposed by Lal (2004b) was used to increase productivity and maximize soil carbon sequestration. The RMP consisted of no-till, N-fertilization for cereals (see Table 3-3 for details), and conserving residues. For each scenario, yearly crop growth (e.g., aboveground vegetative biomass) and soil carbon dynamics (e.g., the amount of soil organic carbon content at 20 cm depth) were predicted using the DSSAT-CENTURY model. To analyze the impact of different scenarios on each of the simulated crops, one representative field, whose initial measured soil organic carbon content was the median value within the measurement range, was chosen, and continuous mono-cropping of each crop was simulated for each scenario.

Soil Carbon Sequestration Rate

The yearly soil carbon sequestration rate for each scenario in each field was "relatively" calculated based on soil carbon changes under the BAU scenario as follows:

$$\text{Sequestration Rate for TRT (kg ha}^{-1}\text{ yr}^{-1}) = \frac{(\text{TRT}_n - \text{TRT}_0) - (\text{BAU}_n - \text{BAU}_0)}{n} \qquad (3\text{-}1)$$

where n is the number of years simulated (20 in this study), TRT_n is the amount of SOC for each scenario in year n (kg[SOC] ha^{-1}), and BAU_n is the amount of SOC for the BAU scenario in year n (kg[SOC] ha^{-1}). Thus, the soil carbon sequestration rate for each scenario represented the net potential soil carbon benefit relative to the BAU scenario over time. The calculated soil carbon sequestration rates for each of the 132 fields were analyzed to test their statistical significances in different scenarios using the Duncan's multiple range test (Duncan, 1955). In addition, three representative fields with the maximum, median, and minimum sequestration rates were chosen to compare the impacts of different cropping sequences on soil carbon sequestration rate.

Results

Representative Field

A representative field was selected based on its soil carbon content in 2006; soil organic carbon content of this field was 0.45%, the median value of measured soil organic carbon content. The field had loamy sand texture (clay: 6%, silt: 14%, and sand: 80%). Surveyed cropping history showed that the selected field was cultivated with peanut and sorghum crops since 2002. Based on the assumed relationship between crop cultivation period and SOM3 fraction shown in Figure 3-2, SOM3 pool fraction in the representative field was initialized as 0.79. Fractions of the other pools were generated by difference and estimated as: SOM1:SOM2:SOM3 = 0.01:0.20:0.79.

Continuous bush fallow: biomass and SOC

Unlike crops, continuous bush fallow grown for more than one cropping season did not simulate harvest at the end of a cropping season. Thus, continuous bush fallow growth for 20 years showed increasing trends of aboveground biomass and soil organic carbon (Figure 3-7). Over time, increasing soil organic carbon resulted in a positive feedback on biomass productivity. Root biomass was not notably increased over time, but roots were able to survive during the dry

winter season with increased drought tolerance. Since bush fallow fields were not managed, there was no impact of different management scenarios on results. Differences in soil carbon and productivity among fields were due to differences in soil texture, initial soil carbon content, and SOM3 fractions.

Continuous mono-cropping system: biomass

When continuous mono-cropping was simulated for the representative field, different crops showed different responses of aboveground vegetative biomass production to management scenarios based on the supply and demand of soil nutrients to crops (Figures 3-8 and 3-9).

Continuous sorghum mono-cropping showed some responses to different scenarios, but their differences across scenarios were weak (Figure 3-8A). There were some years in which fertilization increased biomass productivity, but the differences were not as much as in maize or millet. This result implied that the simulated sorghum cultivar may have been adapted to the low input cropping system with low fertility soils. Relative biomass enhancements showed no significant differences among management scenarios from the BAU scenario (α=0.05) (Figure 3-9).

Continuous maize mono-cropping showed the most distinctive responses to fertilization, compared to other crops (Figure 3-8B). The two fertilized scenarios, FRT and RMP, showed notably higher biomass productivities than others without fertilizations. Relative to the BAU scenario, fertilized scenarios significantly enhanced biomass productivity, by more than 90% on average (α=0.05) (Figure 3-9). In contrast, scenarios without fertilization showed only slightly higher productivity than the BAU scenario with no significances (α=0.05). This provides evidence that N in regions with limited inherent soil fertility is one of the major constraints hampering productivity and SOC accumulation. On average, annual aboveground vegetative biomass was about 8 ton/ha for FRT and RMP and 4 ton/ha for BAU, NTL, and RSD.

Continuous millet mono-cropping showed the most dramatic differences between scenarios over time (Figure 3-8C). The RSD scenario showed significantly higher biomass productivity than the BAU scenario (α=0.05) (Figure 3-9). The FRT scenario (fertilization alone) produced significantly higher biomass than other non-fertilized scenarios (BAU, NTL, and RSD) (α=0.05). Productivity was increased further when no-till cropping was simulated, as shown for the RMP scenario, which produced more than twice as much biomass as the BAU scenario with significance (α=0.05) (Figure 3-9). However, it was noted that the overall biomass productivity decreased over time under all scenarios, regardless of adoption of recommended management practices (Figure 3-8C). This result implied that the simulated millet cropping systems under different scenarios did not provide enough nutrients to meet millet crop nutrient demand.

Continuous peanut mono-cropping did not show any significant differences in aboveground biomass production (α=0.05) (Figures 3-8D and 3-9). This is because the peanut model simulated nitrogen fixation that provided nitrogen needed by the crop.

Continuous mono-cropping system: soil carbon

The soil organic carbon (SOC) accumulation was greatly affected by different management scenarios (Figure 3-10). Overall, all scenarios sequestered soil carbon for all crops relative to BAU. The RMP scenario sequestered the most SOC among all cropping systems, followed by the NTL, RSD, and FRT scenarios. The FRT scenario showed the least soil carbon sequestration potential. Although the FRT scenario increased crop biomass productivities in all fertilized crops (Figures 3-8 and 3-9), the enhanced crop biomass production did not result in soil carbon sequestration, as most crop residues were removed from the field. In contrast, relatively higher soil organic carbon for the RSD and NTL scenarios for all crops showed that, even without fertilization, improved residue management can increase soil carbon. In the RMP scenario, the highest soil carbon sequestration potential was achieved for the continuous millet mono-cropping

(Figure 3-11). On average, the RMP scenario sequestered 30% more soil carbon than the BAU scenario.

It was noted that absolute soil carbon sequestration for the RMP and to some extent the NTL scenarios increased nearly linearly over time for all cropping systems, but the RSD scenario continue to decline slowly but reaching a minimum value. These results imply that the NTL and RMP scenarios are a necessary part of any soil carbon sequestration scheme, although the RSD scenario may be stabilize after 10 to 20 years and certainly with a better sequestration potential than the BAU scenario.

Carbon Sequestration Rate

The relative rate of soil carbon sequestration in each field for each scenario was calculated using Equation 3-1. Histograms of soil carbon sequestration rates for each scenario showed their distributions over 132 farmers' fields in the study area (Figure 3-12). Duncan's multiple range test result showed that all scenarios were significantly different from each other (α= 0.05). The RMP was the most effective scenario (Figure 3-12D) with the median value of about 173 kg[SOC] ha^{-1} yr^{-1}, and the NTL and RSD scenarios followed with median values of 132 kg[SOC] ha^{-1} yr^{-1} and 68 kg[SOC] ha^{-1} yr^{-1}, respectively (Figures 3-12A and 3-12C). The FRT scenario showed a median soil carbon sequestration rate of only about 20 kg[SOC] ha^{-1} yr^{-1} relative to BAU (Figure 3-12B), as most crop residues were removed and tillage practices increased soil organic carbon decomposition rates.

For the RMP scenario, three particular fields with maximum (285 kg[SOC] ha^{-1} yr^{-1}), medium (174 kg[SOC] ha^{-1} yr^{-1}), and minimum (35 kg[SOC] ha^{-1} yr^{-1}) soil carbon sequestration rates were identified. Their soil organic carbon changes over the simulation time period were used to compare cropping sequences (Figure 3-13). Overall, the three cases showed similar

trends among different scenarios in the order of RMP, NTL, RSD, FRT, and BAU, from highest to lowest soil carbon sequestration, but their yearly dynamics were different depending on crop.

The maximum sequestration rate was achieved at a field with mostly (19 out of 20 years) continuous cereal cultivation with no bush fallow (Figure 3-13A). In contrast, the minimum sequestration was from a field with mostly (15 out of 20 years) bush fallow (Figure 3-13C). Although the continuous bush fallow was shown to be effective to conserve soil organic carbon and sustain an increasing trend in biomass productivity (Figure 3-7), the simulated potential to sequester soil carbon was low, relative to BAU. Unlike crop cultivation, management scenarios did not change any management options for the continuous bush fallow before harvest (Table 3-3), thus simulated soil carbon dynamics were similar across scenarios and not much different from the BAU scenario. Consequently, overall soil carbon sequestration potential was low. However, this result may not reflect benefits of bush fallow found in conventional field management practices. For example, only the non-legume-based bush fallows were simulated in this study, thus the positive impact of leguminous bush fallows on soil carbon accumulation (i.e., fixing soil N, improving soil fertility, and increasing crop productivity) (Cherr et al., 2006; Franke et al., 2004) was not taken into account. In addition, physiological aspects of bush fallows may not be adequately simulated in the preliminary model (e.g., low productivity due to limited nitrogen uptake and/or shallow rooting depth). Further improvements on the bush fallow model will be necessary.

The median soil carbon sequestration rate was from a field in which cereal crops were rotated with legumes and bush fallows (10 years of cereals, 6 of legumes, and 4 of bush fallow out of 20 years) (Figure 3-13B). The FRT scenario did not show any soil carbon sequestration

benefit when peanut was cultivated, as fertilization was applied only on cereal crops and no differences were simulated between the BAU and FRT scenarios in those years.

Aggregated Results

As an aggregated regional estimate of the soil carbon sequestration, results from all 132 fields were averaged by scenario (Figure 3-14). It was noted that, when the potential of soil carbon sequestration is estimated, soil carbon changes over time can be differently interpreted depending on the definition of soil carbon baseline values. That is, if one assumes the initial soil carbon content as the baseline, soil carbon sequestration potentials for different scenarios will be estimated differently than sequestration potential based on the BAU soil carbon as the baseline. For example, the FRT and RSD scenarios showed soil carbon depletions over the 20-year time period in their absolute values (Figure 3-14A), but their soil carbon sequestration potentials were positively estimated using Equation 3-1 (Figure 3-14B). This was because soil carbon changes under the BAU scenario were not steady-state but continuously depleted over time, and its depletion was greater than that of the FRT and RSD scenarios (Figure 3-14A). Since this study relatively defined the soil carbon sequestration rate as differences in soil carbon levels between with and without adoption of soil carbon-promoting management practices (Equation 3-1), the BAU-based estimation of soil carbon sequestration potential for each scenario (Figure 3-14B) was analyzed hereafter.

Similar to a representative field, the aggregated result showed a near-linear increase in soil carbon sequestration for both the RMP and NTL scenarios. The RSD and FRT scenarios showed less potential, although soil carbon levels seemed to approach minimum asymptotes that were clearly higher than the BAU scenario, especially for RSD relative to BAU. This result suggested that the RSD and FRT scenarios may be used as valuable soil carbon maintenance strategies. The FRT scenario consistently showed the least soil carbon sequestration among scenarios.

On average, all of the simulated management scenarios showed significantly higher soil carbon sequestration than the BAU scenario (α=0.05) when compared as the increment of rate versus BAU (Figure 3-15A). The average soil carbon sequestration for the RMP scenario was 173 kg[SOC] ha^{-1} yr^{-1}, significantly higher than the BAU, FRT, and RSD scenarios (α=0.05). Without fertilizer applications, the NTL and RSD scenarios had soil carbon sequestration rates of 132 kg[SOC] ha^{-1} yr^{-1} and 71 kg[SOC] ha^{-1} yr^{-1}, respectively. These values were significantly higher than the FRT scenario in which fertilizer was applied, which had an average soil carbon sequestration rate of about 23 kg[SOC] ha^{-1} yr^{-1} (α=0.05). The RSD scenario (sequestration rate of 71 kg[SOC] ha^{-1} yr^{-1}) was not as effective as the NTL or RMP scenarios, but still showed a significantly higher soil carbon sequestration rate than the BAU and FRT scenarios (α=0.05). The FRT scenario sequestration rate of 23 kg[SOC] ha^{-1} yr^{-1} was significantly lower than that for the NTL, RSD, and RMP scenarios, although it was significantly higher than the BAU scenario (α=0.05).

Aggregated increases in crop biomass productivity showed higher variability across simulated fields, as different fields were cultivated with different stochastically-generated cropping sequences. This produced different magnitudes of crop biomass production depending on crops growing in any particular year across the landscape (Figure 3-8). This variability would be reduced when the number of fields increases. However, in general, Duncan's multiple range test showed significances of different scenarios on crop aboveground biomass productions (Figure 3-15B). Two fertilized scenarios, FRT and RMP, showed significantly higher biomass production than others without fertilizations (α=0.05). Among others, the RSD scenario showed significantly higher biomass production than the BAU scenario, but its productivity was less than 50% of fertilized scenarios. In contrast to the high potential of sequestering soil carbon by the

NTL scenario (Figure 3-15A), it showed the least potential for increasing biomass production, and it was not significantly different from the BAU scenario (α=0.05). Comparing the RSD and NTL scenarios, the difference could be from the nutrients more readily released from the incorporated crop residues with the RSD scenario rather than the crop residue left on surface in the NTL. Also, tillage increases organic matter decomposition, which releases nutrients for crop growth. Thus, with decomposition rates lower in the NTL scenario, lower amounts of nutrients would result in lower productivity.

Discussion

Current low-input dryland cropping systems have been limiting crop production and depleting soil organic carbon pools. However, such low and depleted levels of soil carbon provide opportunity for enhanced soil carbon sequestration. Relative to cropping systems with business-as-usual management practices, scenario analyses estimated the potential for soil carbon sequestration if recommended management practices (i.e., fertilization, conserving residues, and elimination of tillage practices) were adopted. When all recommended management practices in the analysis were adopted, the aggregate soil carbon sequestration rate was estimated as 173 kg[SOC] ha^{-1} yr^{-1}, relative to BAU.

Based on the expected minimum amount of carbon tradable in the International Greenhouse Gas Market, 1,000 Mg[CO_2] or 273 Mg[C] (Mooney et al., 2004; Rosenzweig et al., 2002), the aggregate soil carbon sequestration rate of 173 kg[SOC] ha^{-1} yr^{-1} implied that the RMP scenario would need to be practiced for at least 12 years in the 132 fields (assuming their average field area is 1 ha) to trade their soil carbon sequestration in the market. Depending on the carbon credit price traded in the market, carbon credits for the sequestered amount of soil carbon can be estimated. For example, as of March 12, 2007, the CO_2 credit price in the Chicago Climate Exchange is $4.00 per Mg[$CO_2$]. This CO_2–based credit can be converted to carbon-

basis as $14.65 per Mg[C], and the carbon price for the minimum tradable amount of carbon (i.e. 273 Mg[C]) is $4,000. That is, theoretically, smallholder farmers of the 132 fields may be credited with $4,000 after the contract period of 12 years.

Even small doses of fertilizer application showed significant aboveground biomass production improvements in cereal crops, but they did not benefit soil carbon sequestration without implementing changes in residue management and tillage practices. Solely relying on fertilizer applications showed the least potential in sequestering soil carbon. On the other hand, a scenario with improved residue management showed significantly higher potential for soil carbon sequestration and crop biomass production, even without fertilization.

When fertilization is not a feasible option, which is the current situation in dryland agricultural systems in West Africa, the most effective management practice to sequester soil carbon and increase crop productivity would be conversion to no-till farming practices combined with increased on-site residue retention. However, the average crop biomass production simulated under no-till prediction was slightly less than in tilled systems, soil carbon sequestration potential under no-till was significantly higher than a tilled system (α=0.05). Furthermore, carbon credits obtained from soil carbon sequestration may be provided in the form of inorganic fertilizers to enhance crop biomass and yield production further and increase soil carbon sequestration.

The practice of shifting cultivation rotates crop cultivation with bush fallows for the purpose of replenishing depleted soil organic matter. However, simulated results showed that elimination of bush fallows may be more beneficial to increase soil carbon sequestration, if most of crop residues are left and/or no-till agricultural practices are adopted. However, the simulation did not include any addition of nitrogen due to native legume species, and there is also concern

over the preliminary nature of the bush fallow model. Thus, this result may be misleading. If legumes occur in the native vegetation or the bush fallow functions better than the model results, then fallow would accumulate nitrogen faster than simulated in this study and lead to higher crop biomass and soil carbon. If one could replace bush fallows with crops, overall crop production from same number of fields would increase without shifting to new lands.

Although simulation results showed the potential benefits of use of conservation tillage and/or residue management practices, their actual adoption by smallholders may not readily occur until some barriers are removed to reduce smallholders' risks and concerns. Simulation results showed that aggregated crop biomass production with tillage was slightly higher than no-till, and this may have been a result of slower mineralization in the no-till practice without fertilization. Moreover, in the absence of pesticide application, leaving crop residues on-site may increase the risk of plant disease or pest epidemics, although the dry winter climate may help avoid them in dryland agricultural systems. Planting methods that can efficiently plant seeds through crop residues may need to be developed and provided (S.G.K. Adiku, University of Ghana, personal communication, April 2006). Eventually, carbon credits may need to be accessible for smallholders via providing them with fertilizers, herbicides, or pesticides up front and in this manner reduce the risk of crop failures and provide incentives to adopt these recommended management practices.

The potential for soil carbon sequestration also depends on soil ability to effectively store resistant plant materials (Farage et al., 2003). It was argued that the use of agricultural land to sequester carbon is only a temporary, not permanent, solution to the global warming and greenhouse gases problems (Conant, 2002; Sharp, 2000). This is because soils may reach their carbon storage capacity within 20 to 50 years with appropriate agricultural practices (Sharp,

2000). However, in the global carbon cycle, soils simultaneously act as a source as well as a sink (Brady and Weil, 2002). As Farage et al. (2003) emphasized, sequestered soil carbon is not inert but can be decomposed when the balance of soil carbon dynamics is shifted. Therefore, it will be important for smallholders in West Africa not only to adopt recommended management practices to increase soil fertility and crop production, but also to maintain the adopted practices and not lose the sequestered carbon or production potential.

Table 3-1 Calculated genetic coefficient values for the Obatanpa maize cultivar

Coefficient	Description	Value
P1	Degree days (base temperature = 8 C) from seedling emergence to the end of the juvenile phase when tassels are observed.	220.0
P2	Extent to which development is delayed for each hour increase in photoperiod above the longest photoperiod at which development proceeds at a maximum rate, 12.5 hours.	0.0
P5	Thermal time from silking to physiological maturity (base temperature = 8 C).	910.0
G2	Maximum possible number of kernels per plant.	550.0
G3	Kernel filling rate during the linear grain filling stage and under optimum conditions (mg/day).	7.74
PHINT	Phylochron interval; the interval in thermal time (degree days) between successive leaf tip appearances.	68.0

Table 3-2 Transition probability matrix obtained from the surveyed cropping sequence in the Wa, Ghana study area from 1987 to 2005

Crop in year *t*	Crop in year *t+1*				
	Sorghum	Maize	Millet	Peanut	Bush Fallow
Sorghum	0.54	0.02	0.09	0.27	0.08
Maize	0.04	0.89	0.02	0.02	0.03
Millet	0.10	0.05	0.29	0.37	0.19
Peanut	0.25	0.01	0.09	0.53	0.12
Bush Fallow	0.11	0.11	0.05	0.16	0.57

Table 3-3 Outline of production practices used for different management scenarios simulations

Scenario (Abbreviation)	Tillage	Fertilization	Residue Removal		
			Cereals	Legumes	Bush Fallow[1]
Business-As-Usual (BAU)	Hand-hoeing at 20 cm	No fertilization	100%	75%	100%
No-Till (NTL)	No-Till	No fertilization	25%	25%	25%
Fertilization (FRT)	Hand-hoeing at 20 cm	Sorghum: 20 kg[N]/ha/yr Maize: 40 kg[N]/ha/yr Millet: 20 kg[N]/ha/yr Peanut: No fertilization Bush Fallow: No fertilization	100%	75%	100%
Leaving Residues (RSD)	Hand-hoeing at 20 cm	No fertilization	25%	25%	25%
Recommended Management Practice (RMP)	No-Till	Maize: 40 kg[N]/ha/yr Sorghum: 20 kg[N]/ha/yr Millet: 20 kg[N]/ha/yr Bush Fallow: No fertilization	25%	25%	25%

[1] When bush fallow was continued for more than one season, the residue of bush fallow was removed only in the last season.

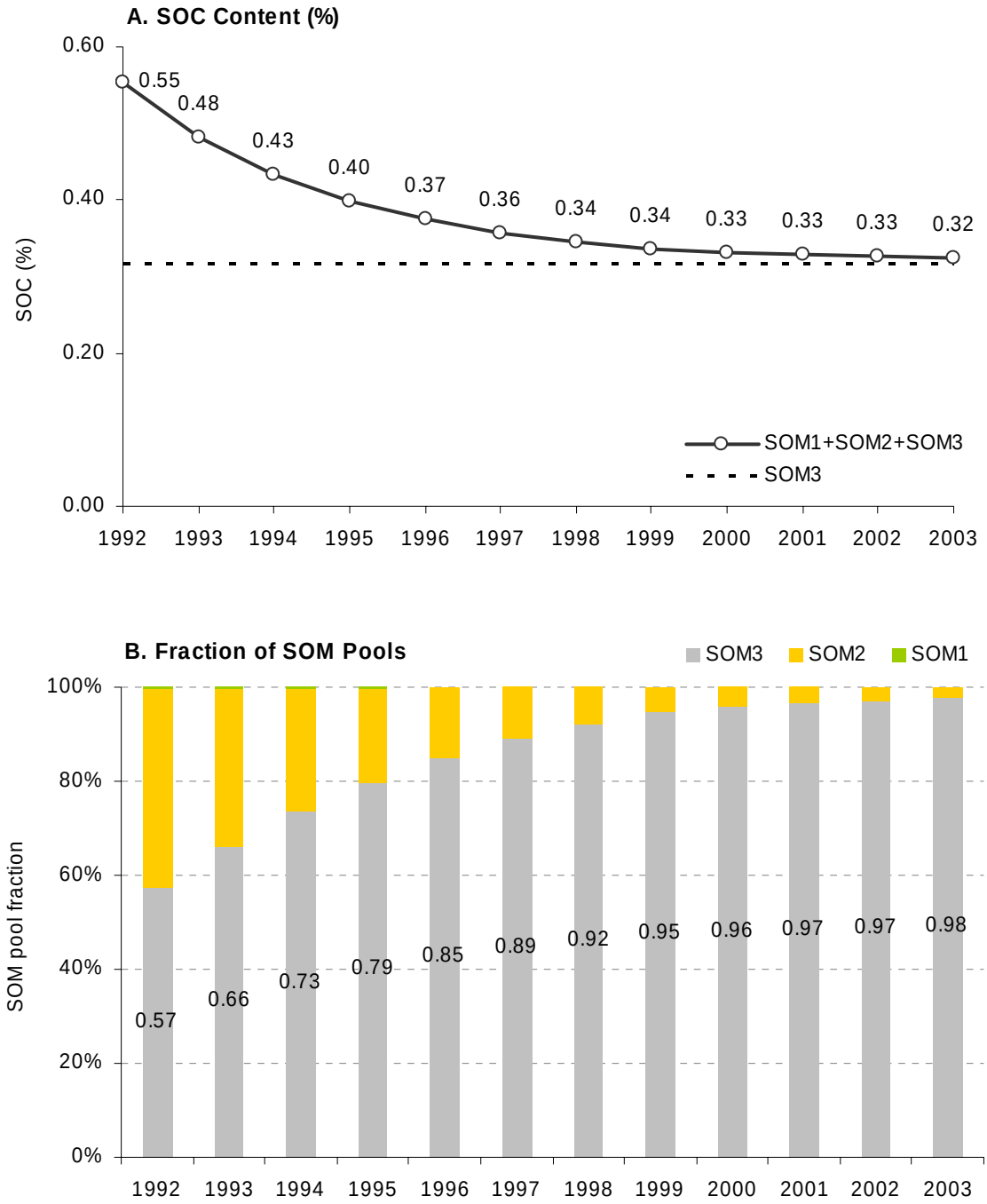

Figure 3-1 SOM fraction changes for 10-year continuous sorghum cropping with no fertilization applications[2]

[2] Adapted from Bostick, W. M., V. B. Bado, A. Bationo, C. T. Soler, G. Hoogenboom, and J. W. Jones. 2007. Soil carbon dynamics and crop residue yields of cropping systems in the Northern Guinea Savanna of Burkina Faso. *Soil and Tillage Research* 93:138-151.

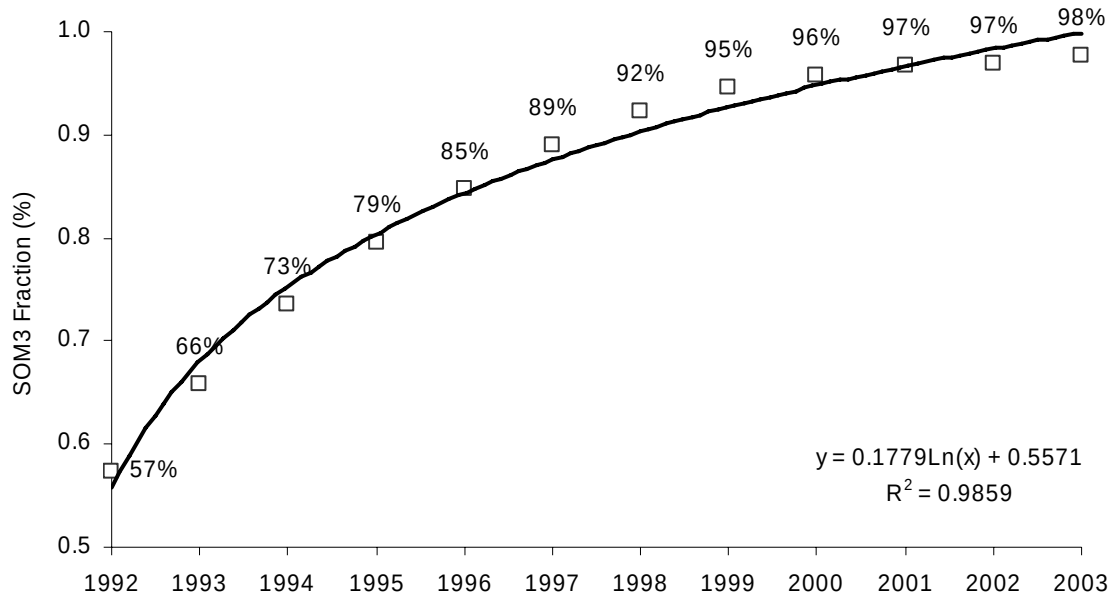

Figure 3-2 Nonlinear regression of the SOM3 pool fraction based on the duration of continuous cultivation with no fertilization

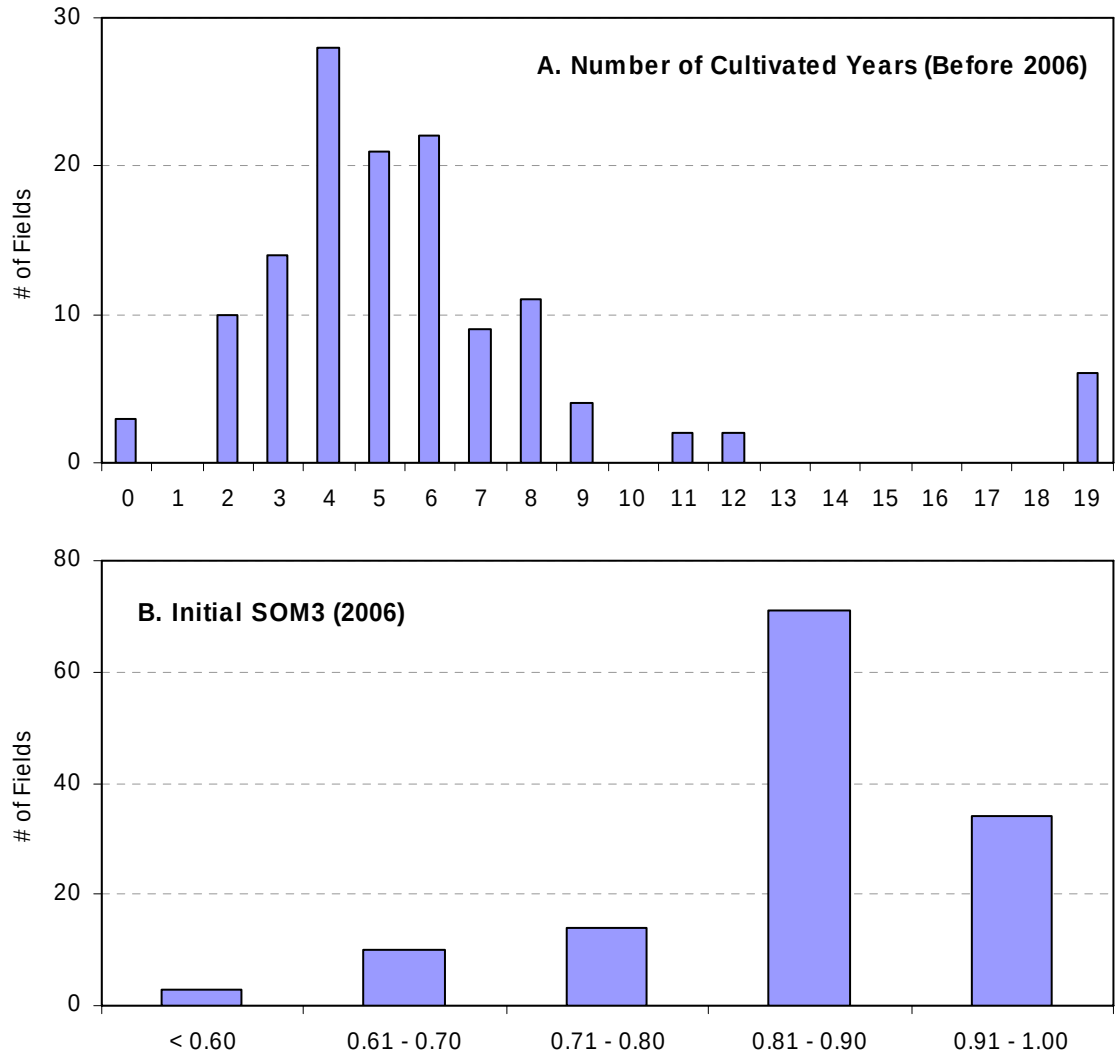

Figure 3-3 Histograms of A) the number of cultivated years and B) the initial SOM3 pool fraction estimated from the number of cultivated years.

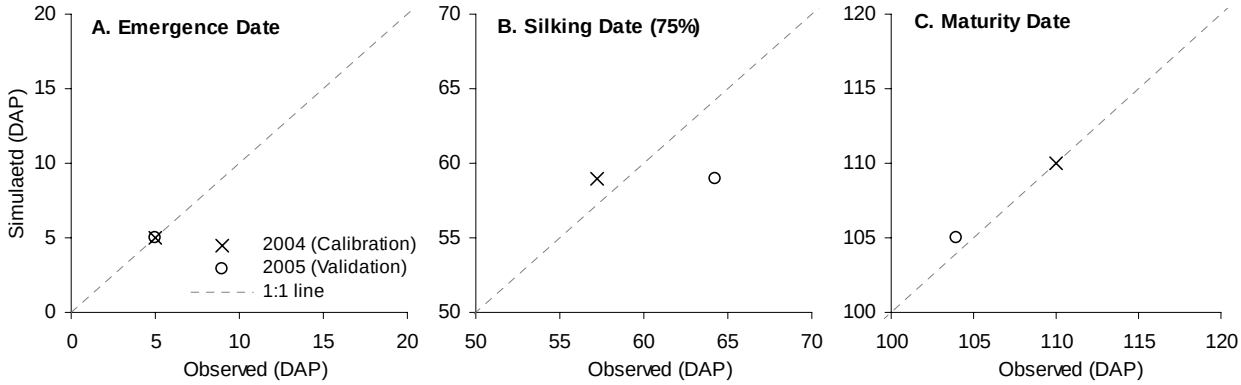

Figure 3-4 Simulated (SIM) and observed (OBS) phenology dates for the Obatanpa maize cultivar.

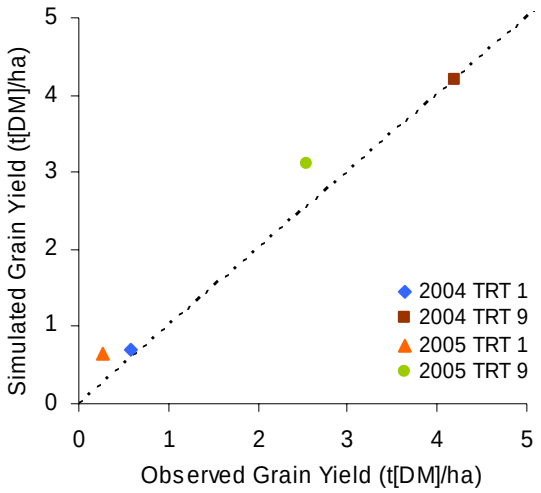

Figure 3-5 Simulated and observed grain yield of Obatanpa maize cultivar in 2004 and 2005 for two different treatments (TRT 1: no inorganic fertilizer, TRT 9: 120 kg[N]/ha, 90 kg[P]/ha fertilizer applied)

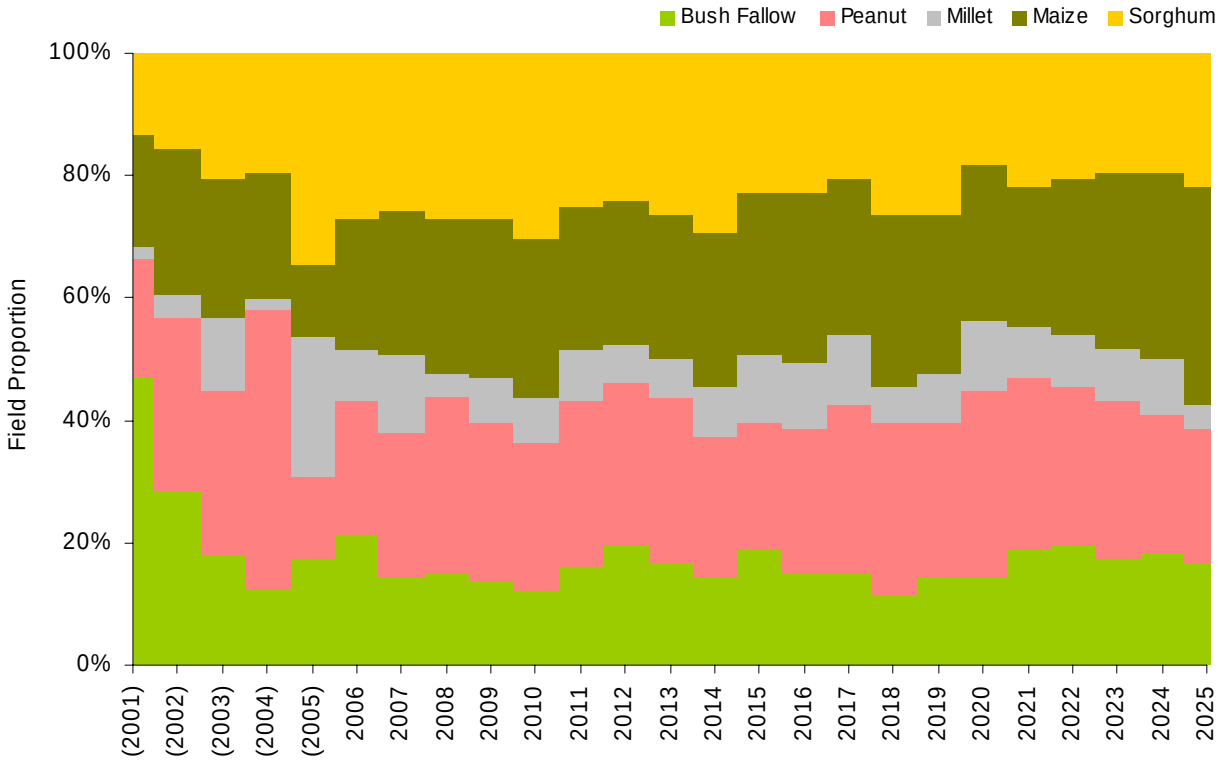

Figure 3-6 Measured (2001-2005) and created (2006-2025) cropping sequence in 132 fields in Wa, Ghana, in proportion of the number of fields each crop is planted.

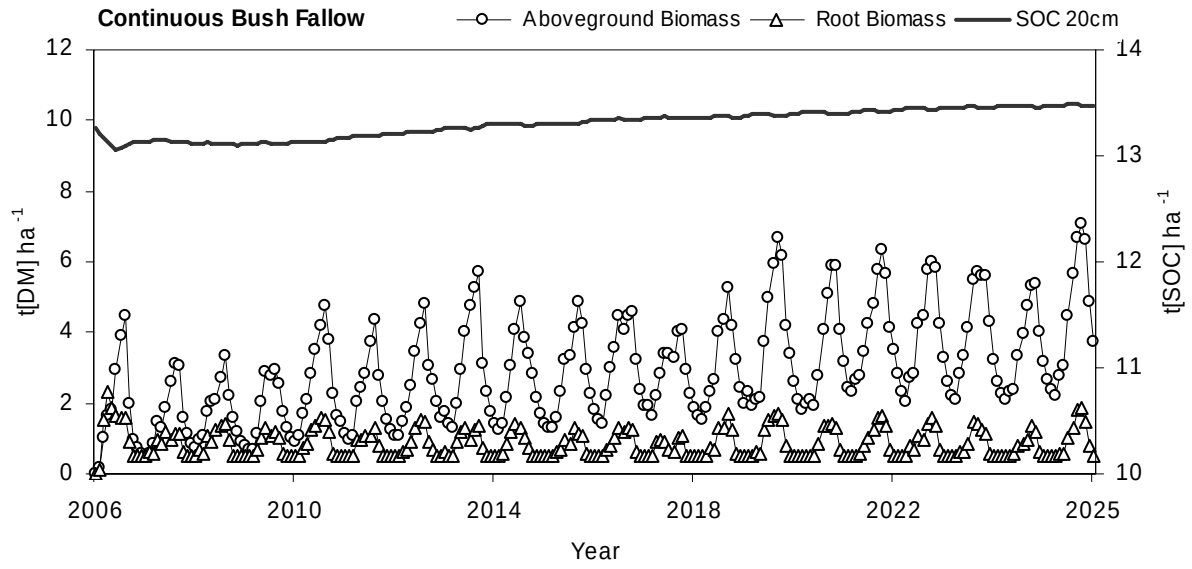

Figure 3-7 Simulated aboveground vegetative biomass, root mass, and soil organic carbon for continuous bush fallow in a representative field in the study area

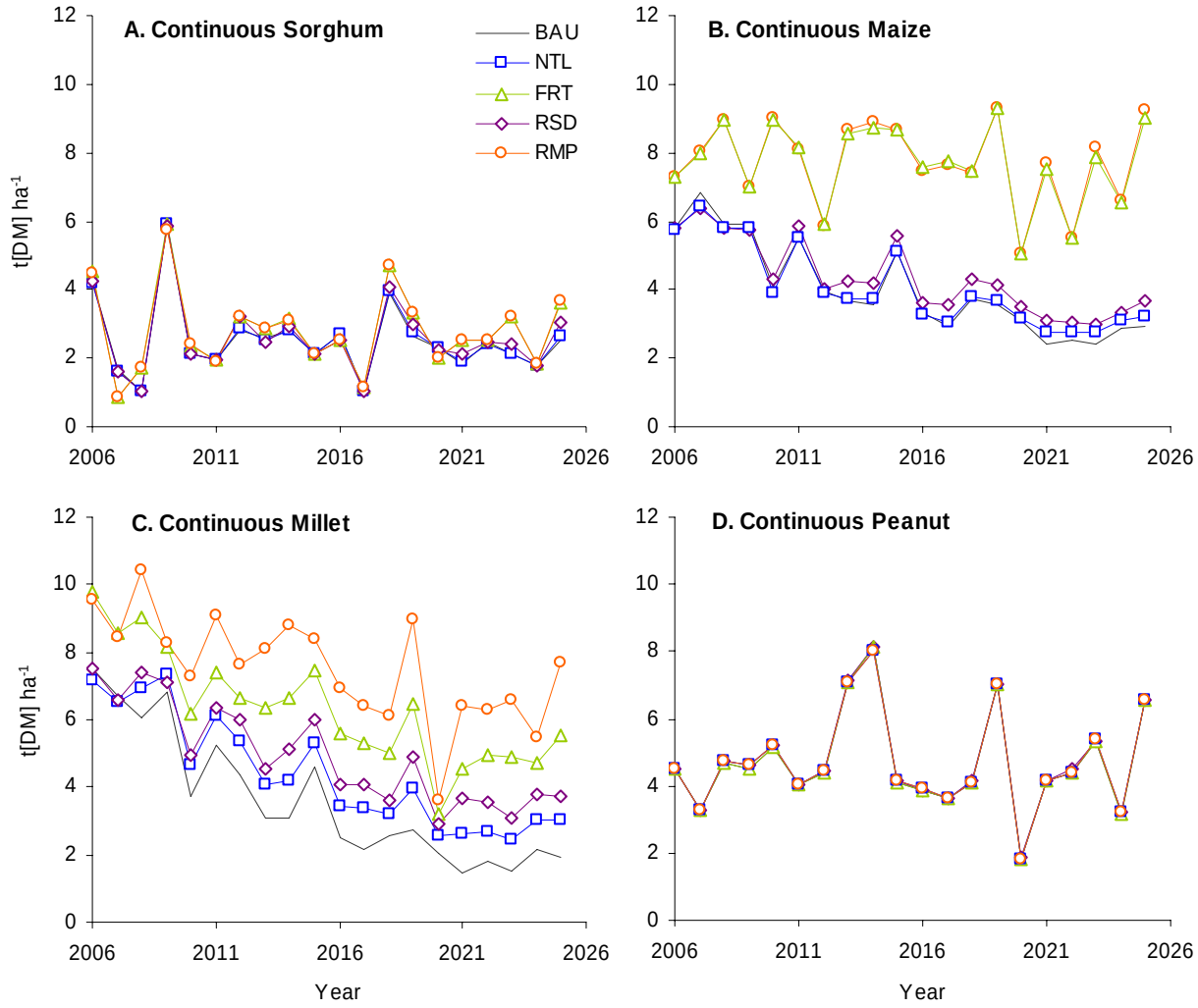

Figure 3-8 Simulated aboveground vegetative biomass in continuous mono-cropping systems at a representative field in the study area for different management scenarios

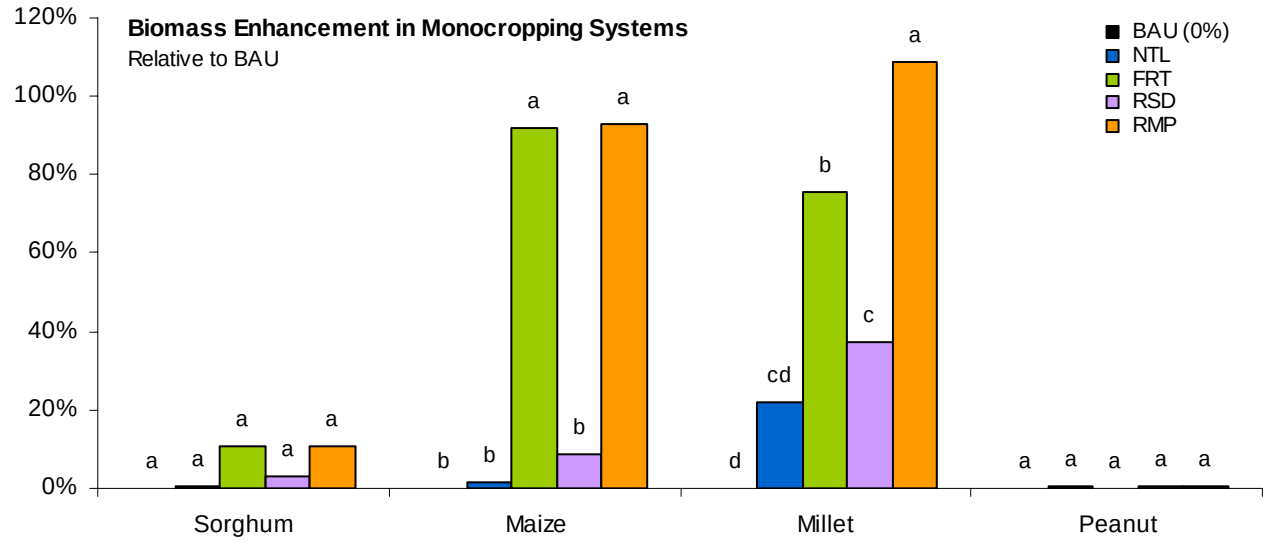

Figure 3-9 Average aboveground crop vegetative biomass enhancements under the simulated management scenarios for continuous monocropping systems of each crop for 20 years, relative to BAU. Different letter represents significant differences in mean values (α=0.05).

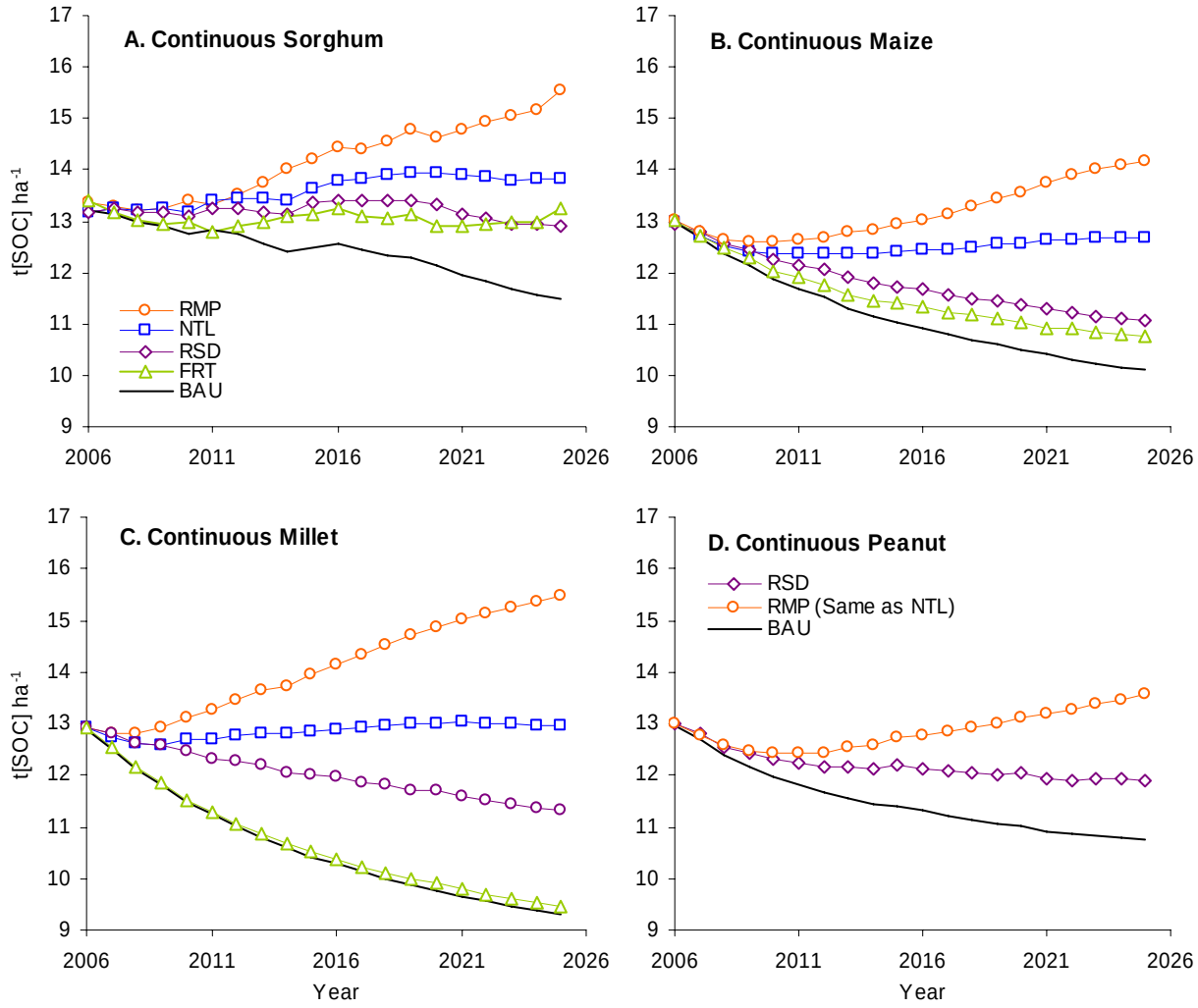

Figure 3-10 Simulated changes of soil organic carbon to 20 cm depth for continuous mono-cropping systems under different management scenarios at a representative field in the study area for 20 years.

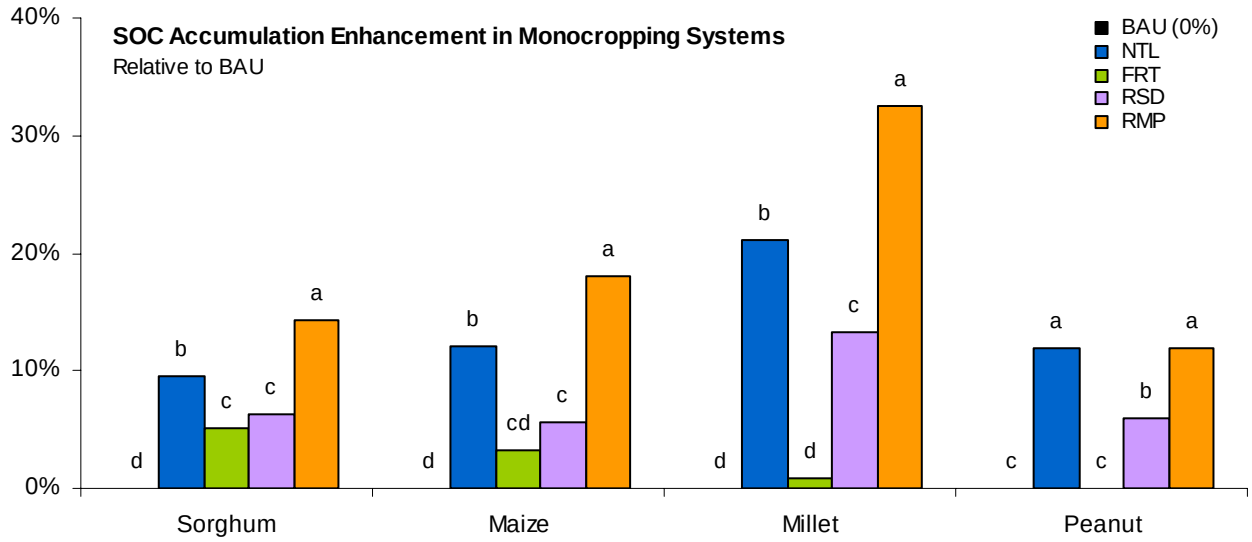

Figure 3-11 Average soil organic carbon accumulation enhancements under the simulated management scenarios for the continuous monocropping system of each crop for 20 years, relative to BAU. Different letters represent significant differences in mean values (α=0.05).

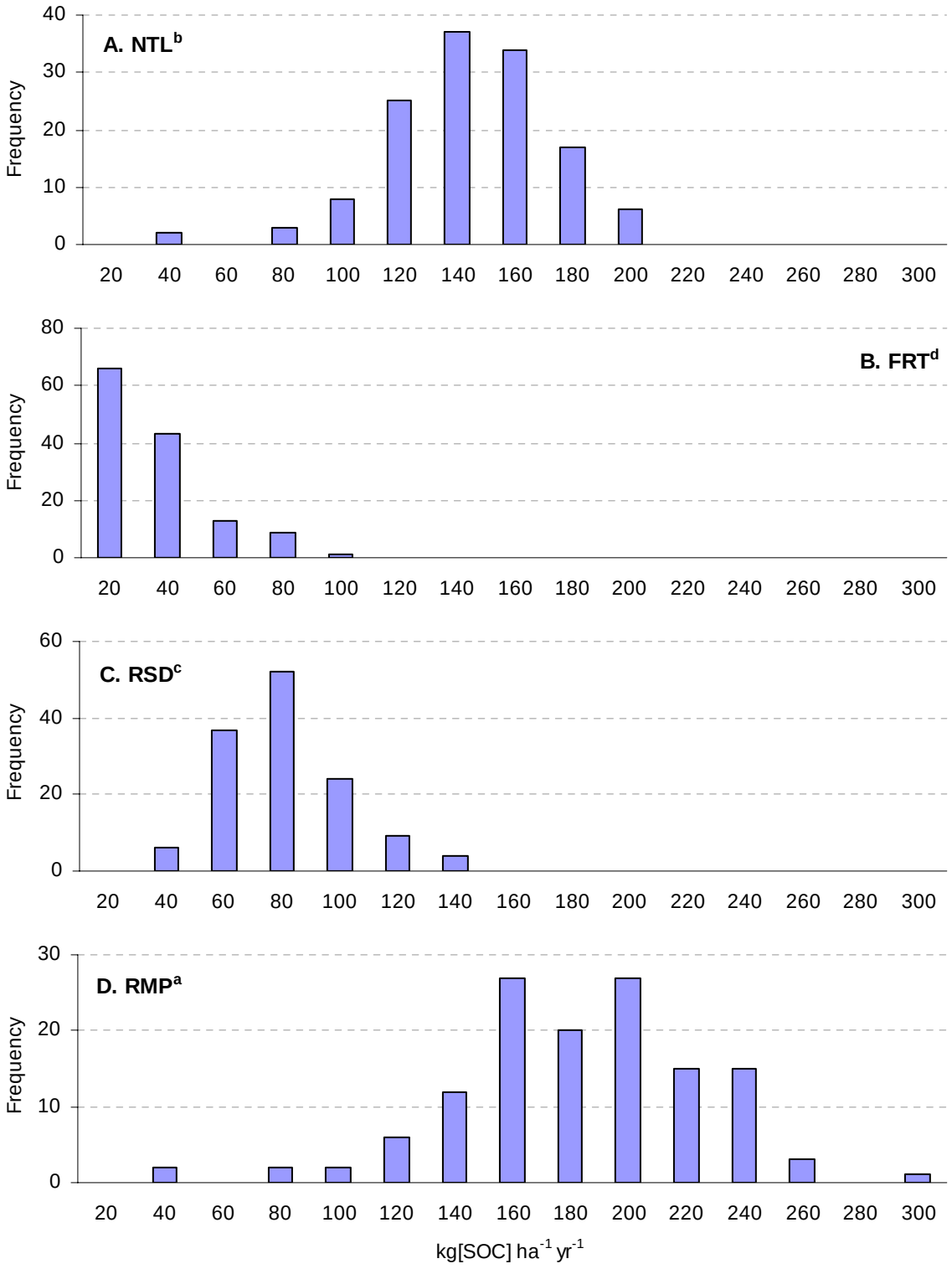

Figure 3-12 Histogram of the simulated soil carbon sequestration rate in 132 farmers' fields in Wa, Ghana, for each management scenario relative to BAU. Different superscript letters represent significant differences in their mean values ($\alpha = 0.05$).

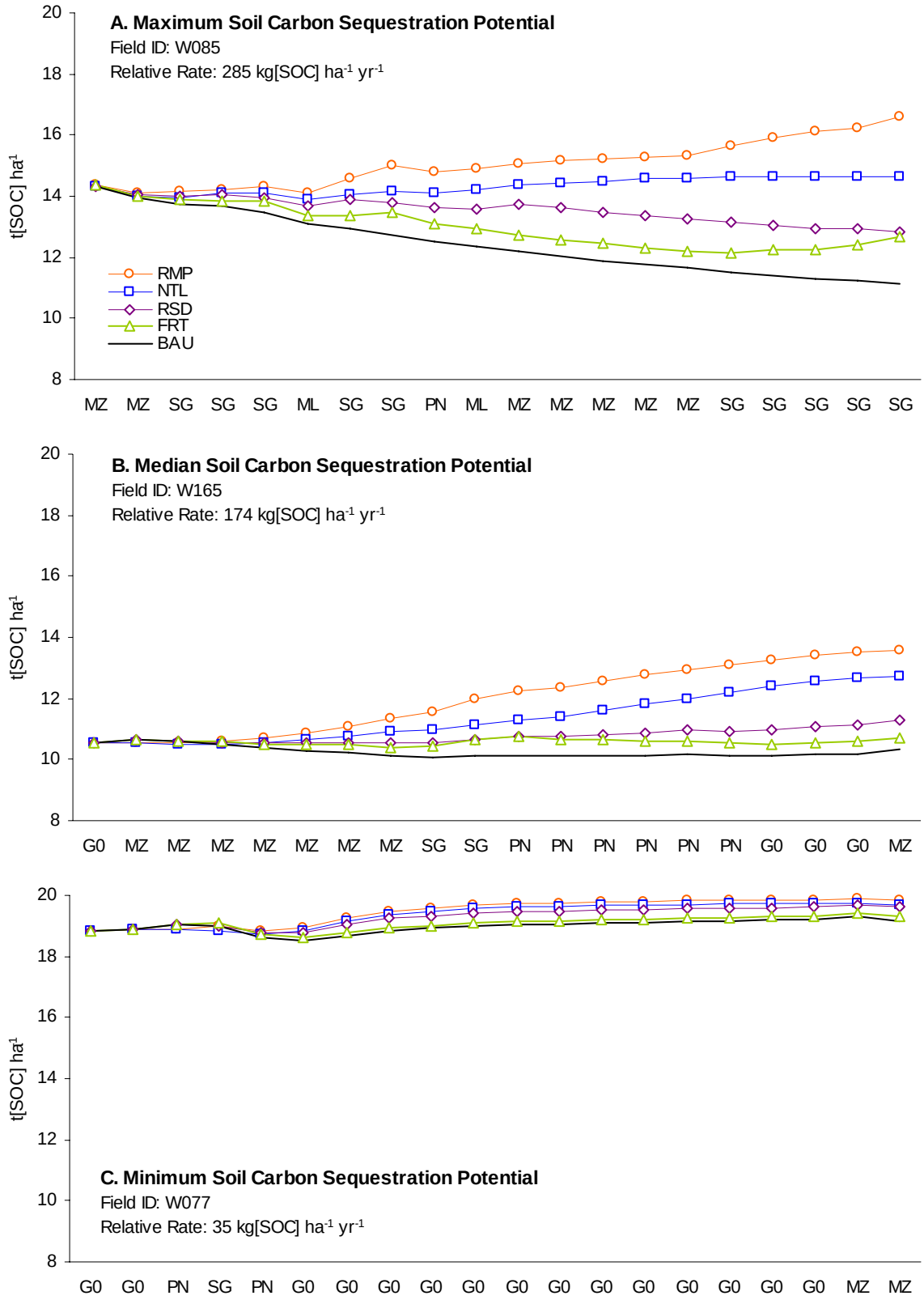

Figure 3-13 Simulated soil carbon accumulation in three representative fields with the maximum, median, and minimum soil carbon sequestration rate relative to BAU.

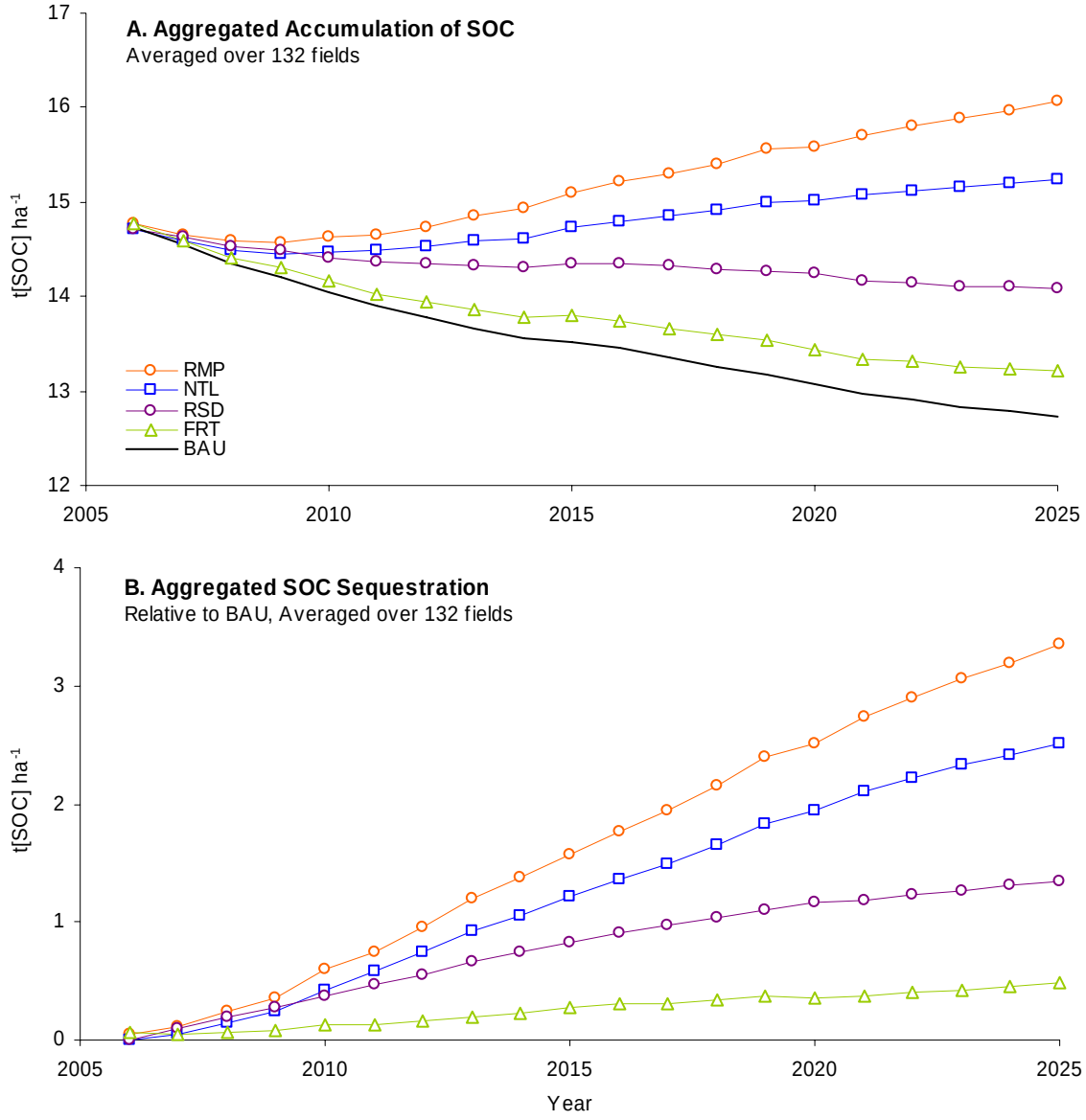

Figure 3-14 Simulated A) soil carbon accumulation and B) sequestration relative to BAU, aggregated over 132 farmers' fields in the study area in Wa, Ghana, for 20 years.

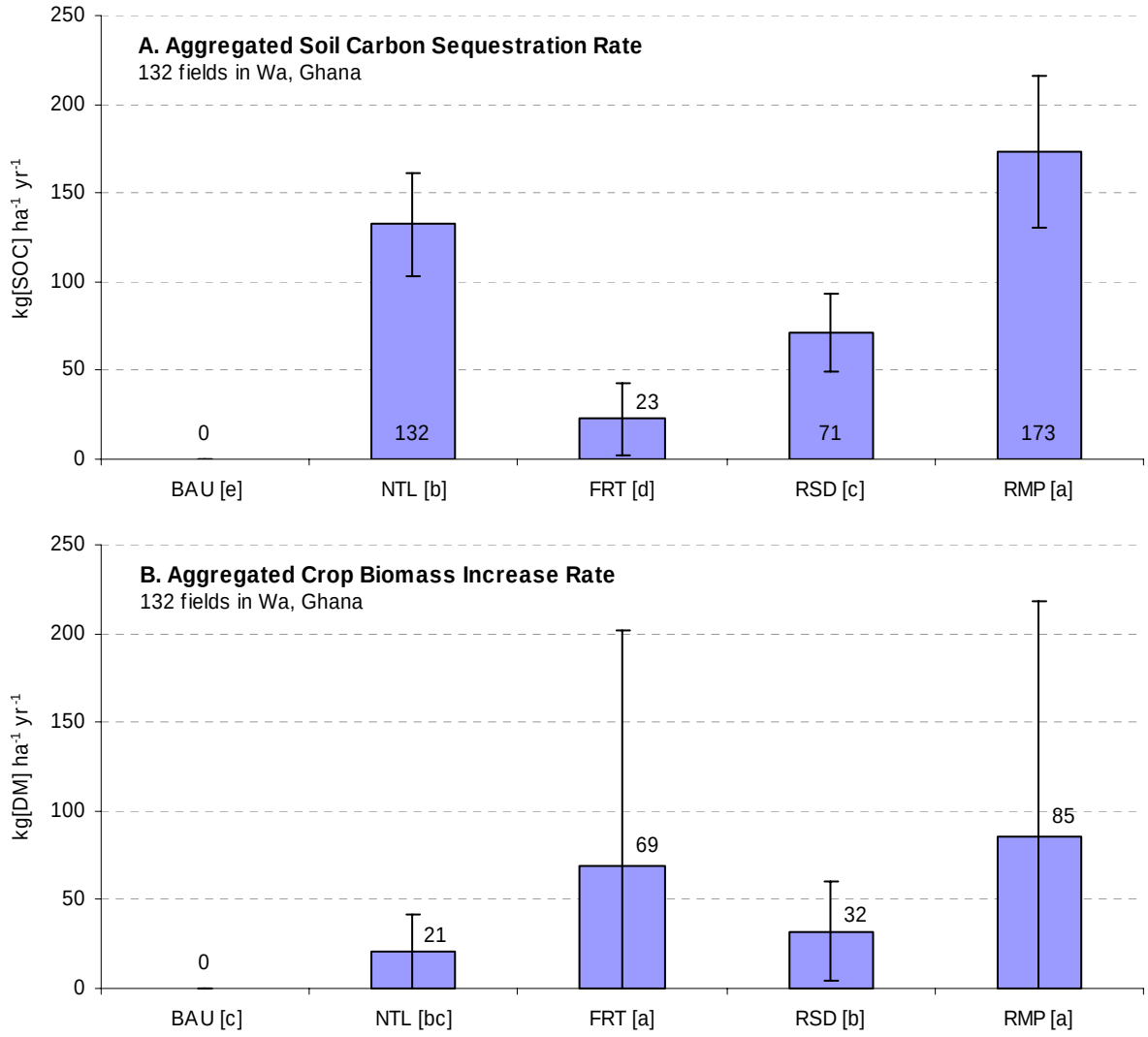

Figure 3-15 Mean and standard deviation of the aggregated soil carbon sequestration rates and the crop biomass increase rates under different management scenarios relative to BAU.

CHAPTER 4
ESTIMATING SOIL CARBON IN AGRICULTURAL SYSTEMS USING ENSEMBLE KALMAN FILTER AND DSSAT-CENTURY

Introduction

Conventional approaches to manage carbon dioxide (CO_2) in the atmosphere include 1) increasing energy efficiency to reduce the need for fossil fuel combustion and 2) increasing use of low-carbon or carbon-free sources of energy, such as nuclear power. While many worldwide efforts are being made to manage CO_2 with these approaches, a third approach, carbon sequestration, has been suggested as a truly radical method considering the development of the energy technology (Reichle et al., 1999). Among various ways to sequester carbon from the atmosphere, soil carbon sequestration is recognized as an option that could also lead to positive benefits to agricultural production in developing countries, by increasing soil organic matter that will help reduce soil degradation, raise agricultural productivity, alleviate poverty, and combat desertification (Antle and Uehara, 2002). To accept this option as a mechanism for reducing atmospheric CO_2 levels, a reliable soil carbon accounting system that can monitor soil carbon changes needs to be developed (Antle and Uehara, 2002). However, the standard errors of soil carbon measurement may be several times higher than the change in soil carbon over one to several years (Jones et al., 2004), making it difficult to accurately quantify changes in soil carbon over time.

Measuring physical entities is an essential procedure for understanding a system. In studies aimed at modeling a system, for example, measurements provide data for the development, verification, and validation of a model. However, one must consider associated uncertainties to properly interpret and use measurements in the quantification process. Maybeck (1979) stated that "any measurement will be corrupted to some degree by noise, biases, and device inaccuracies." Such corruptions in measurements may be significant especially when several

entities must be measured to estimate a desired variable. For example, one may attempt to quantify the amount of soil organic carbon (SOC) in a unit land area with a commonly-used Walkley-Black method (Walkley and Black, 1934) for measuring carbon content in soil samples. The Walkley-Black method estimates carbon content in a soil sample using chromic acid by measuring the amount of oxidizable organic carbon. Other soil measurements (e.g., the soil bulk density, soil sampling depth, and field area) are needed to estimate the mass of soil organic carbon. Thus, the desired output (i.e., the mass of SOC) is a computed value based on relationships among various measurements, each of which has its own uncertainty.

The use of biophysical models can also help estimate SOC and its changes under different weather, soil, and management practices (Jones et al., 2002; Parton et al., 1988; Parton and Rasmussen, 1994). Gijsman et al. (2002) modified the DSSAT (Decision Support System for Agrotechnology Transfer) cropping system model (Jones et al., 2003) by incorporating a soil organic matter-residue module from the CENTURY model (Parton et al., 1988; Parton and Rasmussen, 1994). The combined model, DSSAT-CENTURY, was designed to be more suifor simulating low-input cropping systems and conducting long-term sustainability analyses (Gijsman et al., 2002).

With a mathematical model capable of simulating the states of a system including SOC, one can use a data assimilation method to get the best estimate of SOC. A data assimilation method combines measurements of the current state of a system with predictions made by a mathematical model to produce an estimate of the current state of the system (Daley, 1991). When the system states propagate in time, one may use a sequential data assimilation method, a so-called filter (Maybeck, 1979). The filter is a temporal extension of the data assimilation

method that propagates the assimilation process in time, and estimates of system states are updated whenever new measurements become available (Bertino et al., 2003; Evensen, 1994).

A Kalman filter (Kalman, 1960) is the most commonly used sequential data assimilation algorithm for linear dynamic systems. The Kalman filter combines all of the available measurements, model state estimations, and prior knowledge about the system to optimally estimate the state of the system with statistically minimized errors (Gelb, 1974; Maybeck, 1979; Welch and Bishop, 2003). In principle, a Kalman filter has two sets of mathematical equations - predictors and correctors (Welch and Bishop, 2003). The predictors use a model to predict the state of a system, and then the correctors use a measurement to optimally update the prediction with minimum variance. An optimally estimated covariance matrix is used to use measured information from data-rich areas (i.e., states with less uncertainty) to data-poor areas (i.e. states with high uncertainty) (Keppenne, 2000). For nonlinear systems, two extensions of the Kalman filter, the extended Kalman filter (EKF) (Gelb, 1974) and the ensemble Kalman filter (EnKF) (Evensen, 1994), have been commonly used. See Reichle et al. (2002) for a detailed discussion on comparisons between EKF and EnKF. The EnKF uses a Monte Carlo simulation technique to approximate the probability distribution of system states. Especially for applications with complex and non-linear models, the EnKF is preferred because of its capability to accommodate a wide range of models, account for input and measurement uncertainties, and provide information on the accuracy of estimates (Margulis et al., 2002).

Estimating values of model parameters is a critical step in adapting a model for a new environment. However, the model parameter estimation process is not straightforward in some cases. Depending on the number of parameters in the model, adjusting all model parameters using measured data may not be practical or even numerically possible (Wallach et al., 2001).

However, because model parameters are uncertain, model estimates (e.g., SOC dynamics) are inevitably uncertain and potentially divergent from the true state values, especially over a long term. Although the primary purpose of using a data assimilation method is to achieve the best estimates of system states, the EnKF has also been used for model parameter estimation when parameters were considered as time-invariant model states (e.g.,Anderson, 2001; Annan et al., 2005; Jones et al., 2004; Moradkhani et al., 2005). Using cross-correlations between states and parameters, the EnKF can update unmeasured state variables and parameters. Eknes and Evensen (2002) used the EnKF in a marine ecosystem model, and noted that it was capable of updating state variables of the whole model, even when measurement of only one state variable was assimilated, through the information on cross-correlations between different model state variables.

Maybeck (1979) described a Kalman filter as an "optimal" recursive data processing algorithm with minimized errors. However, in practice, it is difficult to attain optimality in real problems with complex models, because all of the model error sources (e.g., uncertain states, parameters, input data, and model structure), and their statistical characteristics need to be included in the filtering process (Gelb, 1974). Therefore, it is often useful to design a "suboptimal" filter that simplifies or approximates the optimal filter by updating only selected states and/or model parameters (Gelb, 1974). Choosing the most effective and efficient EnKF states and model parameters to design the suboptimal filter is an important preliminary task, but may not be straightforward in some cases and may produce biases in estimates if unselected model states and parameters are incorrect for a site.

To test the estimation accuracy of a filter, an identical twin test is commonly used (e.g., Eknes and Evensen, 2002; Annan et al., 2005). The identical twin test preliminarily uses the

model itself to generate a synthetic 'true' dataset, which is subsequently used to generate synthetic measurements to be assimilated (Annan et al., 2005). Hargreaves et al. (2004) classified the identical twin test as a weak test. However, Eknes and Evensen (2002) stated that the motivation of using the identical twin test is that there are cases where real datasets are not available and tests are needed to confirm the reliable operation of a method. They also pointed out that if a method does not work well with a synthetic dataset, it would not work with a real dataset.

Implementations of the EnKF with simple crop models have been reported in previous studies. Makowski et al. (2003) presented a case study using a simple nonlinear winter-wheat crop model, AZODYN (Jeffroy and Recous, 1999), to assimilate measurements and improve the accuracy of model predictions. Five state variables in the model (i.e., nitrogen uptake, dry matter production, nitrogen-nutrition index, leaf area index, and soil mineral nitrogen supply) were updated with a chlorophyll-content measurement. Jones et al. (2004) used a simple non-linear soil carbon model to estimate SOC and optimize the value of an uncertain soil carbon decomposition rate parameter. However, given the simplicity of their model (e.g., one SOM pool) and its assumptions (e.g., a constant value for the yearly crop biomass residue), that approach did not consider year to year variability and thus may not be generalized. Although the EnKF is flexible regardless of the complexity of a model (Margulis et al., 2002), no study has been conducted yet on the EnKF implementation with a *complex* crop model. Compared to simple models, complex models can help in understanding the dynamics of components in a simulated cropping system as a whole, not only a specific component of interest. In addition if model parameters are cross-correlated with updated systems states, the EnKF can be also used as a model parameter optimizer, conditioned on measurements of correlated system states.

The question that this study addresses is whether an EnKF method used with a complex crop-soil model can provide more reliable estimates of SOC than measurements over time. It is hypothesized that the uncertainty of SOC measurement can be reduced by combining complex biophysical model simulations and measurements using the EnKF method. The steps in testing this hypothesis were (1) to develop an EnKF framework for estimating SOC by using a combination of the DSSAT-CENTURY model simulations and measurements and (2) to evaluate the estimation accuracy of the framework for estimating the SOC dynamics in time based on an identical twin test.

Materials and Methods

Study Site and Cropping System

Our study site is an on-farm experimental plot of 0.2 ha located south of Wa in the Upper West Region of Ghana. The site has a savannah climate with hot and dry weather with one rainy season, generally from April to October (Figure 4-1). Most agricultural cropping practices take place during the rainy season. Cropping fields are generally left with bare fallow during the dry season.

A continuous low-input maize cropping system in Ghana was simulated as a base case scenario for the study site (i.e., maize in rainy seasons and bare fallow in dry seasons). During each rainy season, it was assumed that rainfall contributed 5 kg[N] ha^{-1} to the maize crop, based on the minimum nitrogen in precipitation from the typical range (5 to 8 kg[N] ha^{-1}) for non-industrial temperate regions (Brady and Weil, 2002). Considering the limited resources in the area, a low level of N-based fertilizer applications (20 kg[N] ha^{-1}, split applied at 20 and 40 days after planting) was simulated for a carbon-sequestering practice. After harvesting maize, aboveground crop residues were cut and left on the ground to be naturally decomposed and incorporated into the soil over time. It was assumed that 20% of the residues were consumed by

grazing livestock, which in turn contributed livestock manure of 600 kg ha^{-1} to the soil at the same time.

Detailed soil characteristics of the site were measured to 1 m in depth by J. B. Naab (Savannah Agricultural Research Institute, personal communication, December 2005). For the 0-20 cm depth, the soil order was classified as Alfisols, and its pH was measured as 6.20. The soil water lower limit, drained upper limit, and saturated upper limit were measured as 0.05, 0.17, and 0.32, respectively. The texture was sandy with more than 87% of sand-sized particles, and the soil bulk density was measured as 1.63 g cm^{-3}. The total soil nitrogen content was 0.05%, and the available soil P and K were 23.89 and 23.92 mg kg^{-1}, respectively.

One of the most important parameters in the DSSAT-CENTURY model for simulating SOC dynamics is the initial fraction of the soil organic matters (SOM) in three different pools (i.e., microbial (SOM1), intermediate (SOM2), and passive (SOM3)) of each soil layer (Gijsman et al., 2002). The SOM pool fractions can be estimated by using the radiocarbon dating and acid hydrolysis methods (Falloon and Smith, 2000), but these data were not available in this study. In general, long-term land-use history directly influences the SOM pool fractions (Brady and Weil, 2002). Detailed cropping history of the study site is not known, but a survey with local farmers (J. Koo, Graduate student, University of Florida, unpublished data) showed that the area has been continuously cultivated for a long time so that it is reasonable to assume the passive SOM pool dominates. V. K. Walen (Graduate student, University of Florida, personal communication, March 2006) studied the dynamics of SOM pool fractions at the study site, and proposed generic SOM pool fractions for the continuous cropping system (i.e., moderately depleted SOM) for soil layers up to 1 m depth. When averaged up to 20 cm depth, the fractions of the three pools were SOM1:SOM2:SOM3 = 0.01:0.12:0.87.

Daily weather data were stochastically generated using DSSAT and monthly climate parameters estimated from measured weather data at Wa from 1996 until 2004. The same sequence of generated weather data was used for all replicates of the ensemble in the Monte Carlo simulations.

Designing the Ensemble Kalman Filter Framework

The DSSAT Cropping Systems Model operates on a daily time step and predicts crop growth, development and yield under different management practices. It also predicts dynamic changes in soil water, carbon, and nitrogen that take place in the cropping system (Jones et al., 2003). Given the complexity of this model, we designed a suboptimal EnKF framework with two system state variables, the amount of SOC in top 20 cm of soil layers (SOC, hereafter) and the crop aboveground vegetative biomass at harvest (crop biomass), and one model parameter, the relative soil organic matter mineralization rate parameter *SLNF*. The reason for choosing the crop biomass and the mineralization rate parameter as the EnKF state variables was that they contribute most directly to the changes in SOC over time and are correlated with each other.

The crop biomass was included in the EnKF design so that SOC can be updated at each time step (even if the crop biomass is measured but SOC is not) through the cross-correlation between SOC and crop biomass. Note that taking measurements of the crop biomass is relatively easier and more practical than measuring SOC.

In the DSSAT-CENTURY model, the *SLNF* parameter serves as a multiplication factor, ranging from 0 to 1, to adjust the mineralization process of organic matter in all soil layers in the DSSAT-CENTURY model (Tsuji et al., 1994). The *SLNF* impacts the overall dynamics of soil organic matter between different SOM pools, and its value is time-invariant and specific to a study site. For example, if there are two fields under the identical environmental conditions with different *SLNF* values, the decomposition process of SOM in a field with *SLNF = 0.5* is 50%

slower than the other field with *SLNF = 1.0*, thus relatively conserving more SOM over time. In general, state variables describing crop growth (e.g., crop biomass) are sensitive to the value of *SLNF*, especially under low-input agricultural systems where the mineralization of soil organic matter plays an important role in short-term nutrient cycling (Brady and Weil, 2002). Although accurate prediction of SOC in a specific field over time requires a reliable estimate of *SLNF*, its value cannot be measured and may vary considerably over space due to a number of factors that are not accounted for in the DSSAT-CENTURY model or are not understood at all.

To implement the EnKF, the DSSAT-CENTURY model was modified so that the whole model behaves as a nonlinear function, which is called from a driver program that controls three components of the EnKF: data, model, and data assimilation (Figure 4-2). The design of the sequential data assimilation process can be briefly summarized as follows. For the initial year, the driver 1) generates an initial ensemble of replicates, 2) runs the DSSAT-CENTURY model for all replicates for one year, 3) collects forecasted states, 4) updates states for each replicate by assimilating available measurements, and 5) computes the best estimate of states (i.e., the ensemble mean). In following years, the driver uses updated states from a previous year for each ensemble replicate in step 1).

Implementing an Ensemble Kalman Filter

Treating the SOM mineralization parameter *SLNF* as a time-invariant state variable, we can construct a state vector that includes two dynamic system states, SOC (C) and the crop biomass (B), as well as the constant, but uncertain, *SLNF* (S). With x_t as the state vector with elements representing the EnKF state variables at year *t* (i.e., $x_t = \begin{bmatrix} C_t & B_t & S \end{bmatrix}^T$), a discrete time-step stochastic system with a complex nonlinear model can be written as:

$$x_{t+1} = M\left(x_t, u_t, S, \theta\right) + \omega_t \,,\ \omega_t \sim N\left(0, Q_t\right) \qquad (4\text{-}1)$$

where x_{t+1} is a state vector of the system at *t+1*, $M(\cdot)$ is an underlying model (i.e., the DSSAT-CENTURY model in this study), and ω_t is the model uncertainty at *t*. The model $M(\cdot)$, which propagates system states in time, is a function of x_t (state vector at *t*), u_t (deterministic input dataset at *t*), S, and θ (time-invariant, deterministic model parameters). The model error vector ω_t is represented as a stochastic term following a zero-mean Gaussian distribution with the model error covariance Q_t taking into account un-modeled uncertainties associated with structural model error. The assumption of Gaussian model error distribution implies unbiased error structures and may not reflect the real-world in some cases. If the model errors are biased, the EnKF estimate may diverge from truth, providing inaccurate estimates of states and their uncertainties. However, we limit the scope of this study to the ideal unbiased system.

We assume the model error for the state variables of C and B is uncorrelated in time, with the variances change over time depending on the magnitude of the respective state variable (i.e., heteroscedastic white noise), whereas the model error for S is a random variable that does not change over time. Note that the model error in this study is not same as the root mean square error (RMSE) between truth and predicted states at a given time. Rather, the model error represents the process noise (Welch and Bishop, 2003) that accounts for the uncertainties associated with the model predictions in *one time step*.

A truth vector of the EnKF states, $x_t^{true} = \left[C_t^{true} \quad B_t^{true} \quad S^{true}\right]^T$, was generated using Equation 4-1 using the DSSAT-CENTURY model with a randomly chosen set of initial conditions and parameters and a randomly chosen sequence of model error ω. By randomly adding the SOC and crop biomass measurement errors to truth, a set of measurements, $y_t = \left[C_t^{obs} \quad B_t^{obs}\right]^T$, was generated and represented as:

$$y_t = H \cdot x_t^{true} + \nu_t,\ \nu_t \sim N(0, R_t) \quad (4\text{-}2)$$

where H is an operator that correlates the EnKF states to the measurement (i.e., $H = \begin{bmatrix} 1 & 0 & 0 \\ 0 & 1 & 0 \end{bmatrix}$) and ν_t is a vector of measurement errors at *t* with the zero-mean Gaussian distribution with the measurement error covariance R_t (the measurement error covariance matrix at *t*) given as:

$$R_t = \begin{bmatrix} \mathrm{Var}(C_t^{obs}) & 0 \\ 0 & \mathrm{Var}(B_t^{obs}) \end{bmatrix} \quad (4\text{-}3)$$

assuming no covariance between SOC and crop biomass measurement errors. The R_t is assumed to be independent from the model error covariance Q_t.

Based on the predetermined statistics of model and measurement covariances, an ensemble of initial states x_0^j ($j = 1, \cdots, N$ where *N* is the ensemble size) at *t=0* is randomly generated. At *t>0*, an ensemble of the state vector with size *N* is forecast by the model and propagates in time as:

$$x_t^{j-} = M(x_{t-1}^{j+}, u_t, S_{t-1}^{j+}, \theta) + \omega_t^j,\ j = 1, \cdots, N \quad (4\text{-}4)$$

where x_t^{j-} is the *j*th replicate of the model-forecasted state vector at *t*, x_{t-1}^{j+} is the *j*th replicate of the filter-updated state vector at *t-1*, S_{t-1}^{j+} is the *j*th replicate of the filter-updated parameter S at *t-1*, and ω_t^j is the *j*th replicate of the model error at *t*. Note that the estimation error of S at t>0 is zero, as this parameter is defined as time-invariant. The minus (-) and plus (+) signs denote the model-predicted and filter-updated states, respectively, hereafter.

If we know the true state x_t^{true}, the prior and posterior error covariances, P_t^- and P_t^+ can be calculated as:

$$P_t^- = \overline{\left(x_t^- - x_t^{true}\right)\left(x_t^- - x_t^{true}\right)^T} \quad (4\text{-}5)$$

$$P_t^+ = \overline{\left(x_t^+ - x_t^{true}\right)\left(x_t^+ - x_t^{true}\right)^T} \quad (4\text{-}6)$$

where the overbar denotes the expected values or averages over the ensemble. However, as we do not know x_t^{true} in a real-world application, we approximate the error covariances as (Evensen, 1994; Bergers et al., 1998):

$$P_t^- \cong \overline{\left(x_t^- - \overline{x_t^-}\right)\left(x_t^- - \overline{x_t^-}\right)^T} \quad (4\text{-}7)$$

$$P_t^+ \cong \overline{\left(x_t^+ - \overline{x_t^+}\right)\left(x_t^+ - \overline{x_t^+}\right)^T} \quad (4\text{-}8)$$

The updated ensemble mean $\overline{x_t^+}$ is considered as the best estimate, and the posterior error covariance P_t^+ is interpreted as the error covariance of the best estimate (Evensen, 1994; Burgers et al., 1998).

For each replicate, the measurement vector is generated by stochastically adding a measurement error term (Burgers et al., 1998) as:

$$y_t^j = y_t + \nu_t^j \quad (4\text{-}9)$$

where y_t^j is the *j*th replicate of the measurement vector. Burgers et al. (1998) reported that the variance of an updated ensemble gets too small without treating the measurements as random variables by adding the random perturbations.

Each replicate of the predicted state vector is updated as:

$$x_t^{j+} = x_t^{j-} + K_t\left(y_t^j - x_t^{j-}\right) \quad (4\text{-}10)$$

where K_t is the Kalman gain matrix (with 3 rows and 2 columns) for the EnKF states, which is given by:

$$K_t = P_t^- H^T \left(H P_t^- H^T + R_t \right)^{-1} \quad (4\text{-}11)$$

The updated EnKF states are used as initial conditions for the subsequent year's simulation for the same replicate. At any time step, an ensemble of the updated replicates can be used to estimate the statistics of states, such as mean, variance, and covariance. The definitions, dimensions, and units of the variables described above are summarized in 4-1.

Evaluation of the EnKF Estimation Accuracy

When an EnKF performs properly, the ensemble of replicates should belong to a probability distribution within which truth is a member (Lawson and Hansen, 2004). Assuming truth is known, as in the identical twin test, the RMSE between truth and the best estimate, has been commonly used to assess the accuracy of the EnKF estimates. However, in a real-world application without knowing the truth, the evolution of the posterior ensemble standard deviation can be used as a measure of the EnKF estimation accuracy. The posterior ensemble standard deviation defines the distribution of all replicates around the posterior ensemble mean. As the posterior standard deviation decreases, the posterior ensemble mean should approach the truth.

There may be differences between the ensemble standard deviation and the RMSE between predictions and the truth (Barker, 1991) due to errors and approximation in the EnKF. Too narrow spread in an ensemble (i.e., too small covariances in P_{t+1}^-) may result in giving less weight to new measurements when they become available, and that may lead to increased estimation error and reduced ensemble covariance with a false confidence in time (Anderson, 2001; Hargreaves and Annan, 2002). Therefore, the evolution of RMSE and the ensemble standard deviation for the base-case scenario (Tables 4-3 and 4-4) were compared to evaluate whether the EnKF was performing as expected.

Initial Ensemble

When an ensemble of initial replicates is randomly generated with a Gaussian distribution, a cross-correlation structure can be applied to generate more probable states of the ensemble. In a preliminary study, it was hypothesized that a model spin-up simulation could show the model-inherent cross-correlations between the EnKF state variables. The stronger cross-correlation was expected to help converging estimates to truth the faster, especially for the non-measured parameter *SLNF*. However, the results showed that the cross-correlations were not generic but varied over time responding to the particular environments and farm management scenarios being simulated (i.e., heteroscedastic). For example, the correlation coefficient between SOC and *SLNF* ($r_{C,S}$) was sensitive to the amount of decomposable SOM exist in soil, and the correlation coefficient between crop biomass and *SLNF* ($r_{B,S}$) was sensitive to the organic and inorganic fertilizer input to the cropping system. Thus, it was recognized that defining a prior cross-correlation is not practically possible, and no initial cross-correlation was given in this study.

The initial ensemble replicates of SOC were generated from $N\left(C_1^{obs}, \mathrm{Var}\left(C_1^{obs}\right)\right)$ using the initial measurement as an ensemble mean. The initial ensemble of crop biomass was not randomly generated, but forecast by running simulations from the ensemble of initial replicates. However, aboveground crop residues left from the previous cropping season was randomly generated with $N\left(gB_1^{obs}, \mathrm{Var}\left(gB_1^{obs}\right)\right)$, where g is a constant parameter that represents the proportion of crop biomass production left on the ground for the following cropping season. The true value for the initial crop residue was assumed as gB_1^{obs}. As specified in the base-case scenario, we arbitrarily set the value of g as 0.8, assuming 80% of crop residues are left on the ground as a part of the carbon-sequestering practice.

The true value of the parameter *SLNF* was arbitrarily set as 0.85. There is no available dataset to justify the choice of this value, but it was assumed that the truth is likely to be in the higher range between its 0 to 1 scale, as the study site is located in the savannah climate with higher temperature that generally fosters soil mineralization. However, the initial ensemble of *SLNF* was randomly generated from $N(0.75,0.04)$. The difference (0.10) between the true value and the ensemble mean was the half of the initial ensemble standard deviation. This value was set to reflect our lack of knowledge of *SLNF* for the field under study.

Values of the ensemble mean and variance of the initial SOC, crop residue, and *SLNF* are summarized in 4-2.

Ensemble Size

The EnKF is based on a Monte Carlo approach, which approximates the probability density of the true states using a finite number (*N*) of randomly generated states. Thus, the estimation accuracy of EnKF highly depends on the ensemble size *N*. In general, a larger ensemble should provide better estimates of the system states. However, choosing a sufficiently large value of *N* may be cost-prohibitive when an underlying model in the EnKF is expensive to simulate. The cost of using the complex DSSAT-CENTURY crop model as the underlying model was expensive. Using a computer system decently equipped with dual AMD Athlon^{tm} 64 processors at 2.2 GHz, 2.00 GB of ram, and dual hard drives configured as RAID Level 0, each model run took about 0.25 second, whereas it took only 3.75e-6 second for a simple SOC model used by Jones et al. (2004). Thus, the overall computational cost for the data assimilation process was significant. In addition in all Monte Carlo methods, statistical errors in the ensemble estimates of the first- and second-moments decreases very slowly as *N* increases (Heemink et al., 2001).

A preliminary sensitivity analysis was used to show the impact of *N* to the EnKF estimation accuracy (i.e., the evolution of ensemble standard deviation). Makowski et al. (2006) proposed to use a relative error (i.e., the ensemble standard deviation between truth and the EnKF estimates of system states) to determine the appropriate value of *N*, beyond which gives no further accuracy improvement. When the time-averaged ensemble standard deviation was computed using a base-case scenario (Tables 4-3 and 4-4) for 20 years with *N*=100, ..., 1000, it was shown that the ensemble standard deviation for all three EnKF states was stabilized beyond 200 runs. Therefore, *N*=200 was chosen in this study.

Filter Parameters

To implement the EnKF framework, several filter parameters were estimated, including the measurement and model error variances. The theory of the Kalman filter requires prior knowledge or assumptions of the first- and second-order moments of the measurement and model errors (Welch and Bishop, 2003). The base-case filter parameter values are presented in 4-4.

Error of SOC measurement

The measurement error variance, ν_t in Equation 4-2, can be estimated by conducting an off-line sampling and analysis in advance to determine the variance of the measurement noise (Welch and Bishop, 2003). We assume that there are two independent sources of the SOC measurement error; sampling and lab-analysis. The sampling error is caused by factors related with in-situ soil sampling (e.g., using a limited number of point samples to estimate the actual average of the spatially heterogeneous SOC at the study site), while the lab analysis error is caused by variability in laboratory measurements of subsamples from the same sample. The SOC

sampling and lab-analysis variances can be estimated from in-situ measurements as described below.

- **SOC Sampling Error**: The area of the study site is 0.2 ha, and an intensive point soil sampling survey was conducted in 2003 by the Savannah Agricultural Research Institute (J. B. Naab, Savannah Agricultural Research Institute, personal communication, January 2004). The SOC content in soil samples was measured by the Walkley-Black method (1934). Mean SOC content in the top 20 cm was 0.43% with a standard deviation of 0.11% (26% CV), and this amounts to a mean of 14 ton[C]/ha based on a soil bulk density of 1.63 g/cm^3 (J. B. Naab, Savannah Agricultural Research Institute, personal communication, December 2005). This result implies that, if one point sample is taken in the site, the SOC sampling error from the spatial variability would be approximately 26% of the measured value. However, if one takes a composite sample of *n* spatially independent subsamples, the sampling error can be theoretically reduced by $1/\sqrt{n}$. For example, the sampling error can be reduced to 12% if a composite sampling method is used with five subsamples. Composite sampling is usually used to collect soil from the field for nutrient and chemical analyses.

- **SOC Lab-analysis Error**: In a separate study, J. B. Naab (Savannah Agricultural Research Institute, personal communication, August 2006) used the Walkley-Black method to determine the SOC content in 160 soil samples taken in the study area with three repetitions. The standard deviation of the analysis for each of the soil samples was averaged as 0.04%, and the mean of all soil samples was 0.50%. The coefficient of variation of the lab-analysis was calculated as 8%, and it was within the range of CV values reported by W. M. Bostick (Graduate student, University of Florida, personal communication, June 2005) as 3-18% from a long-term SOC measurement dataset under various farm management systems in Burkina Faso.

  Since we assume the two error types are independent, their variances are additive as:

$$\mathrm{Var}\left(C_t^{obs}\right) = \mathrm{Var}\left(C_t^{sampling}\right) + \mathrm{Var}\left(C_t^{lab}\right) \tag{4-12}$$

where $\mathrm{Var}\left(C_t^{sampling}\right)$ is the SOC sampling variance and $\mathrm{Var}\left(C_t^{lab}\right)$ is the SOC lab-analysis variance. For the base-case scenario, we optimistically assumed that the SOC sampling error is negligible, and the SOC lab-analysis error is 8% based on the value reported by Naab. Different values of the SOC sampling errors assuming a composite sampling method with *N* subsamples were used for sensitivity analysis.

Error in predicted SOC values

In an EnKF framework, the SOC model error is stochastically added to the predicted SOC at each time step, accounting for uncertainty in the predicted state of SOC (Equation 4-4). Although the model error is an important filter parameter in the EnKF framework, it is relatively more difficult to specify in practice than a measurement error, since we can not directly observe the truth of states that are modeled (Welch and Bishop, 2003) or the required boundary conditions, initial conditions, and parameters. Jones et al. (2004) also stated there was little information available on which to base model errors for their EnKF application. In a real world, however, there is a physically probable range of annual SOC changes under a given cropping system. For example, Lal (2003) stated that the annual soil C sequestration rate ranges between 0.05 and 0.20 ton[C] ha^{-1} in tropics. In percent-basis, the range is converted to about 0.3% and 1.4% of an initially measured value. Jones et al. (2004) discussed the physical limits on how much SOC can be newly added or decomposed annually, and proposed the range as between -0.50 and 0.80 ton[C] ha^{-1}. Assuming the maximum error to be about 1/4 of the range, the standard deviation of the SOC model error was calculated as 0.16 ton[C] ha^{-1} (Jones et al., 2004), which was about 1% of a predicted value at t=0. Although this study uses a different underlying model, we assumed the proposed physical limits on annual SOC changes is still valid, and used 1% of predicted values as the base-case for the SOC model error. This value was also within the range of annual SOC changes reported by Lal (2003).

Error of crop biomass measurement

It was assumed that the crop biomass measurements were made from a high-resolution satellite-based remote sensing image that covers the study area. J. Koo (Graduate student, University of Florida, unpublished data) assessed a CV of about 30% of measurements based on

remote sensing. Considering the expansion of this framework to a regional scale in a future study, we used 30% of crop biomass measurements as the biomass measurement error.

Error in predicting crop biomass

Uncertainties associated with crop biomass prediction are caused by uncertain model input data, unknown model parameters, and the simplification of the model. Irmak et al. (2005) computed model prediction errors that ranged from 21 to 29% of mean yields using independent data for soybean, one of the crops in the DSSAT Cropping System Models (Jones et al., 2003). These values are much higher than the 4 to 6% error in predicting maize yields found by Braga and Jones (2004). However, in the Braga and Jones study, careful in-field measurements were made for all crop model inputs, demonstrating reliable model results but only when inputs are well quantified. Because we did not have long-term crop biomass measurement data to set realistic values of biomass prediction error, we used the prediction error reported by Irmak et al. (2005). The base-case value of the biomass prediction error was assumed to be 20% of predicted values.

Sensitivity Analysis

To understand the effects of uncertainties associated with the EnKF states on soil carbon estimates, a sensitivity analysis was performed. From a preset base-case cropping system described earlier with default filter parameter values presented in 4-3, the model and measurement variances were modified as summarized in 4-4. For each of the EnKF state variables, the accuracy of the EnKF estimates was measured by the ensemble standard deviation of the EnKF estimate of SOC.

- **SOC Measurement Error**: The upper and lower boundary values for the SOC measurement errors were based on the conditions where the sampling errors are the most optimistic (i.e., negligible as 0%) or realistic (i.e., 12% of measured values with 5 subsamples), and the lab-analysis errors are the reported minimum (i.e., 4% of measured values) or realistic (i.e., 8% of measured values). Using Equation 4-12, the SOC

measurement errors for the optimistic and realistic conditions were computed as 4% and 14% of measured values, respectively.

- **SOC Model Error**: An assumption of the upper boundary of the SOC model error was set equal to the base-case SOC lab-analysis error (i.e., 8% of predicted values). The lower boundary value was set as 0.3% of predicted values, which was the minimum value within the probable range of annual SOC change in tropics reported by Lal (2003).

- **Crop Biomass Measurement Error**: The upper and lower boundary values for the crop biomass measurement errors were based on the remote sensing-based crop biomass measurement study for three cereal crops by J. Koo (Graduate student, University of Florida, unpublished data). The base-case value (i.e., 30% of measured values) was adopted from the analysis of results for maize. For the upper and lower boundary values, the analysis of results from sorghum and millet, 66% and 18% of measured values, respectively, were used. Although this study focused on a maize-based cropping system, data from the two other cereal crops were used as boundary values, as the classification among different cereal crop species using remote sensing is not always straightforward.

- **Crop Biomass Model Error**: The upper and lower boundary values for the crop biomass model errors were adopted from other studies. For the upper boundary value, 30% of predicted values were used based on the upper range of RMSE of predictions (RMSEP), expressed as a percentage of average yields, reported by Irmak et al. (2005; their 5). For the lower boundary value, 10% of predicted values were used based on the average RMSEP of maize biomass reported by R. Braga (Associate professor, Polytechnical institute of Portalegre, personal communication, August 2006) for the Braga and Jones (2004) study. Since that study was based on detailed site-specific measurements that are not readily available in most studies, especially in on-farm applications, the RMSEP value of 10% was considered optimistic and thus used as the lower boundary of the model error.

- **Initial Estimates of *SLNF***: The initially estimated value of *SLNF* used to create an initial ensemble was set as 0.75 for the base-case. In the sensitivity analysis, the initial estimate of *SLNF* was set to 0.65 (i.e., one standard deviation below the true value) and 0.55 (i.e., one and a half standard deviation below the true value).

- ***SLNF* Uncertainty**: Unlike SOC and crop biomass, there were no data to justify the range of *SLNF* values used to test its sensitivity to the EnKF estimation accuracy. Therefore, it was arbitrarily set to the upper and lower boundaries of the *SLNF* uncertainty level, or 50% more and less than the base-case value.

- **SOC Measurement Frequency**: Given the expensive cost and difficulty involved in soil carbon measurements, the effects of varying the measurement frequency from 1 (annual measurements) to 1/3 and 1/5 years were analyzed. Crop biomass measurements were assumed available every year.

Results and Discussion

Base-Case

For the 20-year simulation time period, the generated true evolutions of SOC and crop biomass dynamically fluctuated reflecting stochastically generated daily weather data, and did not show particularly noticeable trends over time (Figures 4-3A and 4-4B). The true SOC was relatively stable throughout the 20 years of simulated time-period (CV = 2%), reflecting the biophysical limit of the probable SOC changes in a real cropping system. Generated measurements also did not show any trend nor notable biases over time, as the measurement error terms were defined as white-noise (Equation 4-2). In time, the ensemble reliably encompassed truth with smaller estimate variances than the spread based on measurements alone (Figures 4-3A and 4-3B). One standard deviation of the EnKF estimates of SOC and crop biomass encompassed truth in 75% and 85% of the time, respectively, while one standard deviation of estimates based on measurements alone encompassed truth in 70% and 80% of the time, respectively.

The EnKF estimation accuracy over time was measured by the posterior ensemble standard deviation and showed an improving trend for SOC, but not for the crop biomass (Figures 4-4A and 4-4B). Unlike SOC, the crop biomass production was more discontinuous over time due to yearly variable weather conditions. Thus, the crop biomass estimation accuracy was also discontinuous over time, as the crop biomass model error was defined as heteroscedastic (Figure 4-4B). However, the ensemble standard deviation of the EnKF estimates of SOC and crop biomass were consistently lower than measurements (Figures 4-4A and 4-4B).

The ensemble standard deviation for SOC was reduced over time toward an asymptote (Figure 4-4A). The ensemble standard deviation of SOC linearly decreased in initial years until t=6, then stabilized with a continuing slow rate of decrease. At t=20, the ensemble standard

deviation of SOC was 0.4 ton[C]/ha, which was reduced about 60% from the measurement standard deviation of 1.1 ton[C]/ha. When the evolution of the standard deviation reduction, which relatively compares the standard deviation of measurements and the EnKF estimates (Equation 4-13, where σ_{obs} is the measurement standard deviation and the σ_{EnKF} is the ensemble standard deviation), was plotted, a nonlinear improving trend of the EnKF estimation accuracy was also shown (R^2=0.72) (Figure 4-5).

$$\textit{Standard Deviation Reduction (\%)} = \frac{\sigma_{obs} - \sigma_{EnKF}}{\sigma_{obs}} \times 100 \qquad (4\text{-}13)$$

The EnKF estimate of the parameter *SLNF* trended toward the true value in time, but the rate of convergence was very slow (Figure 4-3C). The ensemble standard deviation of *SLNF* was not notably reduced over time either (i.e., 0.20 at *t*=1 and 0.17 at *t*=20) (Figure 4-3C). Although the estimates did not diverge, this slow convergence to truth with almost constant ensemble standard deviation was not expected. We hypothesized that the EnKF estimate of the parameter as well as the state variables would converge to truth. Since *SLNF* was not directly measured but updated using its cross-correlations with SOC and crop biomass, the evolution of the prior covariance matrix P_t^- for the base-case scenario was investigated for the cause of the unreliable estimates. When the model was spun-up (i.e., no updates) assuming no model errors (i.e., perfect model with $\mathrm{Var}\left(C_t^{\mathrm{model}}\right) = 0.0$ and $\mathrm{Var}\left(B_t^{\mathrm{model}}\right) = 0.0$), the time-averaged values of the correlation coefficients for 20 years between SOC and *SLNF* ($r_{C,S}$) and between crop biomass and *SLNF* ($r_{B,S}$) were -0.28 and 0.88, respectively. This result showed expected trends, as increased *SLNF* values should increase the SOM mineralization rate, and, in turn, decreases SOC and increases soil nutrients including nitrogen that benefits soil fertility and crop biomass production. However, when the model was spun-up with the base-case model errors (4-4), the time-averaged $r_{B,S}$ was

considerably degraded from 0.88 to 0.09, whereas $r_{C,S}$ was not notably impacted from -0.28 to -0.29. The cause of the degraded $r_{B,S}$ was the extent of the crop biomass prediction error, which was 20% of predicted values. When the crop biomass model error was added for each replicate (Equation 4-4), the inherent cross-correlation between crop biomass and *SLNF* was degraded due to the randomness of the error term. In contrast, the value of $r_{C,S}$ was not impacted as much, since the extent of the SOC model error was relatively small as 1% of predicted values.

When the sensitivity of three correlation coefficients (i.e., $r_{C,B}$, $r_{C,S}$, and $r_{B,S}$) under the spin-up simulation to the different magnitudes of model errors (e.g., 0%, 25%, 50%, 75%, and 100% of the base-case values) was plotted in time, the evolution of $r_{B,S}$ (Figure 4-6C) showed that even 25% of model errors (Δ) degraded the inherent cross-correlations (□) by more than 50% (Figure 4-6C). The same trend of the degraded cross-correlation was shown for the evolution of $r_{C,B}$ and $r_{C,S}$ as well, but their cross-correlations were relatively weak overall, even for the case without model errors (Figures 4-6A and 4-6B). The evolution of $r_{C,S}$ was relatively more stable to the different magnitudes of model errors than $r_{C,B}$ or $r_{B,S}$, because the extents of the SOC model error and the *SLNF* estimation error were smaller than that of the crop biomass model error. This overall result implies that the extent of model error significantly influences the cross-correlations among the EnKF states, thus impacts the EnKF estimation accuracy, especially for an unmeasured parameter that relies on its cross-correlations with other states to update in the filtering process.

The assumption of the positively agreeing trends between RMSE and the ensemble standard deviation was verified by plotting the evolution of RMSE and the ensemble standard deviation of SOC for the base-case scenario (Figure 4-7). Although the evolution of RMSE was

noisier (R^2 = 0.4) than the ensemble standard deviation (R^2 = 0.7) when fitted to logarithmic models, the two trends in measures of uncertainty in SOC estimates were nearly identical.

Sensitivity Analysis

Different values of the filter parameters defined in 4-4 showed different degrees of influences on the accuracy of the EnKF's SOC estimation. However, out of the seven analyzed filter parameters, the EnKF estimation accuracy was most sensitive to three parameters: the SOC model error, the SOC measurement error, and the SOC measurement frequency.

Effects of SOC model error

Increased SOC model error degraded the estimation accuracy of the EnKF by increasing the ensemble standard deviation of SOC (Figure 4-8A). However, even when the model error is at its assumed upper boundary (i.e., 8% of predicted values), the standard deviation of the EnKF estimates were still consistently lower than the measurement standard deviation over time. At t=20, increasing the SOC model error from 0.3% to 8.0% increased the ensemble standard deviation from 0.3 to 0.9 ton[C]/ha, and the measurement standard deviation was 1.1 ton[C]/ha. Considering the base-case value of the SOC measurement error (i.e., 8.0% of measured values), this result implied that the superior estimation accuracy of the EnKF method was not the result of the given small ratio of model and measurement errors. In addition, even if the model error exceeds the measurement error, the EnKF estimation accuracy is not expected to be worse than the measurement, as the filter adjusts weights between model-predicted states and measurement based on their variances (Equation 4-11). Jones et al. (2004) also reported that the EnKF estimates were better than measurements with less error even when the measurement error was less than the model error.

Effects of SOC measurement error

Higher SOC measurement errors degraded the estimation accuracy of the EnKF, but less so than SOC estimates based on measurements alone. At t=20, increasing the SOC measurement error from 4% to 14% increased the ensemble standard deviations from 0.3 to 0.6 t[C] ha^{-1} (Figure 4-8B). However, the largest relative change in the ensemble standard deviation was shown for the case with the highest measurement error. When the measurement error was 14%, the initial ensemble standard deviation was as high as 1.5 t[C] ha^{-1} at t=1, but reduced to 0.6 t[C] ha^{-1} at t=20 by 62%. In contrast, with a measurement error of 4%, the ensemble standard deviation was reduced by only 35% over time. Most of the standard deviation reductions occurred during first six years for all cases. This result implies that the balance between the model and measurement errors influence the EnKF estimation accuracy.

Although the ensemble standard deviations were sensitive to different values of SOC measurement errors over time (Figure 4-8B), it was shown that the EnKF estimates with different measurement errors were not (Figure 4-9). At t=20, the EnKF estimates from three cases were almost identical (CV = 0.3%). This same trend was reported by Jones et al. (2004) using a simple model.

Effects of SOC measurement frequency

When the ensemble standard deviations from three different SOC measurement frequencies are plotted, one can see that the uncertainty in the updated SOC estimates increased considerably during years when SOC measurements were not made, even though there were annual crop biomass measurements (Figure 4-10). This result occurs due to the propagation of prediction errors. Although the ensemble standard deviations with different measurement frequencies decreased over time when measurements are made and assimilated, the efficiency of measurements (i.e., extent of the reduced ensemble standard deviation with assimilating a

measurement) decreased over time as well. This result implies that when the resources to conduct *in situ* measurements is constrained, the most efficient measurement scheme may be to have annual measurements in initial years instead of distributing them evenly over time.

Insensitive model parameters

The EnKF estimation accuracy was not sensitive to the parameters for the crop biomass model and measurement errors and the uncertainty of *SLNF* (Figures 4-8C, 4-8D, 4-8E, and 4-8F). As stated above, the weak and degraded cross-correlations among the EnKF states resulted in this insensitivity between SOC and other EnKF states.

Conclusion

Following a previous study with a simple model by Jones et al. (2004), this paper presented the development of an EnKF method to improve SOC estimation accuracy using a complex biophysical cropping system model and measurements of SOC and crop biomass. This is the first study reporting the use of the DSSAT biophysical model with a Kalman filter-based data assimilation process.

Compared to simple models, complex models usually require extra model input data, which may introduce data-associated uncertainties with covariances that are difficult to define. The use of a simple model may produce acceptable results if enough uncertainty in the process is included in the model error covariance matrix, Q_t (Welch and Bishop, 2003). However, complex models provide more detailed estimates of the system than simple models, thus help in understanding the dynamics among different components in a cropping system. Along with the dynamics of SOC, the EnKF used in this study assimilated crop biomass data into the model taking into account other correlated components in the system, such as daily weather, soil nutrient and water dynamics, and specific farm management practices. However, depending on

the complexity of the underlying model, it may not be possible to include all of the dynamic model states as EnKF states that are updated with the filter. Thus, we selected two model states and one uncertain model parameter as the EnKF states in this study and designed a suboptimal filter framework.

Although it was seemingly rational to make specific choices of the EnKF states based on our general understanding of cropping systems, we experienced weak cross-correlations among the EnKF states in the simulated particular cropping system. In addition, there was the degradation of inherent cross-correlations due to the extent and randomness of the model errors, especially for the crop biomass. Unless an inherent cross-correlation between two states is relatively strong and their model errors are considerably small, the degradation of inherent cross-correlations will be difficult to avoid.

Consequences of the degraded cross-correlations were not trivial, including an unreliable estimation of the model parameter, *SLNF*. As a result, the overall EnKF framework behaved as if there were two independent and parallel data assimilation processes for each of the EnKF state variables. In addition, the uncertainty in the EnKF estimates rapidly increased without measurements, due to model predictions that included large uncertainties in *SLNF* that were not improved due to its lack of correlation with either SOC or crop biomass. Thus, annually-measured crop biomass did not improve the SOC estimates when there was no SOC measurement. However, when SOC measurements are available, even with the unreliable parameter estimation, the EnKF estimates showed promising accuracy.

Given that SOC measurement uncertainty was reduced by 60% in this study, we concluded that the EnKF method using the DSSAT-CENTURY model provided more reliable estimates of SOC over time. However, the uncertain parameter, *SLNF*, was not reliably estimated and more

research is needed to explore ways of improving this result. A comparison study using models of different complexities would be useful to better understand the advantages and disadvantages of each.

Table 4-1 Summary of terms used in the EnKF

Term	Definition	Dimension	Unit
x_t	State vector at *t* from a reference simulation. $x_t = [C_t \quad B_t \quad S]^T$	3	-
x_t^{true}	Truth at *t*. $x_t^{true} = [C_t^{true} \quad B_t^{true} \quad S^{true}]^T = x_t + \omega_t$	3	-
ω_t	Model error vector at *t*. $\omega_t = [\omega_{C,t} \quad \omega_{B,t} \quad \omega_S]$ and $\omega_t = N(0, Q_t)$	3	-
Q_t	Model error covariance matrix at *t*.	3 x 3	-
y_t	Measurement vector at *t*. $y_t = [C_t^{obs} \quad B_t^{obs}]^T = H \cdot x_t^{true} + \nu_t$	2	-
C_t^{obs}	Measured SOC at *t*. $C_t^{obs} = C_t^{true} + \nu_{C,t}$	1	t ha^{-1}
B_t^{obs}	Measured crop biomass at *t*. $B_t^{obs} = B_t^{true} + \nu_{B,t}$	1	t ha^{-1}
H	Measurement operator	2 x 3	$\begin{bmatrix} 1 & 0 & 0 \\ 0 & 1 & 0 \end{bmatrix}$
ν_t	Measurement error vector at *t*. $\nu_t = [\nu_{C,t} \quad \nu_{B,t}]^T$ and $\nu_t = N(0, R_t)$.	2	-
R_t	Measurement error covariance matrix at *t*.	2 x 2	-
P_t^-	Prior covariance matrix of x at *t*.	3 x 3	-
P_t^+	Posterior covariance matrix of x at *t*.	3 x 3	-
x_t^j	j^{th} replicate of x at *t*.	3	-
y_t^j	j^{th} replicate of y at *t*.	2	-
ω_t^j	j^{th} replicate of ω at *t*.	3	-
ν_t^j	j^{th} replicate of ν at *t*.	2	-
j	Identifier for a replicate in the ensemble. $j = 1, \cdots, N$	-	-
N	The size of an ensemble.	-	-
K_t	A Kalman gain matrix at *t*.	3 x 2	-

Table 4-2 Mean and variance of the initial ensemble of the EnKF states

	SOC	Crop Residue	*SLNF*
Mean	$C_1^{obs} \cong$ 14 (t ha^{-1})	$0.8 \times B_1^{obs} \cong$ 3 (t ha^{-1})	0.75 (yr^{-1})
Variance	$\mathrm{Var}(C_1^{obs}) \cong$ 1 (t ha^{-1})^2	$\mathrm{Var}(0.8 \times B_1^{obs}) \cong$ 1(t ha^{-1})^2	0.04 (yr^{-1})^2

Table 4-3 Values of filter parameters and initial conditions used for the base-case scenario

Variable	Definition	Unit	Value
S	*SLNF* value used to generate true and measured values.	yr^{-1}	0.85
E(S_0)	Expected value of *SLNF* in the initial ensemble.	yr^{-1}	0.75
NMEB	Number of ensemble replicates.	–	200
NMYR	Number of years simulated.	Year	20
$\mathrm{Var}(C_t^{obs})$	SOC measurement variance at *t*	(t ha^{-1})^2	(8% of measured values)^2
$\mathrm{Var}(B_t^{obs})$	Crop biomass measurement variance at *t*	(t ha^{-1})^2	(30% of measured values)^2
$\mathrm{Var}(C_t^{model})$	SOC model variance at *t*	(t ha^{-1})^2	(1% of predicted values)^2
$\mathrm{Var}(B_t^{model})$	Crop biomass model variance at *t*	(t ha^{-1})^2	(20% of predicted values)^2
$\mathrm{Var}(S_0)$	Initial *SLNF* estimation error	(yr^{-1})^2	(0.2)^2

Table 4-4 Variables and their values used for the sensitivity analysis. Values with (*) were used as the base-case.

SOC measurement error (% of measured)	SOC model error (% of predicted)	Crop biomass measurement error (% of measured)	Crop biomass model error (% of predicted)	Expected value of initial *SLNF*	*SLNF* estimation error (yr^{-1})	SOC measurement frequency (year)
4	0.3	18	10	0.75	0.1	1 *
8 *	1.0 *	30 *	20 *	0.65 *	0.2 *	1/3
14	8.0	66	30	0.55	0.3	1/5

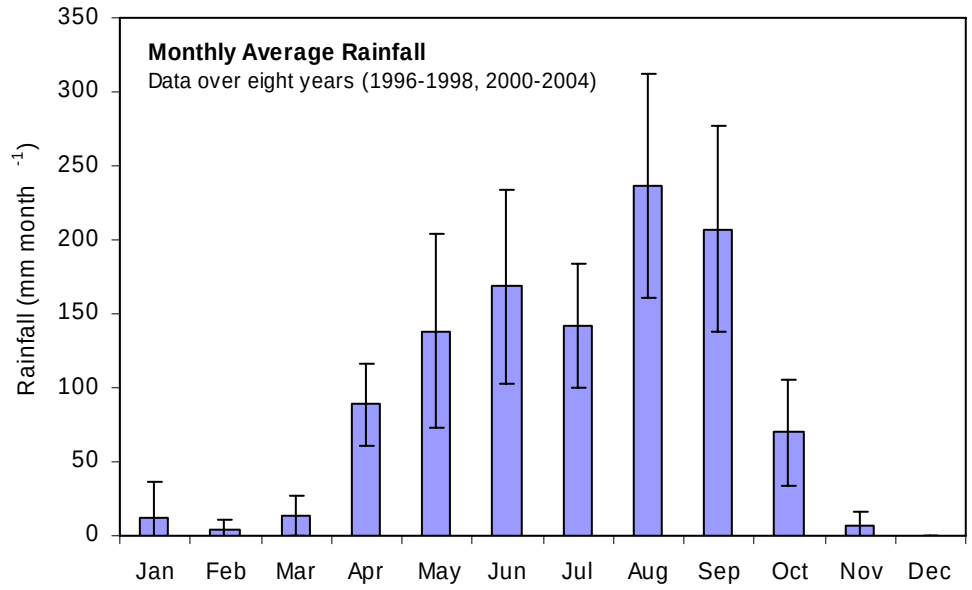

Figure 4-1 Historical monthly precipitation in Wa, Ghana, from eight years of measurement data

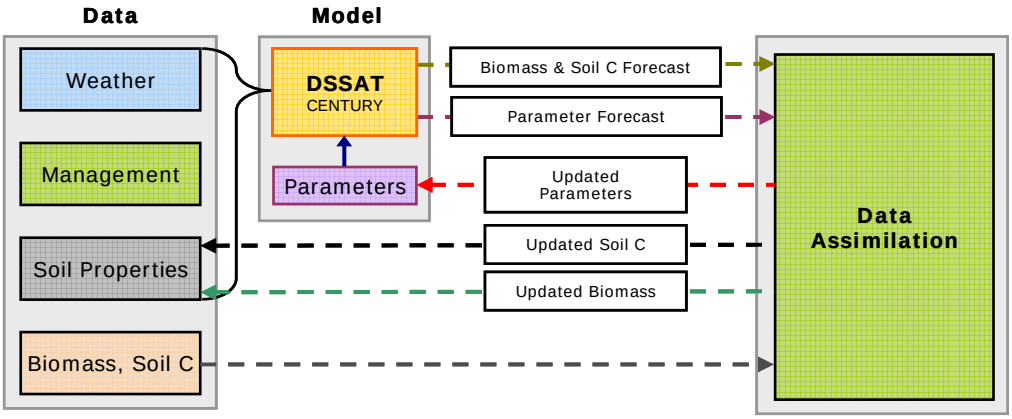

Figure 4-2 Schematic of data assimilation process for estimation of soil carbon sequestration using measurements and a biophysical model, DSSAT-CENTURY.

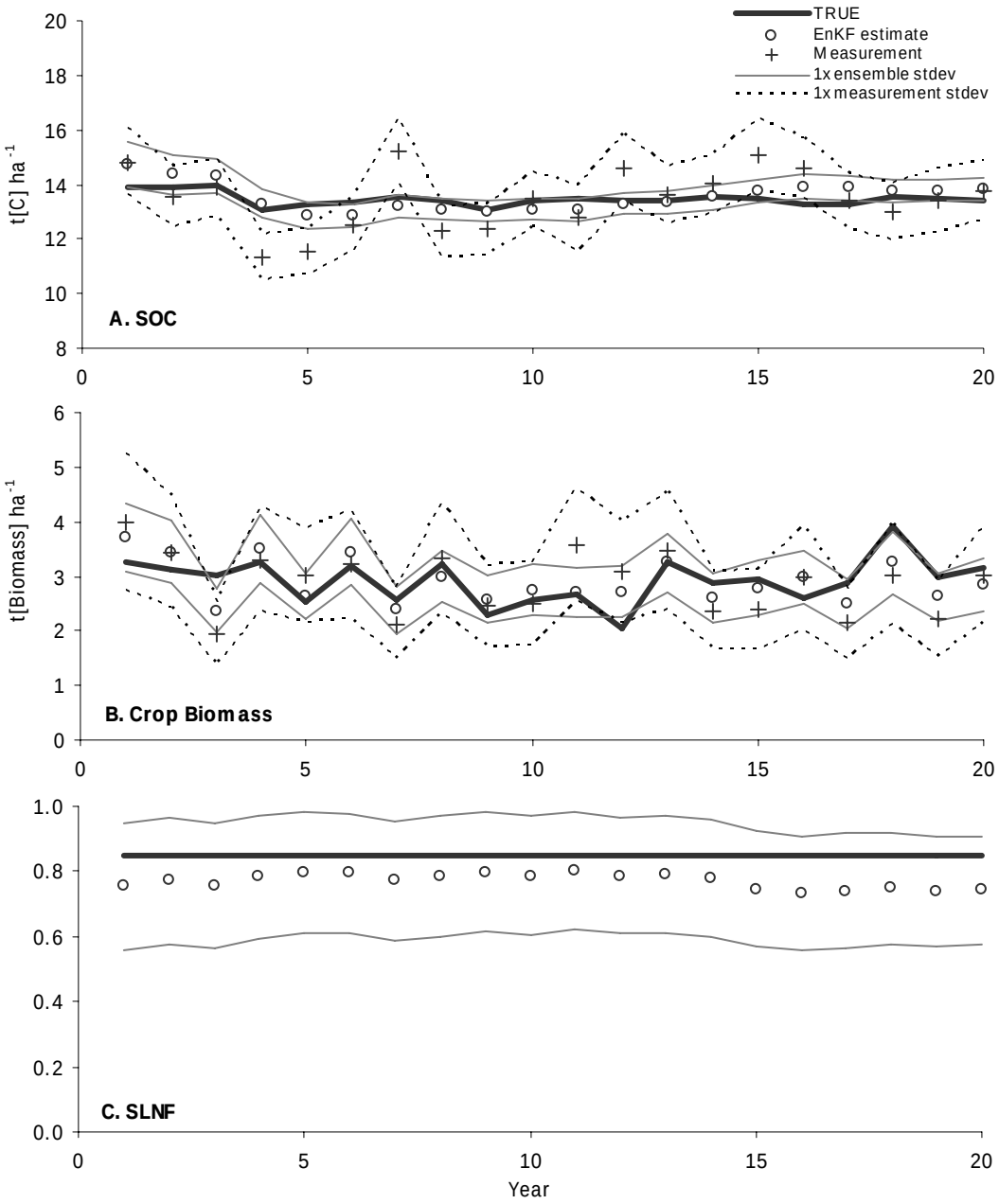

Figure 4-3 Evolution of truth, EnKF estimates, and measurements of the EnKF state variables for 20 years using the base-case scenario

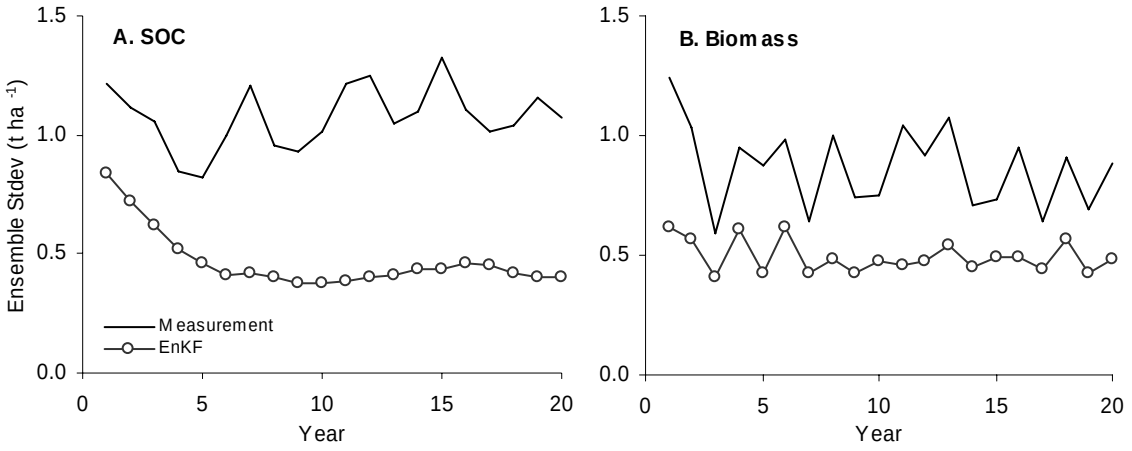

Figure 4-4 Standard deviation of the EnKF estimates and measurements for SOC and crop biomass over time using the base-case scenario

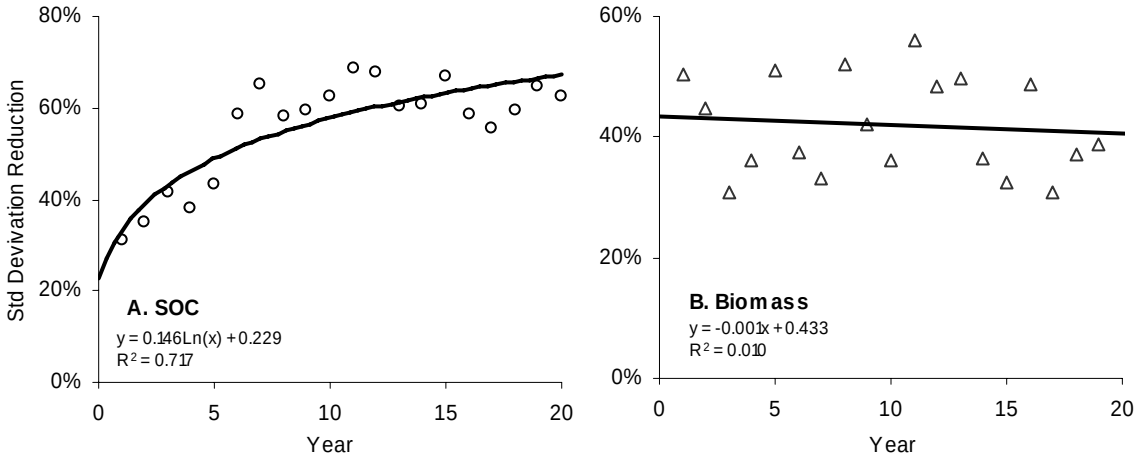

Figure 4-5 Reduction of the standard deviations from measurements to the EnKF estimates over time using the base-case scenario

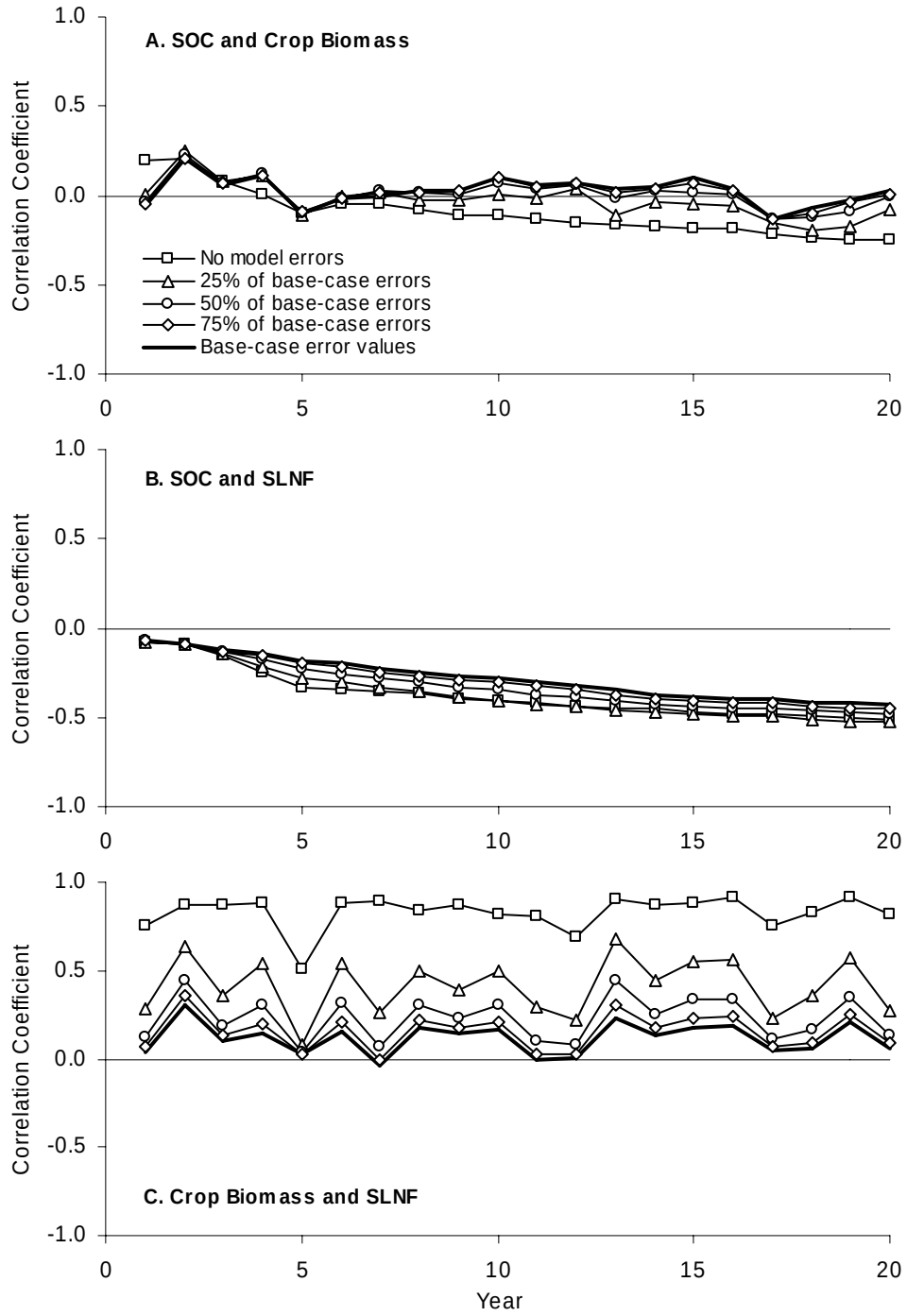

Figure 4-6 Sensitivity of the evolution of the correlation coefficient under the spin-up simulations to the different magnitude of SOC and crop biomass model errors compared to the base-case error values

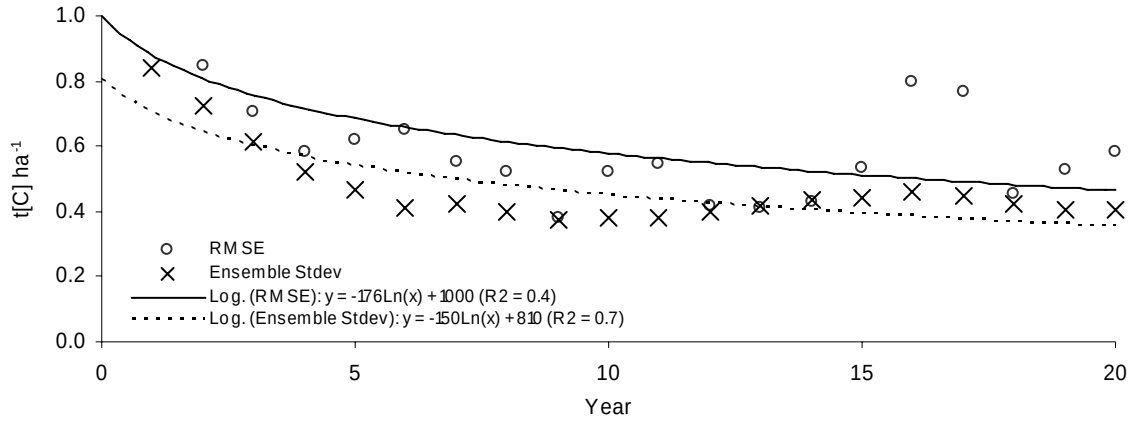

Figure 4-7 Relationship between RMSE and the ensemble standard deviation for the base-case scenario

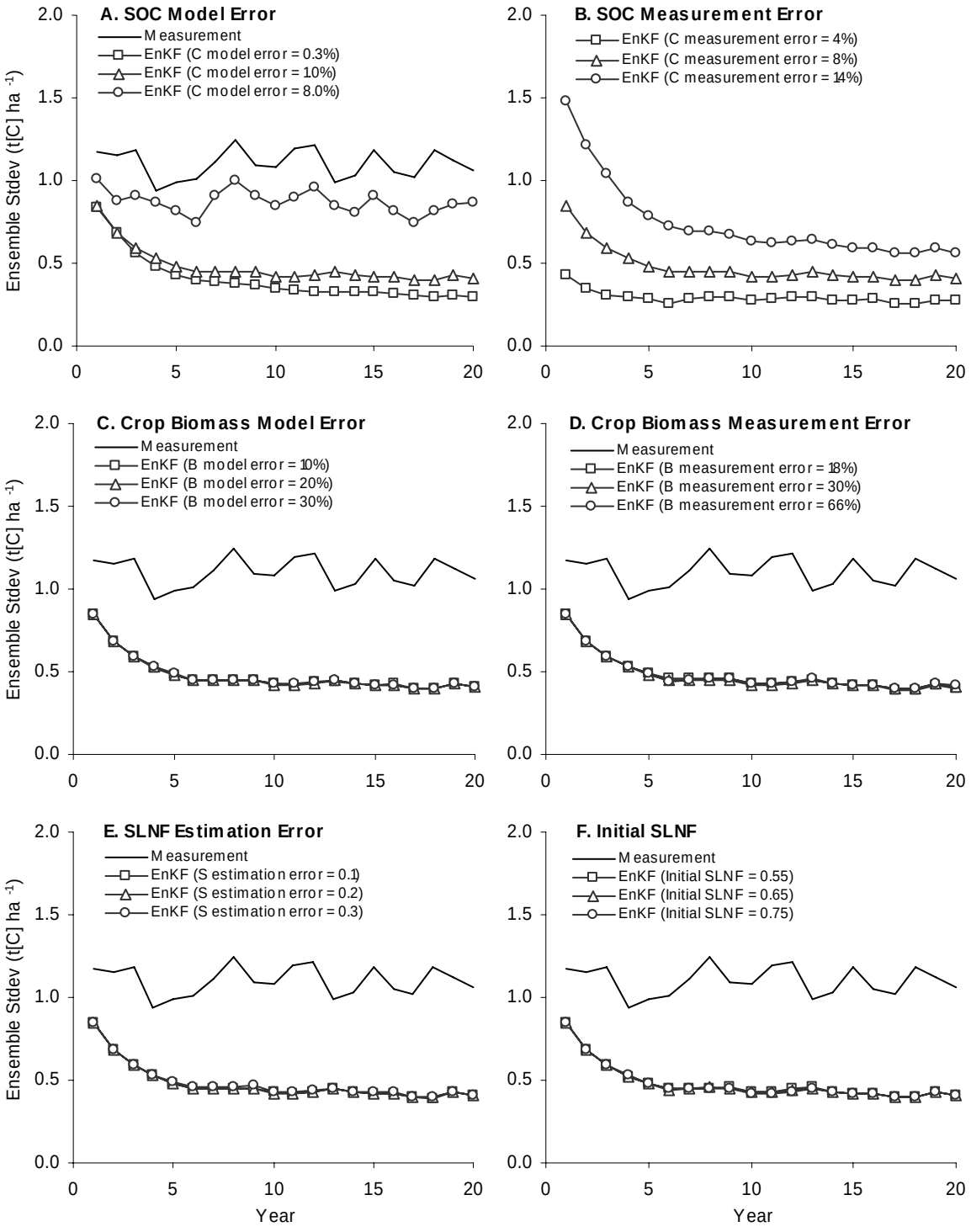

Figure 4-8 Comparison of the sensitivity of the EnKF estimation accuracy to different values of the EnKF filter parameters. Values used in the analysis for each parameter are shown in 4-4.

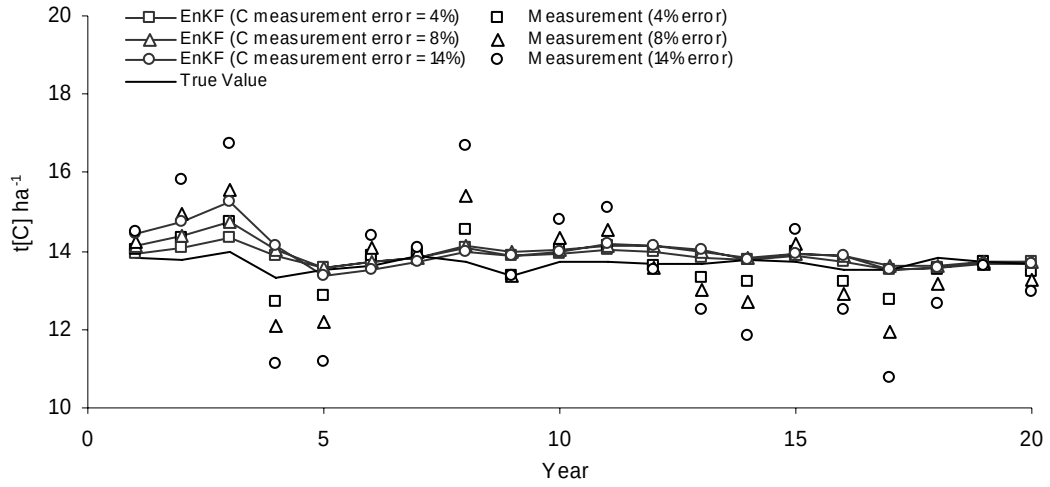

Figure 4-9 Evolution of truth (line), EnKF estimates (symbols with line), and measurements (symbols) of SOC with different measurement errors

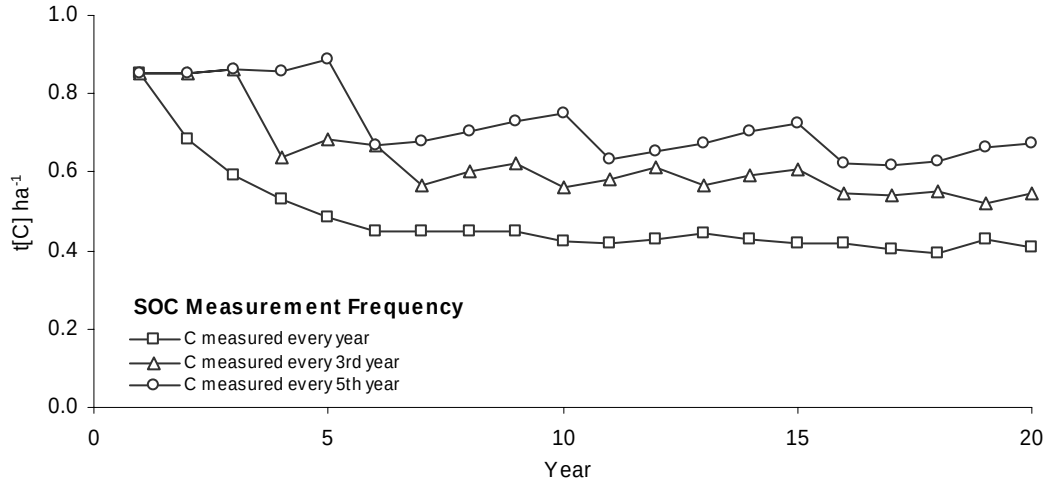

Figure 4-10 Comparison of the sensitivity of the EnKF estimation accuracy to different SOC measurement frequencies (1/1, 1/3, and 1/5 year) after the first year measurement at t=1. The EnKF estimation accuracy was measured by the evolution of the SOC ensemble standard deviation.

CHAPTER 5
ESTIMATING CROP BIOMASS USING HIGH-RESOLUTION REMOTE SENSING AND AN ARTIFICIAL NEURAL NETWORK ALGORITHM

Introduction

It is estimated that the historical depletion of soil organic carbon due to land-use conversion and soil cultivation is responsible for about one third of carbon dioxide (CO_2) emission to the atmosphere (FAO, 2004; Lal, 2003). A large proportion of the lost carbon can be re-sequestered into soils by adopting appropriate management practices in agriculture (Lal, 2003). The CO_2 transfer process from the atmosphere to soils, soil carbon sequestration, is often referred to as a win-win strategy that mitigates greenhouse gas increases in the atmosphere and increases agricultural production in developing countries. Lal (2006) reported strong positive effects of soil organic carbon on soil quality, agronomic/biomass productivity, and advancing global food security. Especially for degraded soils in dryland rain-fed agricultural areas in West Africa, soil carbon sequestration can play an important role to improve crop production as well as to prevent soil erosion and desertification (FAO, 2004). To implement soil carbon sequestration in practice, a reliable soil carbon monitoring system needs to be developed (Antle and Uehara, 2002).

Cropping field management practices that affect soil carbon changes include tillage, cropping history, and crop residues (Bostick et al., 2007). Among these, crop residue is the ultimate source of soil organic matter in cropping systems (Farage et al., 2003) and therefore it greatly affects soil carbon dynamics in the global carbon cycle. When residue management practices are known, the amount of residue returned to the soil after harvest may be estimated by measuring crop biomass production. Therefore, monitoring crop biomass production can provide basic information to estimate source carbon input to soils (Johnson et al., 2006).

At a field-level scale, crop biomass can be directly measured by using destructive plant sampling. However, it would be cost-prohibitive to conduct *in situ* measurements across a large area, especially if 1) the number of fields in the study area is large, 2) the average field size is relatively small, and 3) the locations of fields are scattered throughout the study area. In such cases, satellite remote sensing-based information may be useful to quantify crop biomass over large areas.

Satellite remote sensing images have been used to monitor land-use and land-cover changes over large areas in many disciplines (e.g., Boucher et al., 2006; Inoue, 2003; Kiunsi and Meadows, 2006; Mackin et al., 2006). In agriculture, information on plant activity has been provided by remote sensing using different wavelengths, such as solar spectrum (visible and infrared) (e.g., Broge and Mortensen, 2002; Poss et al., 2006; Rodriguez et al., 2006), microwave (e.g., Kimball et al., 2006; Ranson et al., 1997) and thermal range (e.g., Fitzgerald et al., 2006; Moran et al., 1994). Among these different wavelengths, solar spectrum (400-700 nm region) reflectance is sensitive to the abundance of chlorophyll (Daughtry et al., 2000; Thomas and Gausman, 1977) and thus is used as an indicator of the physiological status of plants. To reduce the multiple bands of remote sensing information into to a single number per pixel that correlates with plant canopy characteristics, various spectral vegetation indices (SVIs) have been calculated as combinations of near-infrared (NIR) and other visible reflectance bands (e.g., blue, green, and red) (Jensen, 1996). Depending on the selection of reflectance bands and primary sensitive variables, many different SVIs have been developed and reported to date. For example, Poss et al. (2006) listed 71 different SVIs in an attempt to find the most significant SVIs for estimating yields of stressed forages. The most widely used SVI is the normalized difference vegetation index (NDVI) (Weier and Herring, 2007). The NDVI was originally developed to estimate green

biomass using NIR and red channels (Tucker, 1979), and it has been shown to be well correlated with chlorophyll density in plant canopy thus with leaf area index (LAI) (e.g., Colombo et al., 2003; He et al., 2006; Koller and Upadhyaya, 2005; Ray et al., 2006). However, the SVIs may not be useful to estimate biomass of matured annual crops and their residues, as their non-green dried biomass values do not necessarily correlate with chlorophyll density.

Without using remote sensing, techniques that have been developed to estimate crop growth include regression analyses, crop models, and artificial neural networks (ANNs). Each technique has (dis)advantages for specific applications. Regression analyses can be easily used (e.g., Schlegel and Havlin, 1995; Singer and Cox, 1998), but their performance is often limited to the specific environment where the model was developed and tested. Use of a crop model is not limited to specific locations as long as reliable local input data are available. Crop models also take into account interrelationships between crop and other components of a cropping system, such as soil, weather, and management. However, crop models often require detailed biophysical input data for cropping systems at a field-level that are not always available. When input parameters are to be estimated without accurate measurements, uncertainty in the model output increases.

An artificial neural network (ANN) has been used as an alternative method to estimate crop production from readily measurable input data such as weather and soil properties without pre-establishing their biophysical relationship (Liu et al., 2001; O'Neal et al., 2002). The ANN was originally developed to reproduce the architecture of simple data processing elements of the human brain (neurons) on computers, and it has been used to process and interpret large quantities of different types of data in many disciplines, including remote sensing (Atkinson and Tatnall, 1997). An artificial neural network consists of a number of interconnected nodes. Each

node receives weighted inputs and threshold results according to a rule, which is defined by training with input and output of a system.

There are different arrangements of nodes in ANNs. Among them, the multi-layer perception (MLP) is one of the most commonly used types (Atkinson and Tatnall, 1997). An MLP network generally contains three types of layers: input, hidden, and output layers (Figure 5-1). First, the input layer has a node for each input data type (e.g., digital number of each band for a satellite remote sensing image). Second, the hidden layer contains nodes that are interconnected from input layers to an output layer or the next hidden layer. The number of hidden layers and the number of nodes in them may be increased for complex problems, but that may cause an overfitting (overtraining) of the network and reduce its generality (Atkinson and Tatnall, 1997). Finally, the output layer presents the output data of the MLP model.

The most common use of ANNs in remote sensing is land cover classification (Bagan et al., 2005; Kuplich, 2006; Liu et al., 2005). Results form these studies have shown higher accuracy than traditional statistical classifications. Other common agricultural applications include LAI estimation (e.g., Walthall et al., 2004), spatial interpolation of weather variables (e.g., Li et al., 2004), crop nitrogen stress detection (e.g., Noh et al., 2006), and soil moisture estimation (e.g., Del Frate et al., 2003). In addition, ANNs were also used to estimate site-specific crop yield with remote sensing data for maize (Jiang et al., 2004) and citrus (Ye et al., 2006). Jiang et al. (2004) used an ANN to forecast winter wheat yield with remote sensing-retrieved input data, such as NDVI, absorbed photosynthesis active radiation (APAR), canopy surface temperature, and water stress index, and average crop yield per unit area in the past for 10 years prior to the study. In their study, daily AVHRR satellite remote sensing images (about 270 images, from October 1998 to June 1999) were available throughout the crop growing season thus the remote sensing-

retrieved input data were calculated on a daily-basis. For the ANN input layer, each of the remote sensing data points was integrated from tillering to harvest as one number and used in each node. When compared with a general linear model (multiple regression), the ANN estimates were more accurate.

When multiple remote sensing images are accessible during the course of a crop season, important physiological properties of crops over the growing season can be estimated and used to adjust states and parameters of crop growth models, and the adjusted crop models can be used to predict the final crop production (Ko et al., 2006; Locke et al., 2002; Moulin et al., 1998). However, in practice, the number of accessible remote sensing images within a crop season is often limited due to environmental and financial constraints. In rain-fed cropping systems, for example, crop season typically coincides with a rainy season. Thus cloud cover interferes with spectral reflectances and reduces chances of acquiring cloud-free non-microwave remote sensing images during the cropping season (Amanor and Pabi, 2007). When the number of available remote sensing images is limited, a different approach is needed to estimate crop biomass or production.

This study deals with spatially-limited field-level *in situ* crop biomass measurements and temporally-limited satellite remote sensing information. The research question addressed was how to estimate field-level aboveground crop biomass at harvest in all crop fields in a study area, given those data limitations. It was hypothesized that, compared to general linear models, an ANN-based approach would improve crop biomass estimation accuracy in fields without measurements in an area where measurements in other fields were available for developing these methods. Based on *one* available high-resolution remote sensing image acquired during a single cropping season and crop biomass measured in some fields, an MLP model was developed. Its

crop biomass estimation performance was compared with two general linear models (linear and multiple regression models).

Materials and Methods

The study area was located in Oumaroubougou, Mali. A total of 34 smallholder farmers' fields, including eight cotton fields, nine maize fields, eight millet fields, and nine sorghum fields, were georeferenced in August 2003. Aboveground vegetative crop biomass from 1 m^2 area in each field was destructively sampled between August 10 and August 19, dried, and measured. Average age of those crops was 86 days (Table 5-1). However, their measured biomass values were highly variable (coefficient of variation (CV) = 62%) (Table 5-1), and this was mainly due to variability in their canopy density with different ages (CV = 13%). Depending on crop species, CV values of biomass measurements ranged from 50 to 65% (Table 5-1). To some extent, this biomass variability was intentionally introduced to take into account inherent heterogeneity in crop biomass across fields at a given time that may be caused by variable environmental and management conditions, such as different crop species, planting dates, soil properties, and planting density (P. C. S. Traore, International Crops Research Institute for the Semi-Arid Tropics, personal communication, April 2007).

Due to the relatively small size of cultivated fields in the study area, a high-resolution remote sensing platform (QuickBird, whose spatial resolution is 2.4 m for multispectral bands and 0.6 m for panchromatic) was selected. The desired time window for the remote sensing image acquisition was around the time when peak biomass occurred, which was between August and September. The image was acquired on August 27. There were lags of from 8 to 17 days between *in situ* biomass measurements and the image acquisition dates. Using global control points collected around the study area, the image was registered to enhance image precision and

to achieve sub-pixel accuracy (W. M. Bostick, graduate student, personal communication, April 2004).

The number of input (independent) variables used in this study was eleven (Table 5-2). From the QuickBird remote sensing image, the reflectance digital numbers of four wavelength channels (blue, green, red, and NIR) for each point in a field where crop biomass was measured were retrieved and used to form the SVI input variables. To be compatible with the scales of other input variables (e.g., SVIs), the reflectance digital numbers were scaled down as follows:

$$\text{Reflectance} = \frac{\text{Digital Number}}{2048} \tag{5-1}$$

where the denominator ($2048 = 2^{11}$) is the maximum value of digital numbers measured by QuickBird multispectral sensors (DigitalGlobe, 2006). Based on the reflectances measured with four wavelength channels in each field, six SVIs were calculated as follows (Yang et al., 2006):

$$NB = \frac{NIR}{Blue} \tag{5-2}$$

$$NG = \frac{NIR}{Green} \tag{5-3}$$

$$NR = \frac{NIR}{Red} \tag{5-4}$$

$$NDNB = \frac{(NIR - Blue)}{(NIR + Blue)} \tag{5-5}$$

$$NDNG = \frac{(NIR - Green)}{(NIR + Green)} \tag{5-6}$$

$$NDVI = \frac{(NIR - Red)}{(NIR + Red)} \tag{5-7}$$

In addition, to take into account different crop types in each field, a dummy variable was included. It was assumed that crop types were classified in a preliminary study, possibly using a

supervised classification method using ground truthing. Xie et al. (2007) reported that a supervised classification method appropriately classified crop fields from non-cultivated fallow land using a satellite remote sensing image from Landsat ETM+. However, among four crops cultivated in the study area, W. M. Bostick (graduate student, personal communication, August 2004) reported that cotton may be readily distinguished from cereal crops, but cereal species (i.e., maize, millet, and sorghum) would not be reliably classified due to their spectral and canopy geometric similarities. Thus, only one dummy variable that distinguishes cotton and non-cotton crops was included (Table 5-2).

The number of output (dependent) variable was one, *in situ* aboveground vegetative crop biomass measurement made in each field in the study area (Table 5-2). Based on the input and output data, two general linear models (linear and multiple regressions) and an MLP model were developed. The general linear models were implemented to comparatively analyze the performance of the MLP model, following the recommendation of Özesmi et al. (2006). They reported that, based on reviewing literature that used MLP models in ecological science, MLP models do not always outperform simpler linear techniques. Two types of general linear models, linear and multiple regression models, were developed with NCSS 2004 software (Hintze, 2004). The MLP model was developed with MATLAB Neural Network Toolbox (MathWorks, 2004). Due to the relatively small size of dataset (n = 34), the performances of the three models were assessed by calculating the root mean square error of prediction (RMSEP) from cross-validation (i.e., leave-one-out jackknife) analyses (Özesmi et al., 2006).

First, six different models were developed using linear regression analyses between each of six SVIs (independent variable) and crop biomass (dependent variable). As a preliminary data analysis, these linear regression analyses were conducted to test if there were simple and useful

linear relationships between SVIs and crop biomass, without introducing other independent variables or further methodologies. Second, a multiple regression model with all of the eleven independent variables was developed. Finally, an MLP ANN model was developed with feed-forward backpropagation network. The MLP model was designed as follows:

- Input layer: Eleven nodes corresponding to independent variables for the input dataset were configured (Figure 5-2).
- Hidden layer: One hidden layer was created. Number of nodes in the hidden layer is an important factor that influences the generality of network. Based on the suggestion of Bishop (1995) that limits the number of hidden nodes to be about 1/10 of the size of training dataset, the number of nodes in the hidden layer was set as three.
- Output layer: One output layer was created with one node that corresponded to the aboveground vegetative crop biomass measurement data in each field.
- Transfer functions and training method: Transfer functions in the hidden and output layers and the network training method were chosen based the results of a preliminary study that tested the sensitivity of data fitting performance to different choices of transfer functions and training methods. Sigmoid and linear transfer functions (logsig and purelin in MATLAB, MathWorks, 2004) were used for the hidden and output layer, respectively, and the MLP network was trained with the resilient backpropagation method (trainrp in MATLAB, MathWorks, 2004), which showed the best performance.

In addition, it was noted that the initial weights, which were randomly set in each run, were the most sensitive parameters to the MLP model performance in the preliminary study. To take randomness into account, ten random seed numbers were randomly predefined. Each random seed number was used to create a different set of initial weights, which was used to train an MLP network. For each of the trained MLP network, its performance was analyzed using cross-validation. Then, the overall performance of using an MLP model was analyzed from the results of ten repetitions of the cross-validation for each MLP network.

Training of the MLP network was stopped early to prevent overfitting (overtraining) problem and improve generalizations. First, the MLP network was trained with 500 epochs for each random seed number. For each training, changes in RMSE over the increase of epochs were

calculated. Second, after ten repetitions of the training, their average RMSE value for each epoch was calculated. Finally, changes of the average RMSE with increases in epochs were plotted and used to determine the appropriate number of epochs, beyond which the RMSE stabilizes.

Results

Linear Regression

The linear regression analyses with six SVIs showed that the correlations between each SVI and crop biomass was significant ($P<0.01$) (Table 5-3). That is, the SVIs showed significant responses to the crop biomass in each field. Among six tested SVIs, NDVI showed the best fitting performance with lowest RMSE (64.70 g[DM] m^{-2}) (Figure 5-3). The NDVI explained 44% of variability in crop biomass measurements (Figure 5-4). However, its coefficient of variation (CV) was relatively high at 47%, which implied its performance to estimate crop biomass may be unreliable in practice. Cross-validation results showed the same pattern of performances among the SVIs. The NDVI showed the minimum RMSEP value (67 g[DM] m^{-2}), but its CV was also high at 49%. Overall, these linear regression analyses showed that, although there are significant correlations, the SVIs may not be reliable estimators for aboveground vegetative crop biomass in the study area.

Multiple Regression

In the multiple regression analysis, all of the eleven independent variables were used, instead of selecting significant variables only. This was done to compare its performance with the MLP model, which was designed to use all of the eleven input SVIs in its input layer. However, when a stepwise (backward) variable selection method was performed, its result selected five variables (i.e. Blue, NIR, NB, NR, and NDNB) (Figure 5-5), based on the changes in R^2 as the model size increased. Combined, those five variables explained 67% of the variability in the crop biomass measurement (Table 5-4). The other six variables increased R^2 by

only 2% (Table 5-4). It was noted that the dummy variable for cotton/non-cotton classification showed very low influence on the overall model (Table 5-4). This implied that uncertain crop species classifications did not impact these overall crop biomass estimation results significantly. Correlation coefficients of the dummy variable and other variables also confirmed that the crop species classification was not an important factor. The correlation matrix of all variables (Table 5-5) showed that correlations were mostly significant ($P<0.01$), except the ones with the dummy variable (e.g., Blue, Green, Red, NR, and NDVI) (Table 5-5). When correlated with the dependent variable (i.e. crop biomass), ten independent variables were significant ($P<0.01$), and only the dummy crop-type variable showed insignificance ($P<0.10$). Overall, significances were found in most input variables, which indicated their potential use to estimate crop biomass.

Regression coefficients for each of the eleven variables and an intercept are shown in Table 5-6. The P-value of each variable showed that none of the eleven independent variables was significant in the multiple regression model ($P<0.10$). However, the model explained about 70% of variability in the crop biomass ($R^2 = 0.69$) (Figure 5-6), and this was higher than that of the linear regression model that used NDVI, which was 44% (Figure 5-4). The RMSE value was 57 g[DM] m^{-2}, and its CV was 43%. However, it was shown that the performance of multiple regression model may not be generalized. When cross-validation analysis was performed, the RMSEP value between estimated and measured crop biomass was increased to 72 g[DM] m^{-2} with CV = 53% (Table 5-7).

Artificial Neural Network

Training of the MLP network was repeated ten times with different initial weights. From the ten repetitions, an appropriate number of epochs was determined as 100 (Figure 5-7). At 100 epochs, RMSE values ranged from 47 to 59 g[DM] m^{-2} depending on initial weights (CV = 6%). Their range did not noticeably fluctuate beyond 100 epochs (Figure 5-7). The RMSE values were

averaged as 50 g[DM] m^{-2}. With 36% CV, the MLP network showed the best performance to fit dataset over two general linear models (Table 5-8). This superior performance was also generalized, compared to the general linear models. In cross-validation analyses, RMSEP values from ten repetitions ranged from 57 to 71 g[DM] m^{-2}. That is, even in the worst case, its RMSEP of the MLP model was still lower than that of multiple regression models (Table 5-7). The RMSEP values were averaged as 60 g[DM] m^{-2}, and this value was also lower than that of both general linear models (Figure 5-9). However, its CV value was high as 44%, which may be still too high to be used as a reliable estimator in practice.

Discussion

Satellite remote sensing images provide important information to estimate plant growth in a regional-scale study. In agriculture, many SVIs have been developed to estimate vegetation status of crops qualitatively and quantitatively. However, the SVIs mostly target the estimation of fresh and green biomass. Thus, they may not be suitable to estimate crop biomass at harvest maturity, which is usually dry following plant senescence. When a series of remote sensing images are available in the course of cropping season, they may be useful to adjust states in a crop model, which can simulate crop growth and forecast crop biomass production. However, this approach may not be useful in a dryland rain-fed cropping system, where crop seasons coincide with rainy seasons and consistently high cloud coverages. Assuming there was at least one good high-resolution remote sensing image acquired during the cropping season around peak-biomass, this study proposed a new method to estimate crop aboveground vegetative biomass at harvest using ANN. Compared to general linear models, overall results of this study showed the potential of using an MLP model as a crop biomass estimating tool. With data of four different crops in 34 fields in a dryland rain-fed cropping system in this study, cross-validation results showed that the crop biomass estimation performance of the MLP model was superior to

general linear models. This result implied that correlations between input and output were not necessarily linear. Unlike the multiple regression model, the MLP model showed better performances in cross-validation analyses. However, even for the MLP model, the CV of crop biomass estimation in cross-validation analysis was high as 44%. Inherent noise in the crop biomass measurement data may be one of reasons for the unreliable estimation. For example, the CV value of biomass measurements for all crops was as high as 62% (Table 5-1), mainly due to heterogeneous crop species and their growth. Further studies with larger datasets may reduce measurement variability and improve crop biomass estimation reliability.

Note that the purpose of this ANN-based method was to regionally estimate crop biomass with available information including satellite remote sensing image and *in situ* crop biomass measurements, not to substitute all of the *in situ* measurement in a given crop season. The MLP model relied on assumed correlations between remote sensing-retrieved input dataset at a given time of a crop season and crop biomass measured at harvest as output data. Because environmental conditions vary between seasons (e.g., weather variability and management practices changes), reflectances of crop fields retrieved from satellite remote sensing image will also seasonally vary. Such variations in input datasets will alter the correlations between inputs and output of the network if they were defined in a different season. Thus, unless the network is trained with corresponding input (i.e., remote sensing image) and output (i.e., *in situ* crop biomass measurements) for a season, the MLP model estimations with new input data in a new season will be inaccurate. In addition, without *in situ* measurements, any region-wide biophysical events (i.e., drought, pest damage, or low solar radiation) that may occur between remote sensing image acquisition and crop harvest will not be taken into account to the crop

biomass estimation process, although they may affect crop production thus seasonally alter the input and output correlations.

Accurate classification of crop species in each field may improve crop biomass estimations, since different crop species with similar reflectances may not produce similar biomass at harvest. However, it was noted that differentiating four crop species used in this study may not be a practical assumption due to physiological and spectral similarities in same type of crops (e.g., cereal crops). Moreover, especially in a regional-level study, there will be many types of crop species in the study area with smallholder farmers' cropping systems. Thus, accurate classification of those crop species will be a challenging task. For example, according to a survey with smallholder farmers in Northern Ghana, ten different crop species were cultivated between 2001 and 2005 (see Chapter 2). However, differentiating crop fields versus fallow land may be possible with high-resolution satellite remote sensing images (e.g., Xie et al., 2007).

It was recognized that optimizing the architecture of MLP network requires careful investigation and sensitivity analysis. Overfitting has been the major issue in ANN applications, however achieving generalization of the network was not straightforward. There were no generic rules other than simplifying the network architecture (Özesmi et al., 2006). Thus, the final MLP network architecture used in this study (Figure 5-2) was defined based on a series of sensitivity analyses (i.e., trial and error) with available options to minimize the network structure. It was also noted that the MLP performance was sensitive to randomly generated initial weights. Further research is needed to systemically optimize the network architecture to improve estimation accuracy and enhance generality of the MLP model for the purposes in this study.

Table 5-1 Crop biomass measured in 34 fields with four crops located in Oumaroubougou, Mali.

	Number of fields	Crop Age (Day)			Crop Biomass (g[DW] m^{-2})		
		Average	Standard Deviation	CV	Average	Standard Deviation	CV
Cotton	8	96	3	3%	110	69	63%
Maize	9	78	7	9%	143	71	50%
Millet	8	98	4	4%	181	118	65%
Sorghum	9	77	6	8%	114	71	62%
Total	34	86	11	13%	136	85	62%

Table 5-2 Input (independent) and output (dependent) data used for the GLM and ANN analyses in this study. Total of 34 fields with four crop types were located in Oumaroubougou, Mali. Reflectances and SVIs were retrieved from a QuickBird remote sensing image.

Crop	Cotton (Dummy Variable)	Relative Reflectance				Spectral Vegetation Indices						Biomass (g[DW] m^{-2})
		Blue	Green	Red	NIR	NB	NG	NR	NDNB	NDNG	NDVI	
Cotton	1	0.12	0.18	0.11	0.43	3.50	2.37	3.95	0.56	0.41	0.60	147
	1	0.13	0.20	0.15	0.30	2.28	1.49	1.99	0.39	0.20	0.33	20
	1	0.12	0.18	0.10	0.48	4.00	2.64	4.62	0.60	0.45	0.64	141
	1	0.13	0.19	0.12	0.35	2.77	1.88	2.95	0.47	0.30	0.49	81
	1	0.13	0.19	0.13	0.29	2.24	1.54	2.17	0.38	0.21	0.37	31
	1	0.13	0.19	0.13	0.33	2.64	1.79	2.53	0.45	0.28	0.43	71
	1	0.12	0.18	0.10	0.43	3.56	2.35	4.19	0.56	0.40	0.61	211
	1	0.12	0.19	0.12	0.36	2.96	1.90	3.05	0.49	0.31	0.51	174
Maize	0	0.12	0.18	0.10	0.35	2.90	2.00	3.45	0.49	0.33	0.55	177
	0	0.12	0.17	0.10	0.36	3.01	2.10	3.52	0.50	0.36	0.56	213
	0	0.13	0.19	0.12	0.32	2.51	1.68	2.63	0.43	0.25	0.45	82
	0	0.12	0.18	0.11	0.33	2.69	1.87	3.00	0.46	0.30	0.50	250
	0	0.12	0.19	0.12	0.33	2.64	1.73	2.76	0.45	0.27	0.47	34
	0	0.14	0.21	0.14	0.30	2.19	1.47	2.20	0.37	0.19	0.37	160
	0	0.13	0.20	0.13	0.33	2.49	1.64	2.51	0.43	0.24	0.43	127
	0	0.14	0.22	0.15	0.31	2.23	1.42	2.00	0.38	0.17	0.33	65
	0	0.12	0.17	0.10	0.34	2.81	1.94	3.21	0.47	0.32	0.53	175
Millet	0	0.13	0.19	0.12	0.32	2.51	1.71	2.58	0.43	0.26	0.44	42
	0	0.13	0.19	0.12	0.33	2.59	1.72	2.76	0.44	0.26	0.47	110
	0	0.12	0.18	0.10	0.38	3.15	2.14	3.69	0.52	0.36	0.57	320
	0	0.13	0.21	0.15	0.29	2.18	1.42	1.96	0.37	0.17	0.32	80
	0	0.13	0.21	0.14	0.30	2.27	1.48	2.16	0.39	0.19	0.37	129
	0	0.13	0.19	0.12	0.32	2.52	1.67	2.63	0.43	0.25	0.45	131
	0	0.13	0.18	0.10	0.38	3.01	2.09	3.79	0.50	0.35	0.58	337
	0	0.12	0.18	0.10	0.35	2.89	1.94	3.38	0.49	0.32	0.54	302
Sorghum	0	0.12	0.19	0.11	0.33	2.62	1.73	2.84	0.45	0.27	0.48	138
	0	0.13	0.19	0.11	0.38	2.99	2.01	3.39	0.50	0.34	0.54	233
	0	0.13	0.19	0.11	0.33	2.63	1.75	2.89	0.45	0.27	0.49	121
	0	0.12	0.19	0.11	0.35	2.81	1.83	3.21	0.48	0.29	0.52	98
	0	0.13	0.20	0.13	0.31	2.42	1.57	2.52	0.42	0.22	0.43	38
	0	0.13	0.19	0.13	0.32	2.42	1.64	2.53	0.42	0.24	0.43	196
	0	0.13	0.20	0.14	0.24	1.77	1.19	1.68	0.28	0.09	0.25	43
	0	0.13	0.20	0.14	0.25	1.86	1.24	1.80	0.30	0.11	0.29	27
	0	0.13	0.20	0.12	0.29	2.26	1.46	2.34	0.39	0.19	0.40	134

Table 5-3 Linear regression results of SVIs and crop biomass (*: Significant at P<0.01)

	Model Development					Cross-Validation	
SVI	Model	R^2	Correlation coefficient (r)	RMSE (g[DM] m^{-2})	CV	RMSEP (g[DM] m^{-2})	CV
NB	-128.95 + 99.9 x NB	0.30	0.54*	72.59	53%	76.75	56%
NG	-138.75 + 154.88 x NG	0.34	0.58*	70.30	52%	74.12	54%
NR	-86.46 + 78.20 x NR	0.42	0.65*	65.95	48%	69.70	51%
NDNB	-184.05 + 720.50 x NDNB	0.33	0.58*	70.72	52%	73.00	54%
NDNG	-33.96 + 629.52 x NDNG	0.37	0.61*	68.86	50%	71.22	52%
NDVI	-136.41 + 588.21 x NDNR	0.44	0.66*	64.70	47%	66.74	49%

Table 5-4 Results of the variable selection analysis (forward stepwise method) (*: selected significant variable with P<0.10)

Model Size	R^2	R^2 change	Variable Names
1	0.4611	0.4611	Red
2	0.5334	0.0724	Blue, Red
3	0.5535	0.0201	Blue, Red, NDNG
4	0.5815	0.0279	Blue, Red, Cotton, NDNG
5	0.6728	0.0913	Blue, NIR, NB, NR, NDNB
6	0.6761	0.0033	Blue, NIR, NB, NR, NDNB, NDVI
7	0.6783	0.0022	Blue, Red, NIR, NB, NR, NDNB, NDVI
8	0.6825	0.0042	Blue, Red, NIR, Cotton, NB, NR, NDNB, NDVI
9	0.6877	0.0052	Blue, Green, NIR, Cotton, NB, NR, NDNB, NDNG, NDVI
10	0.6895	0.0018	Blue, Green, Red, NIR, Cotton, NB, NR, NDNB, NDNG, NDVI
11	0.6895	0.0000	Blue, Green, Red, NIR, Cotton, NB, NG, NR, NDNB, NDNG, NDVI

Table 5-5 Correlation matrix of twelve variables (11 independent and 1 dependent variables) used in the multiple regression analysis (ns: not significant, *: significant at P<0.10, **: significant at P<0.05, ***: significant at P<0.01)

	Blue	Green	Red	NIR	Cotton	NB	NG	NR	NDNB	NDNG	NDVI	Biomass
Blue	--											
Green	0.91***	--										
Red	0.90***	0.89***	--									
NIR	-0.68***	-0.59***	-0.71***	--								
Cotton	0.21ns	0.15ns	-0.01ns	-0.43**	--							
NB	-0.78***	-0.68***	-0.79***	0.99***	-0.41**	--						
NG	-0.80***	-0.75***	-0.82***	0.97***	-0.38**	0.99***	--					
NR	-0.82***	-0.76***	-0.89***	0.95***	-0.26ns	0.97***	0.98***	--				
NDNB	-0.81***	-0.71***	-0.81***	0.97***	-0.36**	0.98***	0.98***	0.96***	--			
NDNG	-0.83***	-0.78***	-0.84***	0.95***	-0.35*	0.98***	0.99***	0.97***	0.99***	--		
NDVI	-0.86***	-0.80***	-0.92***	0.91***	-0.20ns	0.95***	0.96***	0.98***	0.97***	0.98***	--	
Biomass	-0.49***	-0.55***	-0.68***	0.52***	0.18ns	0.54***	0.58***	0.65***	0.58***	0.61***	0.66***	--

Table 5-6 Multiple regression coefficients for all variables (ns: non-significant variable, P<0.10)

Variable	Regression Coefficient	P-level
Intercept [ns]	-13370.10	0.28
Blue [ns]	82.02	0.31
Green [ns]	-25.39	0.60
Red [ns]	-12.14	0.73
NIR [ns]	-12.38	0.14
Cotton [ns]	31.59	0.49
NB [ns]	2186.67	0.36
NG [ns]	90.64	0.96
NR [ns]	461.06	0.14
NDNB [ns]	36808.66	0.39
NDNG [ns]	-20938.47	0.61
NDVI [ns]	-9556.85	0.68

Table 5-7 Summary of the performances of three crop biomass estimation methods

	Model Development		Cross-Validation	
Model	RMSE (g[DM] m^{-2})	CV	RMSEP (g[DM] m^{-2})	CV
Linear Regression (NDVI)	64.70	47%	66.74	49%
Multiple Regression (11 variables)	56.57	41%	71.97	53%
MLP (11 variables)	49.77	36%	60.12	44%

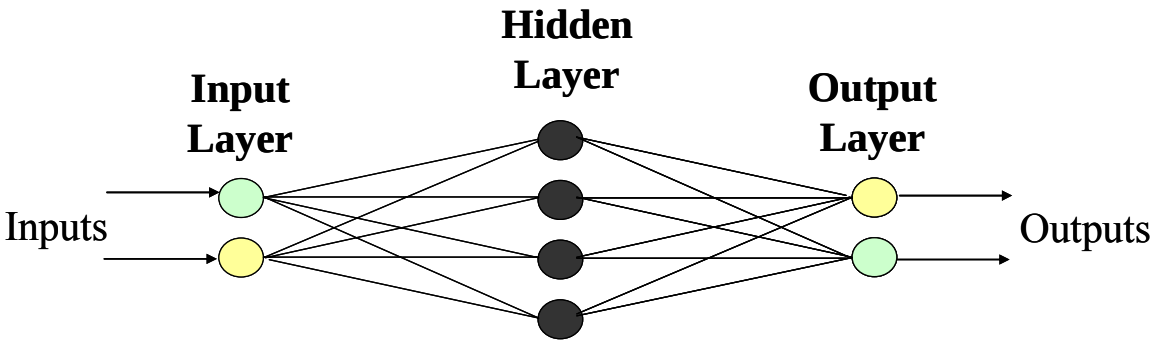

Figure 5-1 Schematic of the MLP algorithm[3].

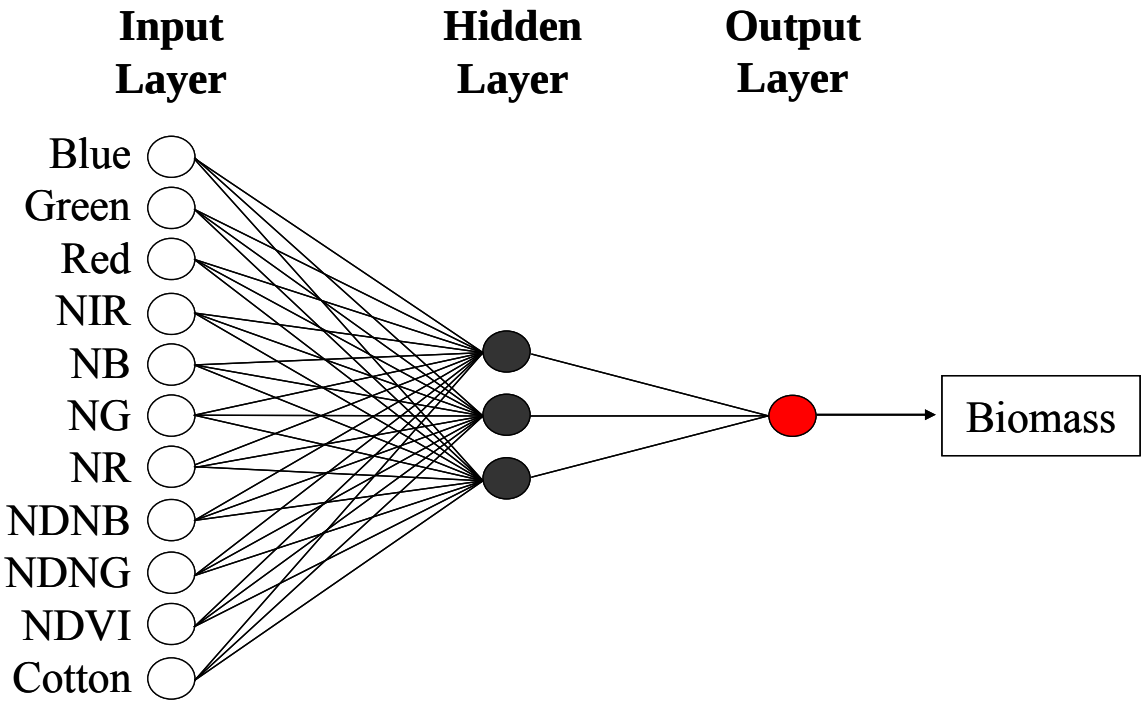

Figure 5-2 Schematic of the MLP model used in this study.

[3] Adopted from Atkinson, P. M. and A. R. L. Tatnall. 1997. Neural networks in remote sensing - Introduction. *International Journal of Remote Sensing* 18, no. 4:699-709.

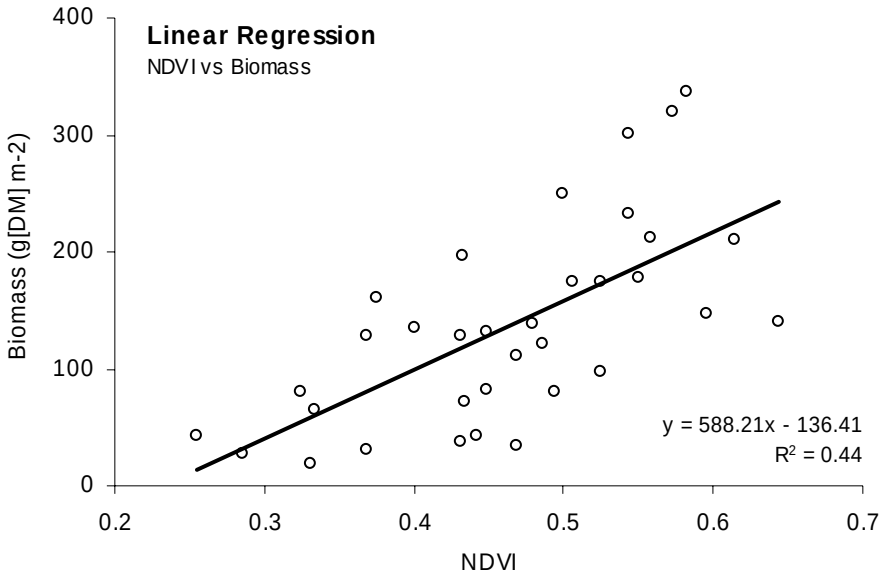

Figure 5-3 Linear regression of NDVI and aboveground vegetative crop biomass in 34 fields in Oumaroubougou, Mali.

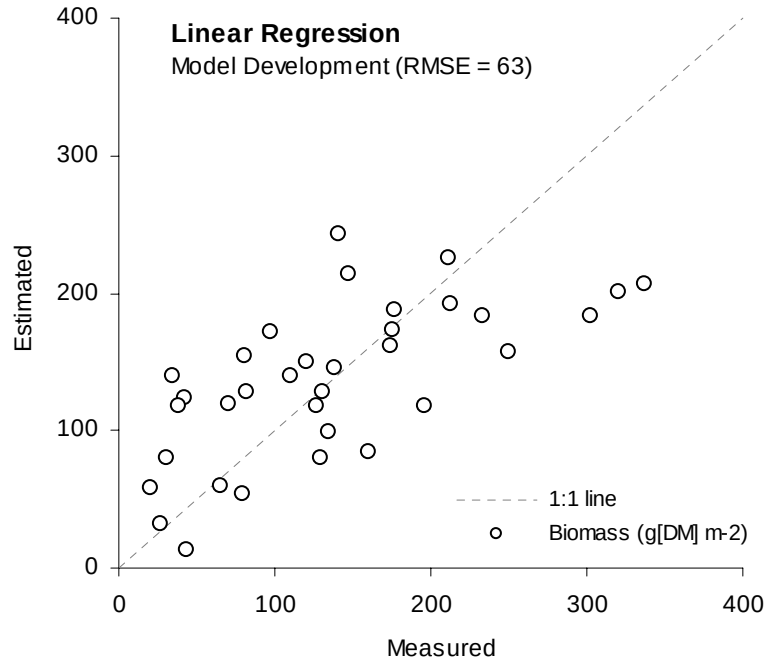

Figure 5-4 Measured and estimated crop biomass using a linear regression model of NDVI

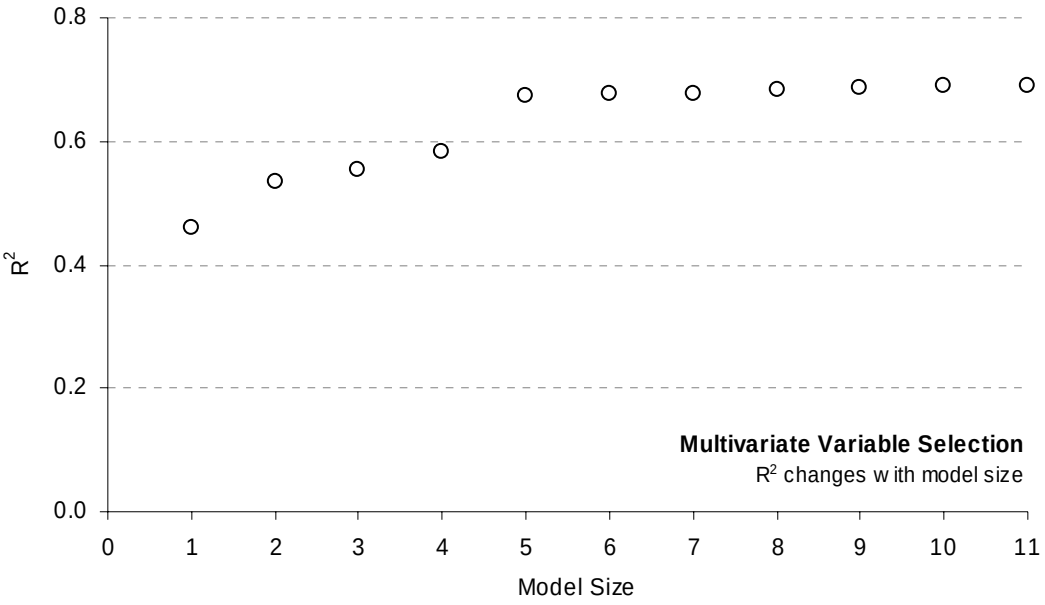

Figure 5-5 Multivariate variable selection analysis result showing the changes of R^2 as the size of multiple regression model increases.

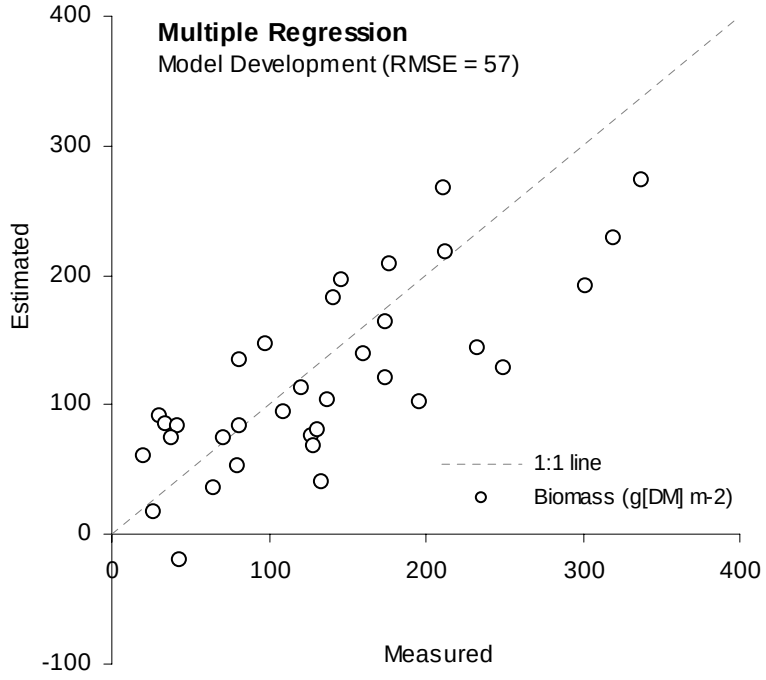

Figure 5-6 Measured and estimated crop biomass using a multiple regression model.

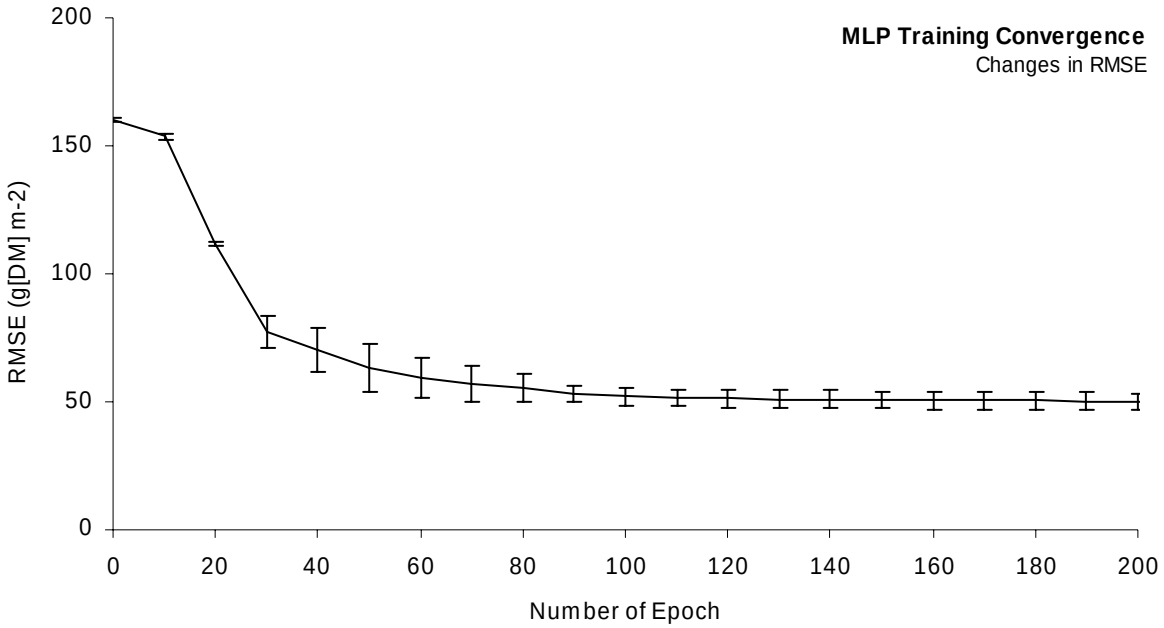

Figure 5-7 Convergence of RMSE from the MLP model training with increasing number of epochs.

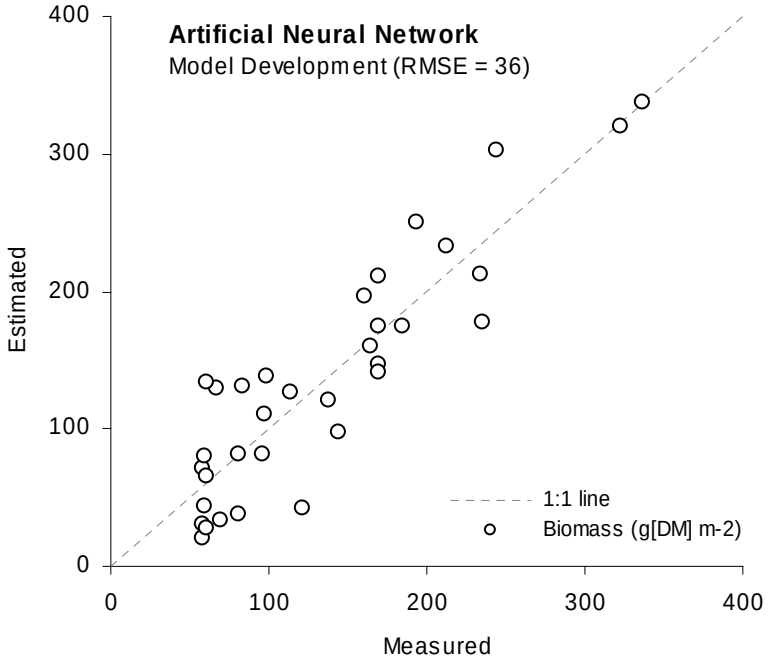

Figure 5-8 Measured and estimated crop biomass using an ANN with MLP model.

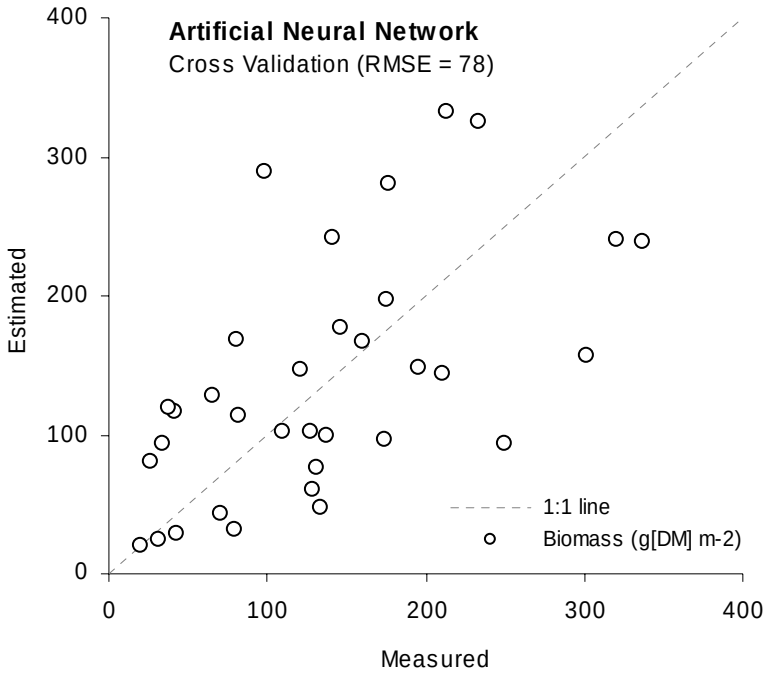

Figure 5-9 Measured and estimated crop biomass from the cross-validation using an ANN with MLP model.

CHAPTER 6
EVALUATION OF USING ENKF TO ESTIMATE SOIL CARBON SEQUESTRATION IN GHANA: CASE STUDY

Introduction

Soil carbon sequestration is defined as "the process of transferring carbon dioxide from the atmosphere into the soil through crop residues and other organic solids, and in a form that is not immediately reemitted." (Sundermeier et al., 2005). Land management practices and the environment affect the changes in soil carbon over time. In agricultural lands, the source of carbon is biomass from crops or wastes from livestock, and thus practices that add or leave more biomass or manure on fields would lead to higher amounts of soil carbon over time and thus carbon sequestration. Practices aimed at sequestering soil carbon are often referred to as a win-win strategy for developing countries to increase agricultural productivity and improve food security while mitigating atmospheric greenhouse gas increase. Lal (2006) reported strong positive effects of soil organic carbon on soil quality, agronomic/biomass productivity, and advancing food security. Especially for degraded soils in dryland agricultural areas in West Africa, soil carbon sequestration can play an important role to improve crop production and prevent soil erosion and desertification (FAO, 2004).

To implement soil carbon sequestration in practice, a reliable soil carbon monitoring system needs to be developed (Antle and Uehara, 2002). Soil carbon may be directly measured on a point-basis, but conducting such *in situ* measurements in a large area where soil carbon varies spatially is cost-prohibitive. In addition, standard errors of *in situ* soil carbon measurements may be several times higher than the change in soil carbon over one to several years at the field scale (Jones et al., 2004), making it difficult to accurately quantify changes in soil carbon over time.

In general, soil processes are spatially correlated. Thus, soil properties can be sampled across the landscape and their values can be regionally estimated and aggregated using spatial interpolation methods, such as kriging (Goovaerts, 1999). Based on the spatial correlation of soil carbon, geostatistical techniques have been suggested to optimize soil carbon measurement schemes (e.g., Conant and Paustian, 2002; Mooney et al., 2004). Mooney (2007) used spatial autocorrelation of soil carbon over landscape to reduce standard errors associated with soil sampling. They reported that confidence intervals were narrowed, which could increase carbon credits by reducing transaction costs in carbon markets. However, because the ultimate source of the soil carbon in agricultural land is crop biomass residues (Farage et al., 2003), soil carbon under different management practices may be highly variable in time even on a relatively small spatial scale. This field-level variability of soil carbon in agricultural lands is an important characteristic that causes the coexistence of multiple spatial structures with different ranges (e.g., Walter et al., 2003; Yost et al., 2002).

The use of biophysical models may be helpful to estimate soil carbon values and changes in soil carbon over time as affected by different weather, soil, and management practices in a field (e.g., Jones et al., 2002; Parton et al., 1988; Parton and Rasmussen, 1994). Most soil carbon models were designed to operate on a field-scale (e.g., Gijsman et al., 2002). These soil models include scale-specific components, such as processes, input data, state variables (Heuvelink, 1998). However, in terms of monitoring soil carbon or carbon sequestration, policy makers need an aggregate estimate of soil carbon over some large area or region (Falloon et al., 1998). Large-scale simulation models can be used to estimate regional soil carbon sequestration potential (e.g., Falloon et al., 1998), but those models may not suitably account for variations in crop production factors and management practices at smaller spatial scales (Schlecht et al. 2006). When model

output is required at a larger scale than the scale at which it operates, aggregation of the model output is necessary. Heuvelink and Pebesma (1999) explored different methods to spatially aggregate outputs from a point-based model. They discussed the options of aggregating inputs to models or running models with point inputs then aggregating model outputs. They concluded that an optimal method would be 1) interpolation of model inputs, 2) site-specific model implementation within the region of interest, and 3) aggregation of model outputs to the desired larger regional scale.

Jones et al. (2006) spatially extended a previously published method that assimilates soil carbon measurements into a dynamic point soil carbon model (Jones et al., 2004) to estimate soil carbon changes over time and space. Using a simple one-pool field-scale soil carbon model (Jones et al., 2004), the study explored the design of a stochastic data assimilation framework using the ensemble Kalman filter for 12 fields in Northern Ghana. They used a sensitivity analysis to evaluate the effects of soil sampling methods and uncertainty in measurements and the model on aggregated soil carbon values. However, this study was based on a relatively simple cropping system and included only a small number of fields with the same field management practices in each field and readily available *in situ* measurements to estimate the initial spatially variable soil carbon and its corresponding uncertainty. In practice, however, cropping systems in Northern Ghana are highly diverse in their crops and management practices and occur in multiple fields with different environmental conditions. Moreover, when resources to make regional *in situ* measurements are limited, initial conditions in all fields may not be readily available.

The overall goal of this study was to assess the potential of using data assimilation taking into account the more realistic spatial variability among fields in a large area than the previous

studies. This study extends the data assimilation method presented in the Jones et al. (2006) study and applies it to a more complex cropping system in large area in northern Ghana. The general objective was to obtain estimates of soil carbon aggregated over many fields when there are limited and uncertain *in situ* measurements in time and space, The specific objective of this study was to assess the ensemble Kalman filter assimilation approach by comparing its soil carbon estimates and associated uncertainties with those based solely on *in situ* measurements of soil carbon in a subset of fields and spatial interpolation of values for fields that are not measured. A total of 132 fields in Northern Ghana were used in the study for comparing the two methods, which used *in situ* measured initial soil carbon in each field and *in silico* generated measurements in a subset of the fields, simulated over a 20-year time period.

Materials and Methods

Study Area

The study area was about 18 km^2 and is located south of Wa, Upper Western Region of Ghana (Latitude: 9.89 and 10.12, Longitude: -2.58 and -2.50) (Figure 6-1). Crop production provides the main source of household income in the area, and the average farm size is about 1 ha (Braimoh and Vlek, 2004). The climate is classified as a "Aw" type (dry winter region) with one pronounced rainy season (Osei and Aryeetey-Attoh, 1997). Average annual rainfall (1953-2004) was about 1000 mm, and the rainy season generally started in April and ends in October (J.B. Naab, Savannah Agricultural Research Institute, personal communication, October 2005).

The study area consisted of 132 fields managed by smallholder farmers. The area of each field was not measured, but based on a survey in this region by Braimoh and Vlek (2004). It was assumed that each field was 1 ha in area. Soil analyses of composite samples taken from 132 fields in the study area in April 2006 showed very low soil organic carbon contents in most of the fields, ranged from 0.3% to 1.3% (median value of 0.44%) (Figure 6-2A). Some lowland

fields with frequent floods and compound fields (i.e., fields adjacent to farm households) with routinely applied domestic animal manure showed relatively high soil carbon contents. Soils in the fields were mostly sandy in texture (median sand-sized particle content of 78%) (Figure 6-2B). A positive linear relationship was found between soil carbon content and silt and clay content with the correlation coefficient value of 0.77 (Figure 6-3). The majority of soils were classified as Alfisols (J.B. Naab, Savannah Agricultural Research Institute, personal communication, August 2006).

True and Measured Soil Carbon

As a theoretical case study, this study assumed that recommended management practices (RMP) to enhance soil carbon sequestration would be implemented in the 132 fields for a 20-year simulation time period. In Chapter 3, the RMP scenario had the maximum potential crop productivity as well as the highest soil carbon sequestration. This scenario included no-till practice, inorganic N-fertilization of cereals, and retention of a majority of crop residues in the field. Starting with the *in situ* measured soil carbon content in the 132 fields in 2006 (Figure 6-2A), Chapter 3 simulated soil carbon content and crop biomass production in each of the 132 fields under the RMP scenario over the 20-year period, from 2006 to 2025. In this chapter, it was assumed that those simulated soil carbon changes over time were the *true* soil carbon trajectories. This time series was used to generate a random sequence of *in silico* soil carbon measurements, and to comparatively test the estimation accuracy of two different soil carbon monitoring methods. Simulated cropping systems in 2006 were used as the initial conditions.

Each year, it was assumed that soil carbon measurements were made in 25% of the fields to simulate an *in situ* sampling schedule. This limited number of measured fields was used as an example that could reflect the time and financial constraints that would not allow annual *in situ* measurements in all fields in the entire region. The 25% sampled fields were randomly selected

over the landscape in each year. As an example, Figure 6-4 shows 25% selected fields in 2006. On average, each field was visited about five times throughout the 20-year time period. Measurement error plus sampling error was added to the true value, assuming the error was normally distributed with zero mean. This error was assumed to be 8% of the measured value (see Chapter 4 for more details).

Soil Carbon Monitoring Methods

To monitor soil carbon and estimate soil carbon sequestration with limited *in situ* measurements in time and space, two soil monitoring methods were defined and compared. Firstly, based on the generated *in situ* soil carbon measurements (i.e., the *in computero* measurements in this study) in 25% of fields, Method A used a spatial interpolation method (i.e., cokriging with soil texture) to estimate soil carbon in the other 75% of fields. Measurements (25% of fields) and the spatially interpolated estimates (75% of fields) were then combined to spatially aggregate soil carbon in each year. Secondly, Method B applied a data assimilation method to the same generated *in situ* soil carbon measurement dataset used by Method A in 25% of fields, but it also simulated soil carbon changes all other fields thereby estimating soil carbon all of the 132 fields.

Method A: Spatial Interpolation

Spatial analysis of the 2006 *in situ* soil samples in 132 fields resulted in semivariograms of soil carbon (Figure 6-5A) and soil texture (Figure 6-5B) and the cross variogram of soil carbon and texture (Figure 6-5C) with similar spatial models, each with the same range of 900 m. These spatial structures were used to estimate soil carbon in unmeasured fields. The cokriging method based on the correlated spatial structure between soil carbon and texture provided the best estimates (Figure 6-5C). Since soil texture in each field in the study area was known, soil carbon in the unmeasured fields (75%) was spatially interpolated with soil texture in those fields and

measured soil carbon content in the other 25% of fields using cokriging. Additionally, the following assumptions were made for implementing Method A:

- Field boundary: The boundary of each field was assumed to be known and to remain constant during the subsequent 20-year time period. In this study, the area of each field was assumed to be 1 ha. The field was assumed to be managed homogeneously in all cropping seasons.
- Soil sampling: A composite sampling method with five subsamples was assumed to be used in each field. In the lab, the Walkley-Black (1934) method was used to analyze carbon content of each soil sample. These assumptions were used to the estimate the uncertainty in measured soil carbon values in this study. The bulk density and soil texture data were also assumed to be measured for each of the 132 fields prior to the study and to remain constant over the 20 years.
- Spatial structure: It was assumed that the spatial structures of soil carbon and texture in the study area (Figure 6-5) did not change over the 20-year time period. Cokriging was used in each year for the 75% of fields that were not sampled in an attempt to minimize estimation errors. Estimation errors from kriging and cokriging were compared with *in situ* measurements in the study area in 2006 when soil carbon was measured in all fields. Results showed that the standard deviations estimated by cokriging were significantly lower than those of kriging (α=0.05) (Figure 6-7), even though the estimated soil carbon values were not significantly different from each other (α=0.05) (Figure 6-6). Point cokriging was the method used to estimate soil carbon at the centroid of each field that was not sampled each year using GSTAT 2.4.1 (Pebesma and Wesseling, 1998).
- Soil carbon estimation error: In each year, the standard deviation of soil carbon estimate was calculated differently depending on the availability of *in situ* measurement in a given field.

For a field with *in situ* measurement, the soil carbon measurement error defined in Chapter 4 (i.e., 8% of measured value) was used as the estimation standard deviation. For a field with spatially interpolated soil carbon value, the cokriging standard deviation, which included a nugget that corresponds to soil carbon measurement error, was used. This conditional standard deviation calculation was implemented by defining known variable measurement errors in the cokriging process using GSTAT 2.4.1 (Pebesma and Wesseling, 1998).

Method B: Data Assimilation

Method B used a data assimilation approach (an ensemble Kalman filter, EnKF) to assimilate *in situ* soil carbon measurements with model-estimated values using a simple soil carbon model. With a yearly time step, the model can be represented in the following equations:

$$X(z_i,t)_m = X(z_i,t-1)_m - R(z_i)_m \cdot X(z_i,t-1)_m + b \cdot U(z_i,t-1) + \varepsilon_X(z_i,t)_m \quad (6\text{-}1)$$

$$R(z_i)_m = R_0(z_i)_m + \varepsilon_R(z_i)_m \quad (6\text{-}2)$$

where $X(z_i,t)_m$ is the m^{th} ensemble replicate of soil carbon state in a field located at z_i in year *t*, $R(z_i)_m$ is the m^{th} replicate of soil carbon decomposition rate parameter at z_i, $R_0(z_i)_m$ is the initial estimate of $R(z_i)_m$, b is the fraction of fresh organic carbon added to the soil carbon pool and remains after one year, $U(z_i,t-1)$ is the amount of crop residue added to the soil at z_i in year *t*-1, and the $\varepsilon_X(z_i,t)_m$ and $\varepsilon_R(z_i,t)_m$ are the model error and the error in the initial estimate of *R*, respectively, and they are assume to be normally distributed following (Jones et al., 2007):

$$\varepsilon_X(z_i,t)_m \sim N\left(0, \mathrm{Var}(\varepsilon_X)\right) \quad (6\text{-}3)$$

$$\varepsilon_R(z_i,t)_m \sim N\left(0, \mathrm{Var}(\varepsilon_R)\right) \quad (6\text{-}4)$$

where $\mathrm{Var}(\varepsilon_X)$ and $\mathrm{Var}(\varepsilon_R)$ are the variances of model prediction error for soil carbon change in one year and of estimation error for *R*, respectively. To be used as the best estimate of soil carbon for a given field in each time step, an ensemble mean was calculated as:

$$\hat{X}(z_i,t) = \frac{\sum_{m=1}^{N} X(z_i,t)_m}{N} \qquad (6\text{-}5)$$

where *N* is the size of the ensemble. The standard deviation of $\hat{X}(z_i,t)$ was estimated by calculating the ensemble standard deviation. A complete description of the EnKF method using this simple model is given by Jones et al. (2004; 2007).

The same *in situ* soil measurement data and the soil sampling scheme described in the Method A section (i.e., annual *in situ* measurement in 25% of fields, including the initial year) provided input data to the EnKF. For the 75% of fields not measured in the initial year, cokriging-estimates were used to initialize soil carbon for the EnKF. The following assumptions were additionally made:

- Uncertainty in measuring soil carbon: When an *in situ* soil carbon measurement was made in a specific field, its measurement error was assumed to be 8% of the measured value (see Chapter 4 for more details).
- Uncertainty in modeling soil carbon: Following the discussion of Jones et al. (2004) on the physical limits on how much soil carbon can be newly added or decomposed annually, the soil carbon model error was assumed to be 1% of the predicted value (see Chapter 4 for more details).
- Crop biomass production: For each crop species cultivated in the area, its average biomass production under the recommended management practices was assumed to be known from other studies in the study area (e.g., from *in situ* measurements and/or estimates using remote

sensing). In this study, preliminarily simulated crop systems in the study area under the RMP scenario for a 20-year period in the past were used to calculate average biomass production for each crop species (Table 6-1). This value was used for all fields with that particular crop in each year. We assumed that the crop species growing in the fields were known. For example, a high-resolution remote sensing image around the peak crop biomass production in every cropping season could be used to classify crop species in each field. Since estimation error for the crop biomass production in each field would affect the estimation accuracy of soil carbon, the soil carbon model error was assumed to include the uncertainty associated with crop biomass estimation errors. The carbon fraction of the crop biomass was assumed to be 40% (Jones et al., 2004).

– Calibrating model parameters: Two model parameters, the initial soil decomposition parameter ($R_0(z_i)_m$ in Equation 6-2) and the crop residue fraction parameter (b in Equation 6-1) were required in the model (Jones et al., 2006), but their values were unknown. For $R_0(z_i)_m$, the initial value of *R* used by Jones et al. (2004), 0.01, was used as an *a priori* estimate for the study area. The value of *b* may be calibrated in reality if: 1) there are available *in situ* soil carbon and crop biomass measurement data for a representative field in the past, and 2) those measured soil carbon and crop biomass values are used to find a value of *b* that minimized the root mean square error (RMSE) between measured and modeled soil carbon values. In this study, *in computero* generated soil carbon measurement (i.e., the simulated results under the RMP scenario plus randomly generated measurement errors) and crop biomass estimations (i.e., estimated values based on the simulated crop species classification) with an independent weather dataset for a representative field were used. The *Excel Solver* software (Microsoft Corporation, http://microsoft.com/excel) was used in the

calibration process. The dataset used in the calibration process and results are shown in Figure 6-8. The calibrated value, 0.01, was used as the initial estimate of *R* in all fields. Physically, the calibrated initial *R* value of 0.01 represented that annually about 1% of the total soil carbon is decomposed. In a previous study, Jones et al. (2004) used 0.02 (2%) as the base-case scenario value. The low value of this decomposition parameter value implied that most of the carbon in the soil was stable and not readily decomposable (Brady and Weil, 2002). Although the calibrated initial value may not represent the actual value in all fields, yearly filter-updated values of *R* for each field were expected to improve the accuracy of estimates. As a result, values should converge to their correct values over time. Uncertainty of the initial *R* estimate was assumed to be 25% of the estimated value with a Gaussian distribution.

– Ensemble size: When values of all the model and filter parameters were selected, an appropriate ensemble size was determined by using a sensitivity analysis in which a comparison was made of the effect of ensemble size on ensemble standard deviation. The ensemble size was varied from 100 to 2000. The relative sensitivity of the ensemble standard deviation for each field in each year to the increment of ensemble size was calculated as follows:

$$Sensitivity = \frac{\left|\sigma_{X,N_2} - \sigma_{X,N_1}\right|}{100} \qquad (6\text{-}6)$$

where $N_2 = N_1 + 100$ and σ_{X,N_1} and σ_{X,N_2} were the ensemble standard deviations of soil carbon estimates with the ensemble sizes of N_1 and N_2, respectively. With a preset sensitivity threshold value of 5%, the size of ensemble beyond which the sensitivity values did not

exceed the threshold value was estimated to be $N = 1500$ (Figure 6-9). This is the number of ensemble members that was used in the EnKF.

Aggregating Soil Carbon Estimates

For each soil carbon monitoring method, an estimated regional aggregate of soil carbon in year t, $\hat{A}(t)$, was estimated by summing the estimated soil carbon in each field across all 132 fields as follows:

$$\hat{A}(t) = \sum_{i=1}^{f} \hat{X}(z_i, t) \tag{6-7}$$

where $\hat{X}(z_i, t)$ is a soil carbon estimate at field z_i in year t (i.e., Method A: cokriging-estimated soil carbon value, Method B: ensemble mean as shown in Equation 6-5) and f is the number of fields (i.e., 132). The estimation variance of the aggregate soil carbon value, $Var\left[\hat{A}(t)\right]$, was estimated by adding the estimation variance in each field along with covariances across fields as follows:

$$Var\left[\hat{A}(t)\right] = \sum_{i=1}^{f} Var\left[\hat{X}(z_i, t)\right] + 2\underbrace{\sum\sum Cov\left[\hat{X}(z_i, t), \hat{X}(z_j, t)\right]}_{i<j} \tag{6-8}$$

where $Var\left[\hat{X}(z_i, t)\right]$ is the soil carbon estimation variance (i.e., Method A: soil carbon measurement variances for measured fields and cokriging variances for unmeasured fields, Method B: ensemble variance) at field z_i in year t and $Cov\left[\hat{X}(z_i, t), \hat{X}(z_j, t)\right]$ is the soil carbon estimation covariance between fields z_i and z_j in year t.

A covariance matrix of soil carbon across 132 fields was required for $Cov\left[\hat{X}(z_i, t), \hat{X}(z_j, t)\right]$ in Equation 6-8. In each year, the covariance matrix was calculated differently depending on the soil carbon monitoring method. For Method A, a covariance matrix of soil carbon over all fields

was calculated from an ensemble of soil carbon realizations (N=1500) with $\hat{X}(z_i,t)$ and $Var\left[\hat{X}(z_i,t)\right]$, assuming measurement errors are normally distributed. For Method B, an ensemble of filter-updated soil carbon over all fields in year t was used.

Performance Analysis

The EnKF provides estimates of uncertainties in soil carbon estimates for each field and year. The standard deviation values of soil carbon estimates obtained from the EnKF were analyzed vs. time. In addition, an error estimate for each method was computed to provide an estimate of the accuracy of each approach. This was done by calculating the RMSE between estimated and true values for each approach over the simulation time period. The RMSE was first calculated for each field, and a field with the median RMSE value for Method B was selected to analyze the estimation accuracy of each approach at a field-level. The RMSE in each field was calculated with the following equation:

$$RMSE = \sqrt{\frac{\sum_{t=1}^{n}\left[\hat{X}(z_i,t) - X(z_i,t)\right]^2}{n}} \tag{6-9}$$

where $\hat{X}(z_i,t)$ is the estimated soil carbon at field z_i in year t, $X(z_i,t)$ is the true soil carbon at field z_i in year t, and n is the number of simulated years (i.e., 19 years, from 2007 to 2025). Then, the RMSE of each method was also calculated for the regionally aggregated soil carbon and compared as follows:

$$RMSE = \sqrt{\frac{\sum_{t=1}^{n}\left[\hat{A}(t) - A(t)\right]^2}{n}} \tag{6-10}$$

where $A(t)$ is the true estimate of regionally aggregated soil carbon in year t.

Estimating Soil Carbon Sequestration

In each field, a base-line soil organic carbon value was estimated for the 20-year time period. This value is indicative of the amount of soil organic carbon stock that would have occurred if the recommended management practices were not adopted. In this study, simulated soil carbon in each field under the business-as-usual management scenario in Chapter 3 was used as the base-line value. Then, soil carbon sequestration in each field was estimated by subtracting the base-line value for a given field in a given year from the estimated soil carbon value for the RMP scenario. Assuming the base-value was exact in this study, the uncertainty associated with the estimated soil carbon sequestration was thus identical to that of the soil carbon estimate in a given field. Although the base-value may not be known in practice, errors associated with the base-value did not influence the comparative analysis between two soil carbon monitoring methods.

Mean soil carbon sequestration rate (i.e., estimated amount of soil carbon annually sequestered per unit area) in a given year was calculated as follows:

$$\text{Mean Sequestration Rate} = \frac{\left[\hat{X}(t_0+n)-\hat{X}(t_0)\right]-\left[X_B(t_0+n)-X_B(t_0)\right]}{n} \qquad (6\text{-}10)$$

where $\hat{X}(t)$ is the estimated soil carbon per unit area in year t, $X_B(z_i,t)$ is the base-line soil carbon per unit area in year t, t_0 is the initial year (i.e., 2006), and n is the number of years elapsed since the initial year. For Method B, the value of $\hat{X}(2006)$ was assumed to be same as that of Method A, as Method B estimated soil carbon values from 2007 using the estimated soil carbon from Method A in 2006 as the initial value. After a number of years occur (e.g., more than 6 years), one could also use linear regression to estimate mean sequestration rate over those

years. This could be done for both Method A and Method B, possibly improving each method. However, this approach was not evaluated in this study.

Results and Discussion

Field-Level Performance

First, the performance of each field is discussed using the RMSE estimates based on deviations of soil carbon relative to true values (Equation 6-10). When the RMSE values of estimated soil carbon for the 20-year time period for each field were analyzed, their distributions over 132 fields showed that RMSE values for Method A were higher than those for Method B, and the difference was significant (α=0.05) (Figure 6-10). When correlated with the number of *in situ* measurements made in each field, it was shown that, in general, the RMSE decreased as more *in situ* measurements were available for both methods (Figure 6-11). This shows that repeated measurements in a given field over time would improve estimation accuracy. In Method B, a field with the median RMSE value was W165 (RMSE = 0.9 Mg[SOC] ha^{-1}); this field was used as a representative field in the comparison.

True and estimated soil carbon from Method A for the field W165 are presented in Figure 6-12A. For this particular field, measurements were made four times (in 2007, 2015, 2017, and 2021) during the 20-year time period. In those years, estimated soil carbon from Method A were relatively close to true values (RMSE = 1.4 Mg[SOC] ha^{-1}) in contrast to the other years when estimates for this field were made by using cokriging to spatially interpolate values (RMSE = 2.2 Mg[SOC] ha^{-1}). Overall, the RMSE was about 2.0 Mg[SOC] ha^{-1} for the 20-year time period. However, it was noted that the spatially interpolated soil carbon values were overestimated in most years. For example in 2016, true soil carbon was 12 Mg[SOC] ha^{-1}, but the interpolated value was 14 Mg[SOC] ha^{-1}. Such overestimations may be the result of soil carbon measurements in nearby fields within the spatial correlation range, whose soil carbon levels were

higher than that of W165. For example, there were three fields with soil carbon measurements within the correlation range of 900 m of this field (W019, W032, and W021) in 2016. Their measured values were all higher than the true value of W165 in 2016 and averaged 15 Mg[SOC] ha^{-1}. Unlike a biophysical model-based approach, this spatial interpolation method does not take into account temporal correlation in soil C. Thus errors in estimated values may be high for variables that are temporally correlated in nature when this is not considered in the estimation method. In years when measurements were not available, the standard deviations of estimated soil carbon over time were highly variable and unstable (Figure 6-12B). The average standard deviation was about 1 Mg[SOC] ha^{-1} and 3 Mg[SOC] ha^{-1}, in years with and without measurements, respectively. There was no distinctive pattern in the standard deviations with time.

Compared to the estimates obtained using Method A, estimates made using the EnKF were closer to truth (Figure 6-12A) with smaller standard deviations (Figure 6-12B) throughout the 20-year simulation time period regardless of when measurements were made. The RMSE between estimated and true soil carbon was about 1 Mg[SOC] ha^{-1}. Unlike the mostly overestimated estimates of Method A, Method B underestimated soil carbon in some years and overestimated it in others (Figure 6-12A). This result may be caused by other uncertainties in the model, such as crop biomass and soil carbon decomposition parameter. For example, in between 2015 and 2020 when peanut was cultivated continuously in this field, underestimations were more distinctive (see Chapter 3). In the true values obtained from the more complex model, soil carbon may have been more positively influenced from the continuous legume cultivations. However, the simple model does not take these details into account and model parameter values were assumed to be constant over time.

Standard deviations for estimates from Method B were consistently lower than those from Method A. Initially in 2007, however, the standard deviation of estimated carbon from Method B was as high as that of Method A. This occurred because, for this particular field (W165), *in situ* measurements were not made until 2008. Thus, the ensemble Kalman filter used in Method B updated soil carbon estimate in this field based on measurements made in other fields, whose spatial correlations with this field were not strong, in 2007. The standard deviations rapidly dropped in 2008 when the first measurement was made. In following years, the standard deviations remained low even in years with no measurements.

Regional-Level Performance

Regionally, the aggregate soil carbon estimate (summation of estimated soil carbon over 132 1-ha fields) from Method A were relatively unstable (Figure 6-13A) with higher estimated standard deviations (Figure 6-13B) in comparison with Method B. Overall, the RMSE between estimated and true soil carbon values was about 44 Mg[SOC] region^{-1} yr^{-1} for Method A. There were some years with large underestimates (e.g., 2008) and overestimates (e.g., 2020) (Figure 6-13A). As the measurement scheme randomly selected 25% of fields per year, such biases in the estimates may be due to relatively lower or higher soil carbon in selected fields measured in those years. When soil carbon in the measured fields were averaged and compared with truth, annually fluctuating biases in the measurements were seen (Figure 6-14). For example, in 2008, true soil carbon in 132 fields averaged 14.6 Mg[SOC] ha^{-1}, but the average soil carbon in the 33 of 132 measured fields was 13.8 Mg[SOC] ha^{-1}. Likewise in 2020, true soil carbon in 132 fields averaged 15.6 Mg[SOC] ha^{-1}, but the average soil carbon in the 33 measured fields was 17.1 Mg[SOC] ha^{-1}. Although fields measured in each year were randomly selected, biases in the magnitude of soil carbon measurements in a given year may still exist due to the heterogeneous

soil carbon distribution within the overall landscape. As shown for the field-level analysis, the spatially interpolated estimates are influenced by this heterogeneity.

Soil carbon estimates from Method B were closer to truth than Method A (Figure 6-13A). The RMSE between the estimated and true soil carbon for the overall simulation time period of 19 years (i.e., from 2007 to 2025) was calculated using Equation 6-10, and its value for Method B was 29 Mg[SOC] region^{-1} yr^{-1}, which was about 38% less than that of Method A, which was 46 Mg[SOC] region^{-1} yr^{-1}. When the standard deviations for the aggregated estimations from two methods were calculated (Equation 6-8) and compared, the values from Method B were consistently lower and more stable than those of Method A throughout the time period (Figure 6-13B). This result confirmed that the data assimilation approach (Method B) improved the accuracy of soil carbon estimates compared to the measurement-based spatially interpolated estimates from Method A.

Estimating Soil Carbon Sequestration

Base-line soil carbon changes during the 20-year time period (Business-As-Usual in Figure 6-15A) were subtracted from the estimated soil carbon values from estimates in which RMP management was assumed, using both methods (Figure 6-15A) to estimate changes in soil carbon sequestration values (Figure 6-15B). Over the 20-year time period, changes in soil carbon sequestration were nearly linear with time (Figure 6-15B). As a result, true annual soil carbon sequestration rate per unit area was relatively stable, especially for the second half of the time period (i.e., between 2016 and 2025) (Figure 6-16). Relatively low soil carbon sequestration rates in initial years (truth) may be the result of slow mineralization of organic matter under no-till practices in those years (see Chapter 3). Overall, true soil carbon sequestration rate for the 20-year time period was 173 kg[SOC] ha^{-1} yr^{-1}, when it was calculated in 2025.

Comparing the two soil carbon estimation methods, soil carbon sequestration rate from Method A had higher variability than Method B over time (Figure 6-16). Depending on which year the rate was calculated, the estimated soil carbon sequestration rates were overestimated (e.g., 208 kg[SOC] ha^{-1} yr^{-1} in 2020) or underestimated (e.g. 114 kg[SOC] ha^{-1} yr^{-1} in 2022) showing instability as shown in Figure 6-15A. However, in 2025, estimated soil carbon sequestration rate was 161 kg[SOC] ha^{-1} yr^{-1}, which was randomly close to the true rate for that particular year (i.e., 173 kg[SOC] ha^{-1} yr^{-1}), differing by about 7%). However, its standard deviation was 187 kg[SOC] ha^{-1} yr^{-1}, higher than the estimated mean rate (Figure 6-17). Compared to Method A, Method B estimated more stable soil carbon sequestration rates throughout the time period (Figure 6-16). The RMSE values between true and estimated soil carbon sequestration rates from Method A and Method B were 86 kg[SOC] ha^{-1} yr^{-1} and 35 kg[SOC] ha^{-1} yr^{-1}, respectively, for the 20-year time period. However, as shown in Figure 6-15, underestimates in soil carbon occurred between 2015 and 2025, which resulted in underestimated sequestration rates in those years as well. At the end of the 20-year time period, Method B estimated soil carbon sequestration rate as 155 kg[SOC] ha^{-1} yr^{-1} in 2025, about 11% lower than the true rate. The standard deviation of the estimated rate was 87 kg[SOC] ha^{-1} yr^{-1}, about 50% lower than that of Method A (Figure 6-17).

Conclusion

To regionally monitor soil carbon and soil carbon sequestration, two approaches were compared, a spatial interpolation method (Method A) and a data assimilation method (Method B). Based on *in situ* measured initial conditions and *in computero* generated truth, and randomly generated measurements of soil carbon, the two methods were analyzed for a study area in Northern Ghana over a 20-year time period. Comparative analysis of estimations showed, in

general, a superior estimation accuracy with less uncertainty when using the EnKF data assimilation method relative to the spatial interpolation method.

With annual soil carbon measurements made in 25% of randomly selected fields, estimation accuracy of the spatial interpolation method (Method A) was affected by biases that occurred when different fields were randomly sampled. Because this method is based on spatial correlations among fields within a particular distance, interpolated carbon in a given field and year was influenced by measurements made in nearby fields. In this method, temporal correlation of soil carbon that occurs in nature is not taken into account. In contrast, the EnKF data assimilation method (Method B) used an underlying biophysical model to estimate soil carbon changes in time, thus constraining estimates over time and creating temporal persistence in soil carbon estimates. As an alternate approach to Method A, a temporal regression method could be used with measurements and co-kriging. For example, a linear regression could be conducted using soil carbon estimates from Method A in Figure 6-13A over the 20-year time period to reduce annual variability in estimates.

Compared with the previous study by Jones et al. (2006), this study showed the potential of using a data assimilation framework to monitor regional soil carbon based on more complex cropping systems in a larger area. In reality, however, assumptions made in this theoretical study may be still idealistic compared to reality (e.g., fixed field boundary, simple one-pool soil carbon model, constant crop biomass production for each crop species, and no uncertainty in base-line soil carbon values). Improvements in those assumptions may be made to perform a more robust test. For example, the one-pool soil carbon model may be replaced by a model with two pools (e.g., labile and stable pools) to take into account different decomposition rates for different types of organic matter in soils (e.g., Bostick et al., 2007). Nevertheless, when two proposed

approaches are compared as in this study, the main result (i.e., more accurate estimations with a data assimilation method relative to a spatial interpolation method) is not likely to change, although the estimation accuracy can be enhanced when uncertainties in measurements and model inputs are reduced. Because *in situ* measurements are uncertain and limited in time and space, as they are in most cases in reality, a data assimilation method will provide more accurate soil carbon estimation by incorporating temporal and spatial correlations of soil carbon.

Table 6-1 Average crop aboveground vegetative biomass production over 132 fields in the study area for 20 years (simulated results adopted from Chapter 3)

Crop Species	Aboveground Vegetative Biomass (kg/ha)
Sorghum	2882
Maize	7570
Millet	8079
Peanut	4067
Bush fallow	3637

Figure 6-1 Location of study site, Wa, Ghana, in West Africa (Latitude: 10.02, Longitude: -2.38). Satellite image and the country boundary was generated by Google Earth™ Mapping Service (http://earth.google.com).

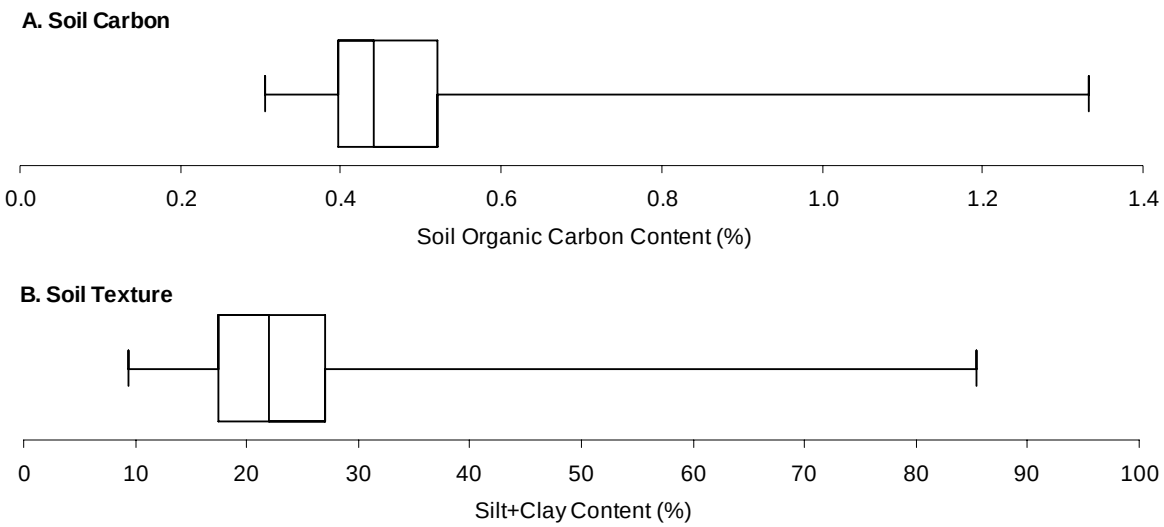

Figure 6-2 Percentile charts of soil carbon content and soil texture of 132 fields in the study area in Wa, Ghana. Composite soil sample in each field was taken in April 2006 and measured by J.B. Naab (Savannah Agricultural Research Institute, personal communication, August 2006).

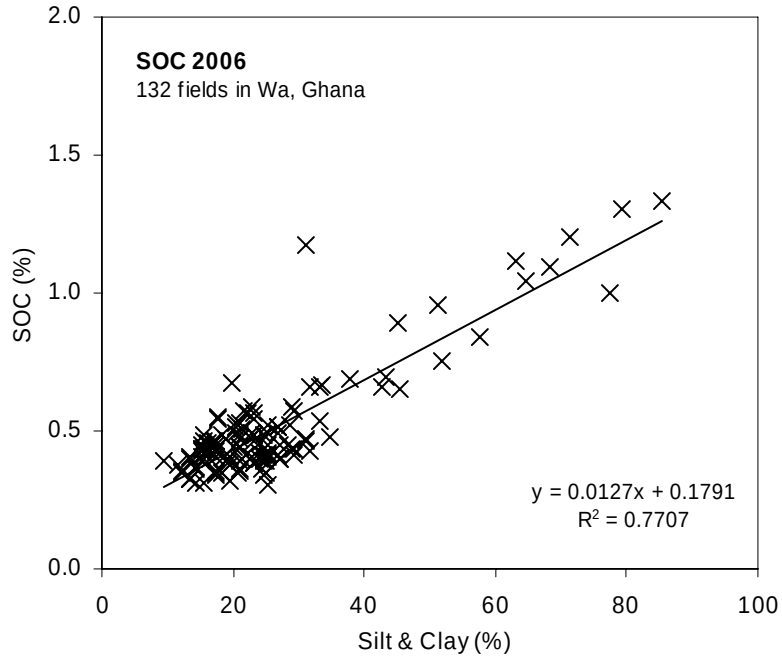

Figure 6-3 Linear relationship of soil carbon content (SOC) and soil texture (silt and clay content) based on *in situ* measurements in 132 fields in the study area in 2006.

Figure 6-4 Fields selected to measure soil carbon in 2006 (25%, or 33 of 132 fields).

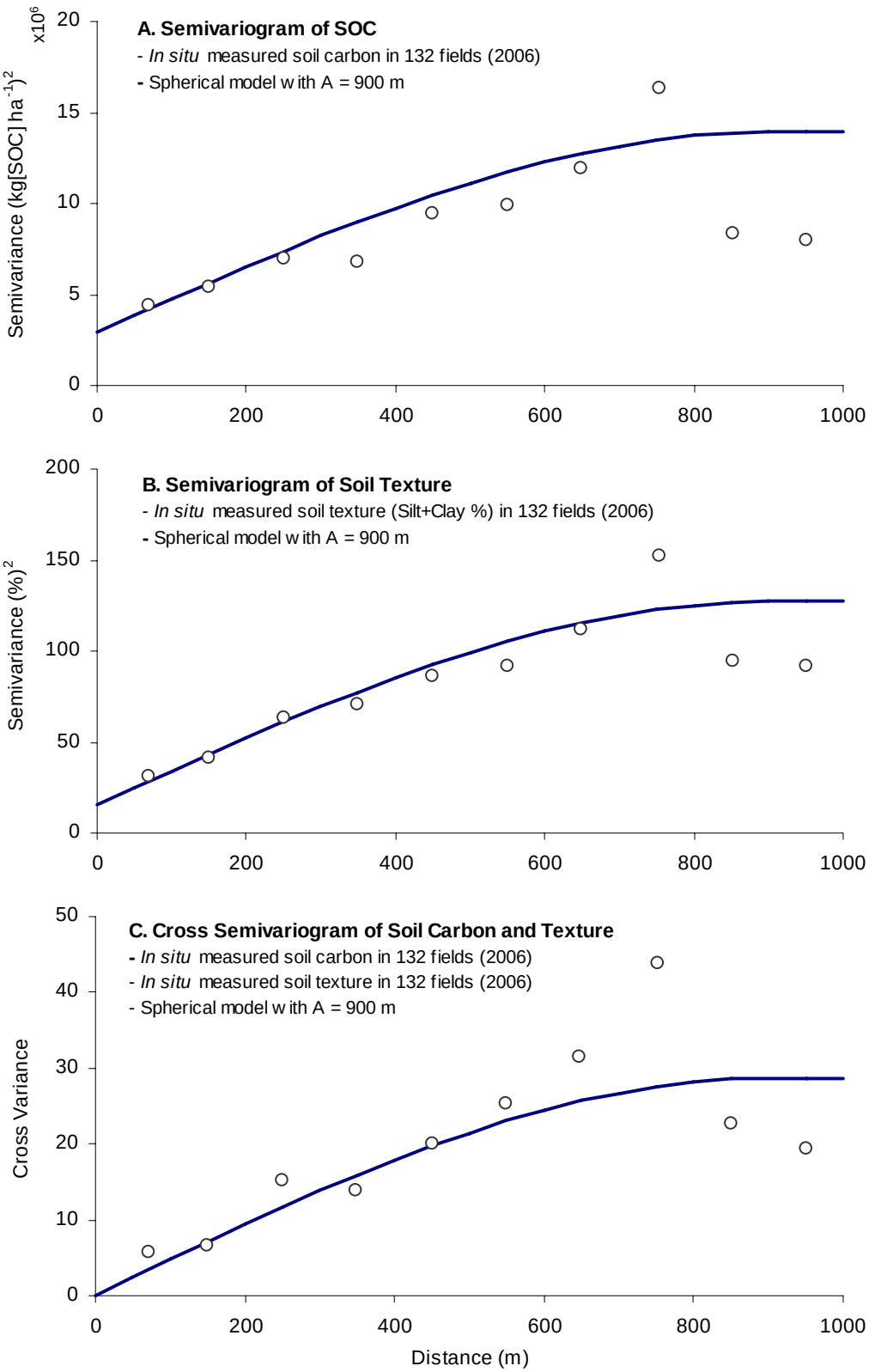

Figure 6-5 Spatial structures analyzed with *in situ* soil carbon and texture measurements in 2006

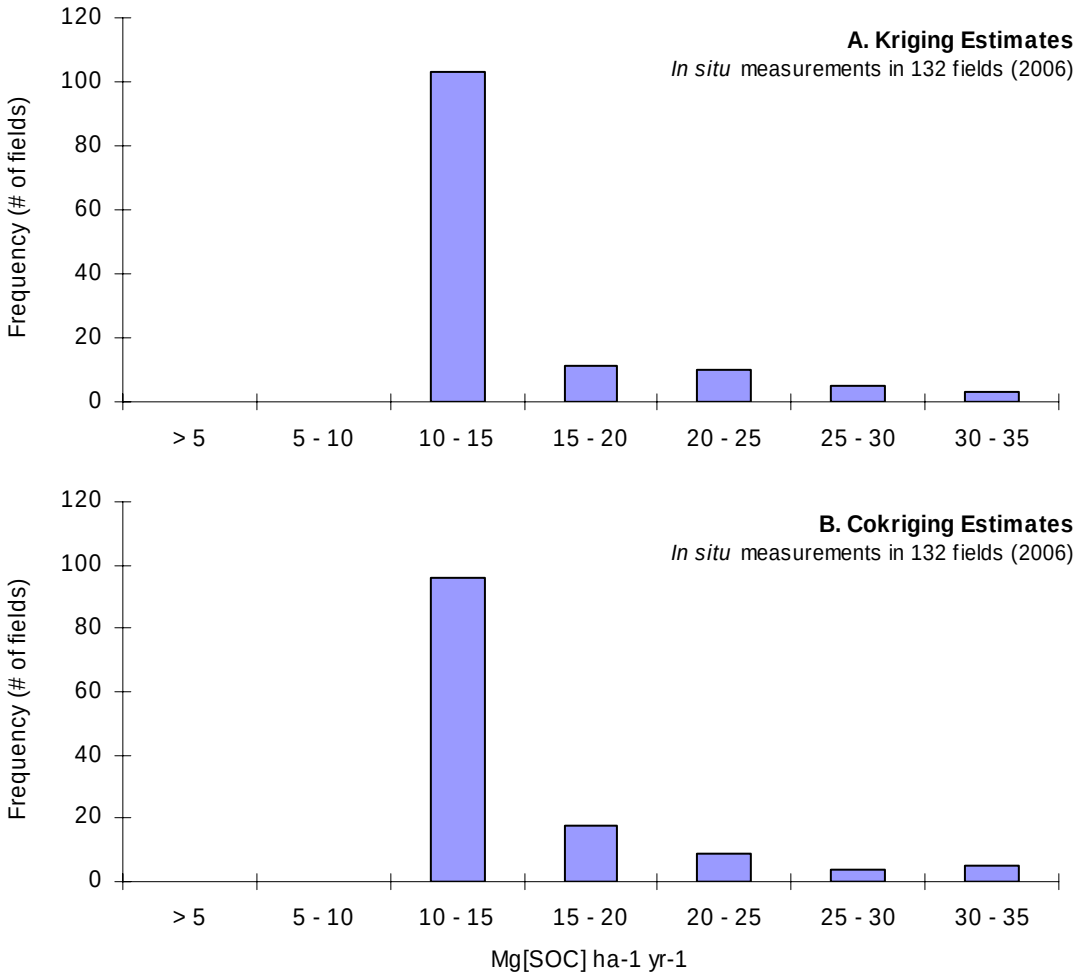

Figure 6-6 Spatially interpolated estimates in 132 fields in the study area by A) kriging and B) cokriging with soil texture in 2006.

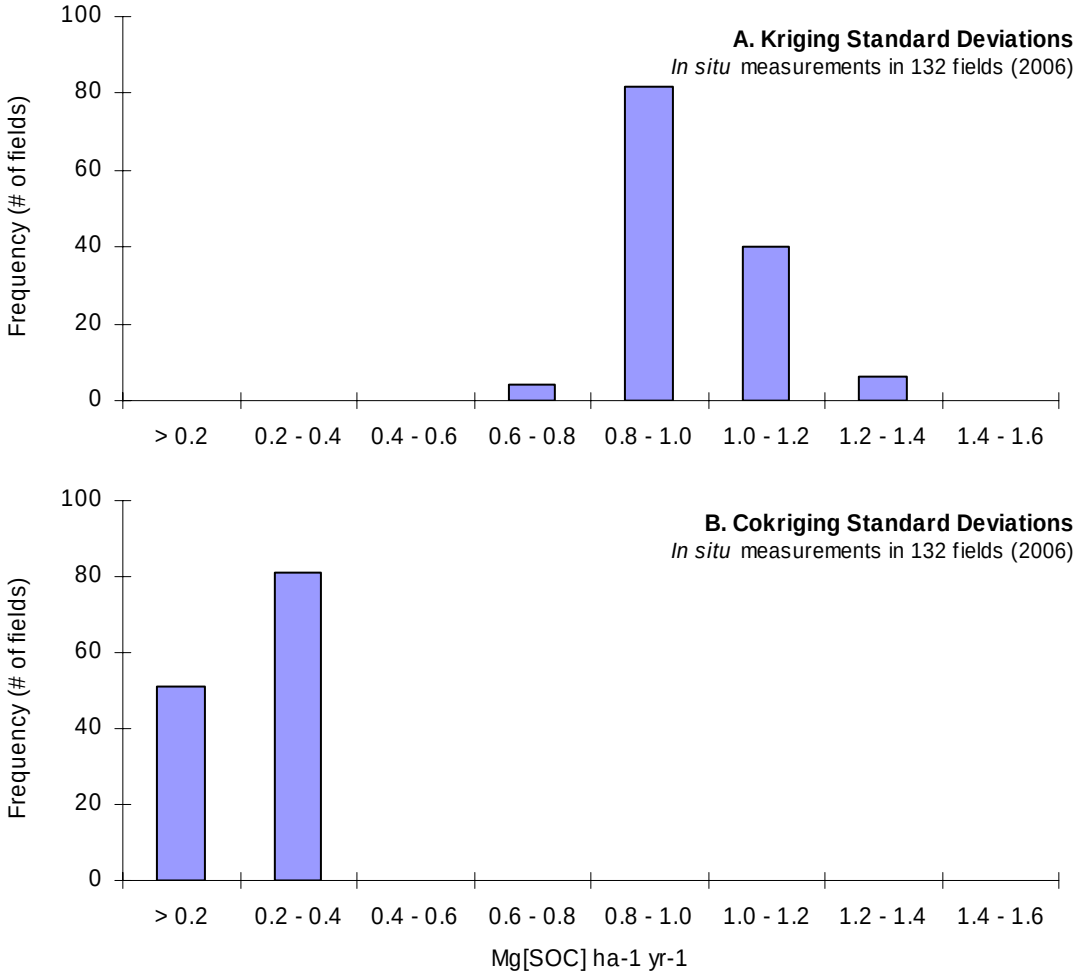

Figure 6-7 Standard deviations for spatially interpolated estimates in 132 fields in the study area by (A) kriging and (B) cokriging with soil texture in 2006.

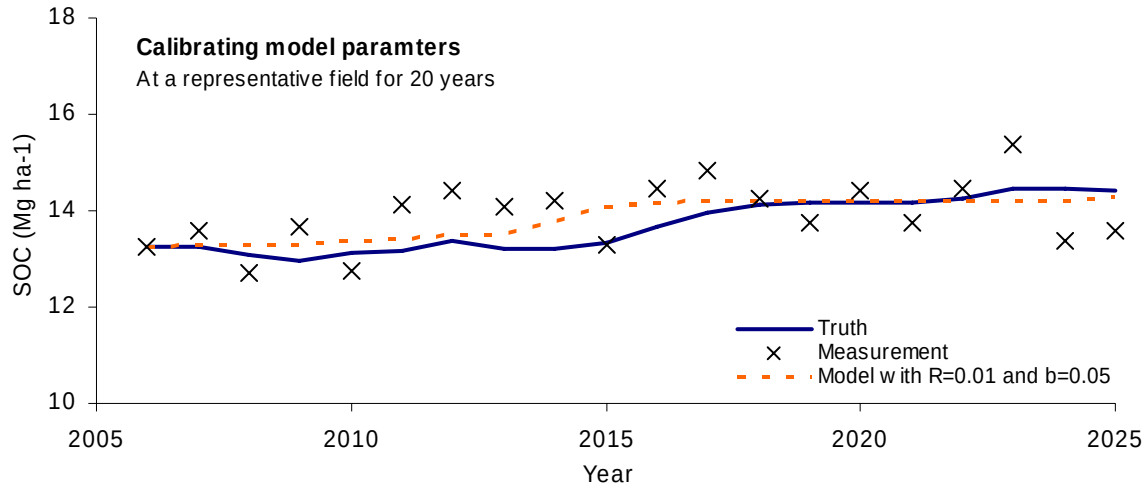

Figure 6-8 Truth, measured, and modeled soil organic carbon at a representative field for 20 years. Modeled soil organic carbon used calibrated parameter values that minimized the RMSE with measured values.

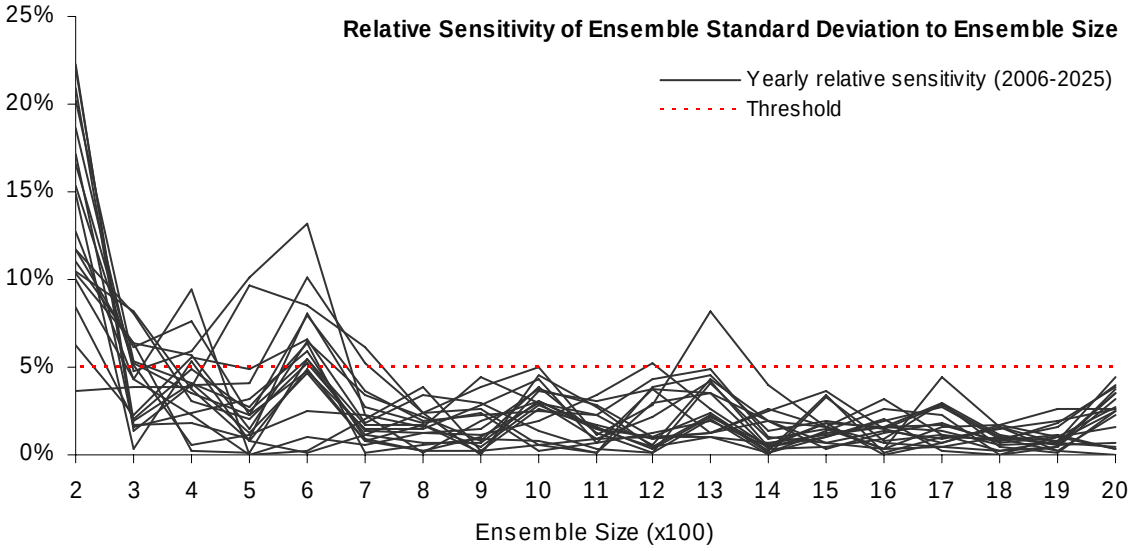

Figure 6-9 Relative sensitivity of the ensemble standard deviation to the ensemble size for estimating soil carbon in 132 fields for each year. Each line represents changes of the relative sensitivity for each year.

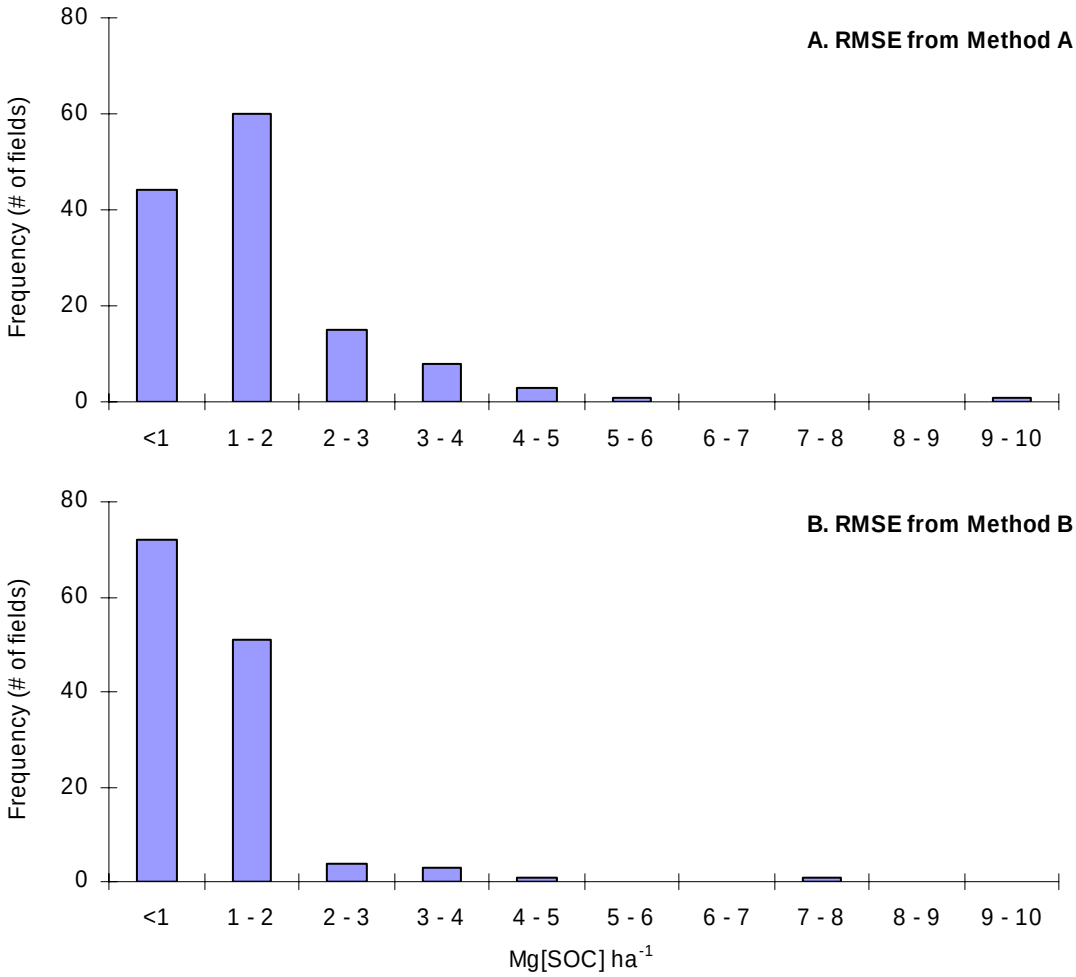

Figure 6-10 Histograms of the root mean square error values calculated for each of 132 fields with two methods for 20 years

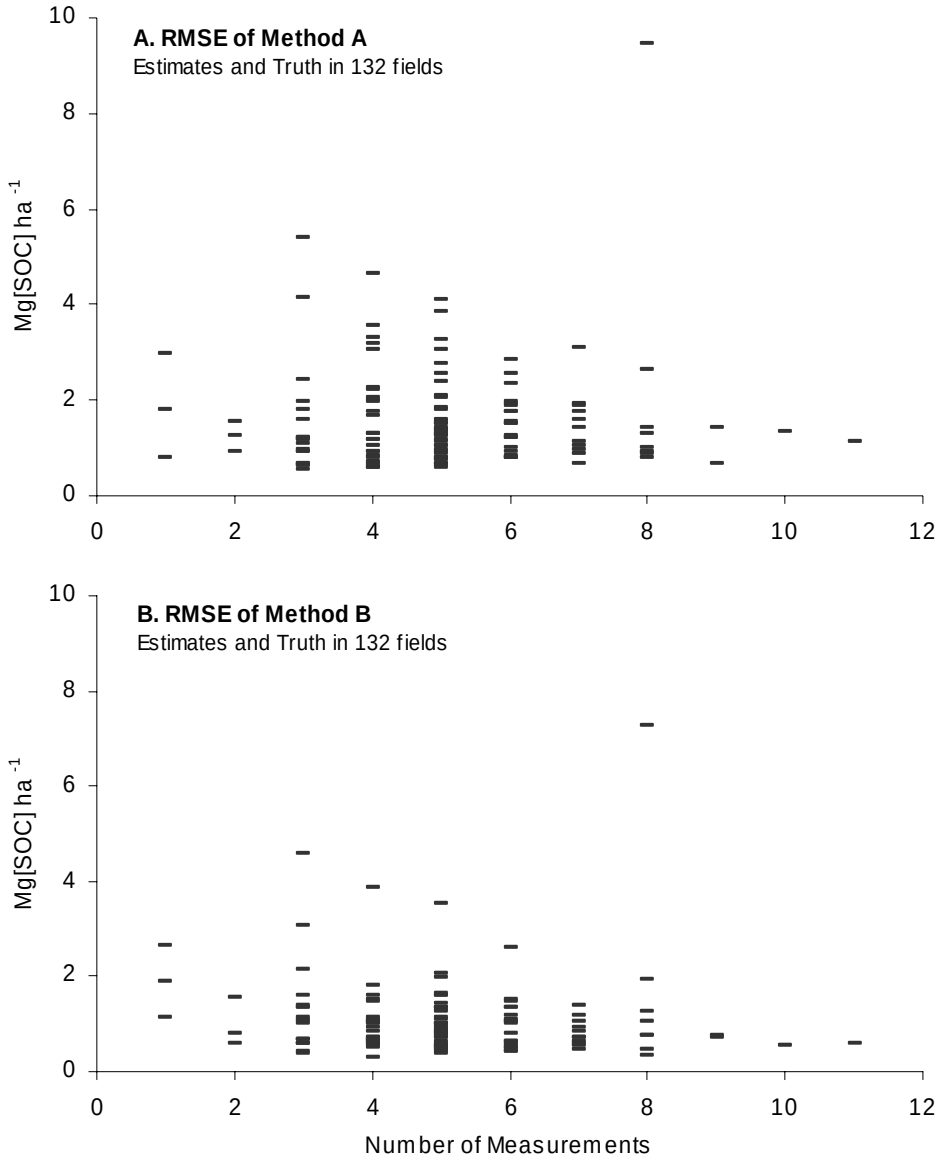

Figure 6-11 Distributions of RMSE values between true and estimated soil carbon in 132 fields from two methods, correlated with the number of *in situ* measurements made during the 20-year time period.

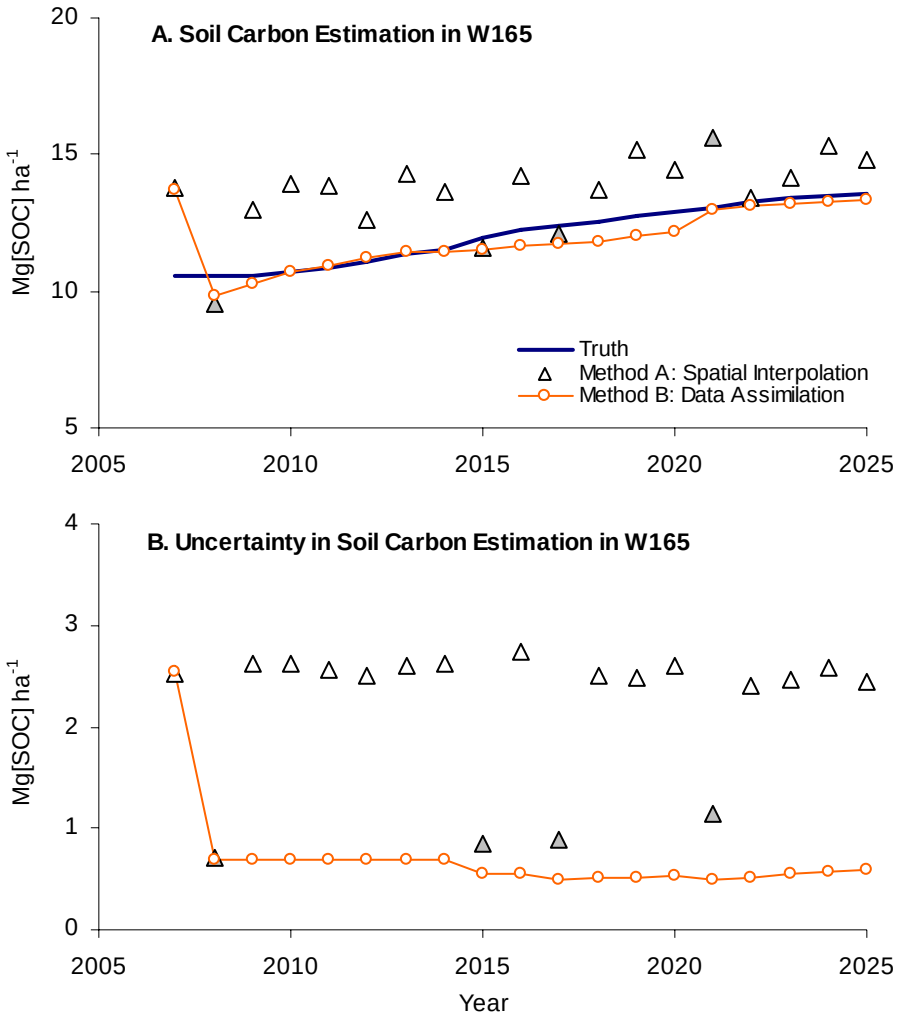

Figure 6-12 True and estimated soil carbon using two methods at a field with the median RMSE value between truth and estimations made with Method B. Filled triangles represent *in situ* measurements and corresponding measurement uncertainty. Hollow triangles represent spatially interpolated soil carbon using cokriging and cokriging standard deviations.

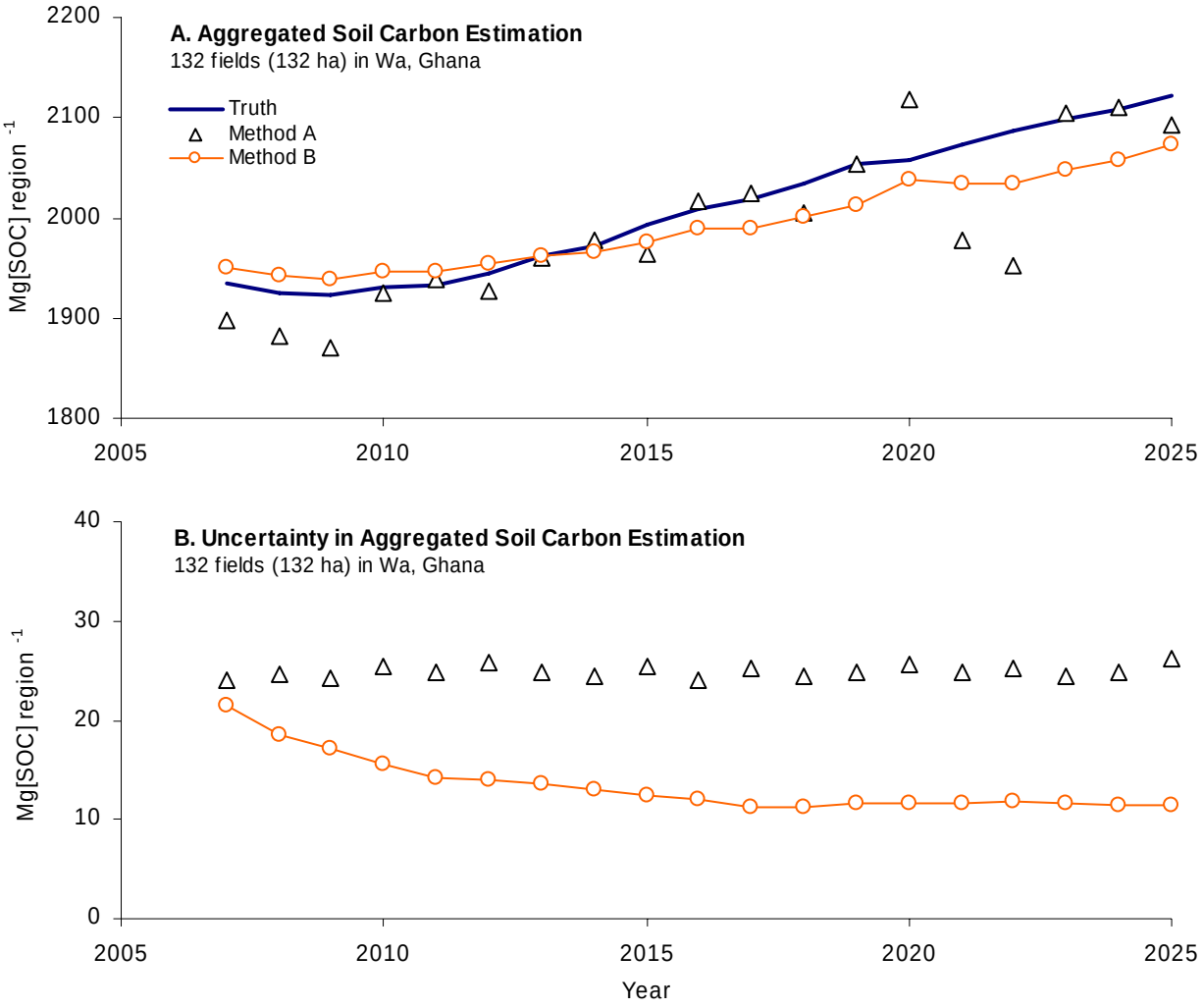

Figure 6-13 Regionally aggregated soil carbon estimated for 132 fields in the study area by two different methods.

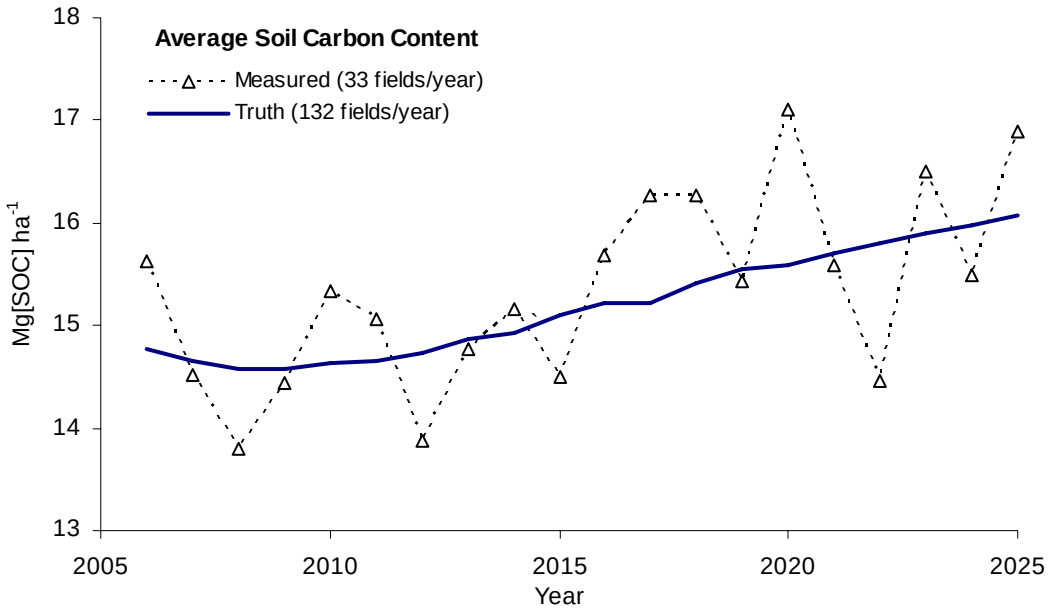

Figure 6-14 Average soil carbon measured in 25% of field and true soil carbon averaged in all fields in each year.

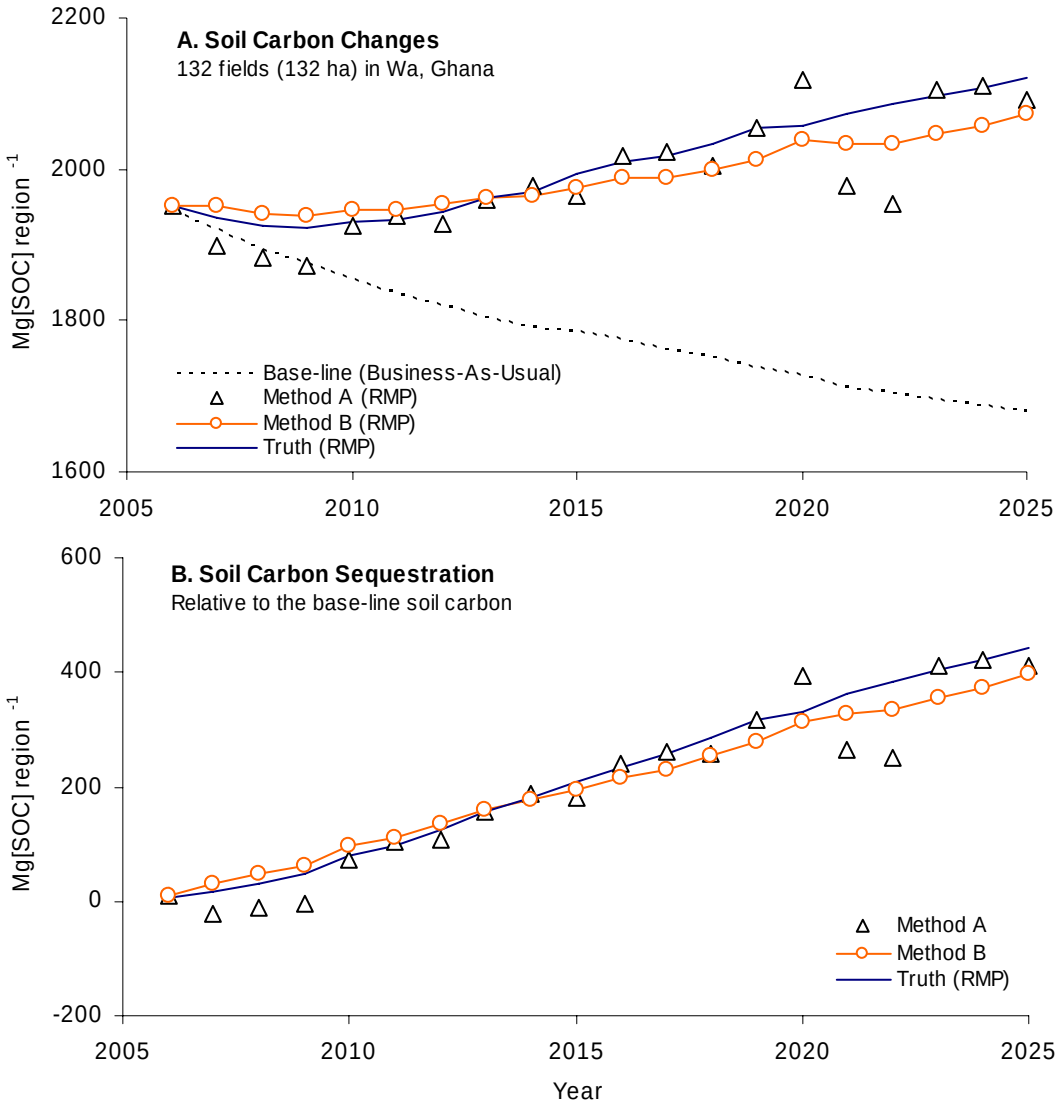

Figure 6-15 Soil carbon changes estimated from two methods and true values under the business-as-usual (base-line) and recommended management practices (RMP). Soil carbon sequestrations were calculated relatively from the base-line values.

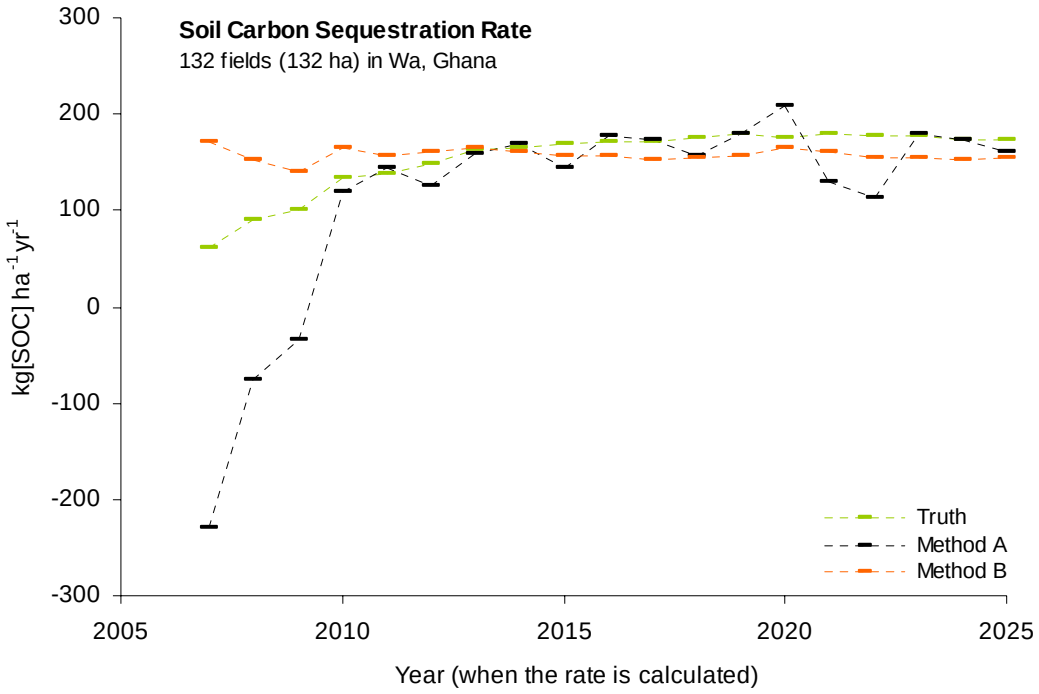

Figure 6-16 Estimated soil carbon sequestration rates from two methods, compared with the true rates. The rates changes depending on in which year the rate was calculated.

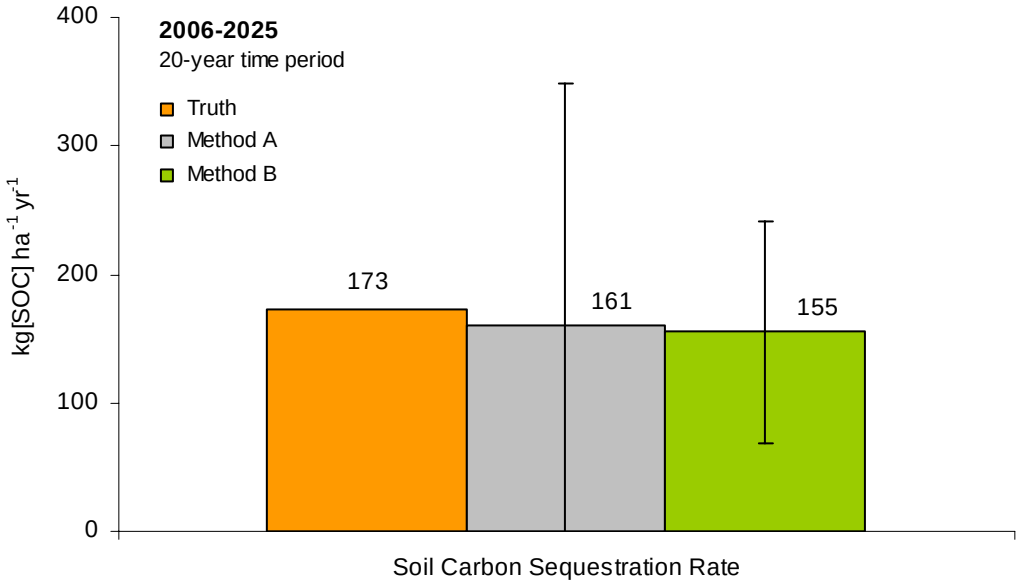

Figure 6-17 True and estimated soil carbon sequestration rates. Bars represent one standard deviation of estimations.

CHAPTER 7
CONCLUSION

This dissertation presents a study of a new approach to monitor soil carbon and estimate soil carbon sequestration using a data assimilation method.

Following the outline presented in Chapter 1, topics include the characterization of the study area in Ghana (Chapter 2), the estimation of soil carbon sequestration potential in an area containing many smallholder farmers' cropping systems (Chapter 3), the implementation and evaluation of a data assimilation method to estimate soil carbon at a field-scale (Chapter 4), the estimation of crop biomass using a remote sensing image and an artificial neural network (Chapter 5), and the implementation of a data assimilation method to spatially aggregate soil carbon estimates for use in monitoring regional soil carbon sequestration (Chapter 6).

The characterization of the study area in Northern Ghana in Chapter 2 showed that overall soil quality was not ideal for low-input crop production, although most smallholder farmers in the study area relied on the native soil fertility with minimum input to their cropping systems. Many of commonly used field management practices, such as intensive tillage, whole plant removal, high temperature, low soil moisture, and residue burning may have resulted in soils in the area with depleted soil organic matter. Thus soils are degraded and crop production is limited.

However, the depleted levels of soil carbon may provide an opportunity for soil carbon sequestration. Scenario analyses using the DSSAT-Century cropping systems model based on *in situ* measurements in Chapter 3 estimated the potential for soil carbon sequestration in the study area under the assumption of adopting recommended management practices, including no-till practice, inorganic N-fertilization of cereals, and retention of a majority of crop residues in the field. When all recommended management practices in the analysis were assumed to be adopted, the regionally aggregated soil carbon sequestration rate averaged 173 kg[SOC] ha^{-1} yr^{-1}.

Assuming that the minimum tradable amount of carbon in carbon markets is 1,000 Mg[CO_2], it was calculated that the smallholder farmers of 132 fields can sell their soil carbon credit with a 12-year contract. Based on the current market price of $4.00 per Mg[$CO_2$] in the Chicago Climate Exchange (CCX) (as of March 2007), it was estimated that the proposed carbon contract would be worth $4,000. However, it was noted that the carbon credit price in potential future markets are still highly uncertain and may fluctuate considerably over time (Williams et al., 2005). For example, the European carbon market (European Carbon Exchange, ECX) crashed in May 2006, with their carbon price dropping from over €30 per Mg[CO_2] in April 2006 to about €10 per Mg[CO_2] (Brahic, 2006). As of March 2007, the carbon price in the ECX is listed as about €1 per Mg[CO_2].

Regarding a carbon contract with smallholder farmers, it was emphasized that farmers would need to adopt recommended management practices and also maintain the adopted practices throughout the contract period. This is because the sequestered soil carbon can be decomposed when the balance of soil carbon dynamics is shifted.

Following a previous study with a simple model by Jones et al. (2004), Chapter 4 described the development of a stochastic data assimilation method using an ensemble Kalman filter to improve soil carbon estimation accuracy using a complex biophysical cropping system model (i.e. DSSAT-Century) and *in situ* measurements of soil carbon and crop biomass at a field-level. Results showed that the data assimilation method provided more reliable estimation of soil carbon over time, compared to use measurements alone. The uncertainty in soil carbon estimation from *in situ* measurements was reduced by 60% relative to measurements alone.

In Chapter 6, two soil carbon estimation methods were presented expanding the spatial scale from a field to the region. One was a spatial interpolation method (i.e. cokriging of soil

carbon with soil texture) and the other method was a data assimilation method (i.e., an ensemble Kalman filter with a simple soil carbon model). A comparison of these two methods was presented using the same scenario of hypothetically projected cropping systems. Results showed that the data assimilation method estimated aggregated soil carbon changes with higher accuracy compared to the spatial interpolation method. It was noted that an annual estimation accuracy of the spatial interpolation method was highly subject to the biases in measurements in a given year, which were introduced when fields were randomly selected for sampling. The spatial interpolation method made use of the spatial correlation of carbon within a calculated correlation range. Thus, interpolated soil carbon values were only influenced by measurements made in nearby fields, without taking into account soil carbon estimations and/or measurements made in the past. As a result, the estimated soil carbon over time from the spatial interpolation method showed a pattern of temporal variations. In contrast, the data assimilation method used an underlying dynamic model to estimate soil carbon changes in time over the entire area and thus temporal correlations in soil carbon were a part of this method.

Due to the remoteness of the study area and difficulties involved in conducting temporally and spatially intensive *in situ* measurements in reality, high-resolution remote sensing imagery was used in Chapters 5 and 6 to provide crop biomass important information to scale-up estimates of soil carbon to a regional-level. Chapter 5 analyzed the potential of using an artificial neural network to estimate crop biomass over the landscape with spatially limited *in situ* measurements. Results showed that, in general, this approach estimated crop biomass with higher accuracy, compared to the general linear models with spectral vegetation indices. Chapter 6 assumed that the high-resolution remote sensing image was used to classify plant species in each field, and the classification result was used to estimate crop biomass. When this approach is

implemented in practice, it will be essential to acquire a good quality high-resolution remote sensing images of the study area annually. These images would be needed not only for estimating crop biomass, but also for assuring the adoption of recommended management practices at the field-level.

When a data assimilation framework was designed, the choice of the underlying model was an important issue. There were tradeoffs between complex and simple models. Complex models provide more detailed estimates of the system than simple models do, thus help in understanding the dynamics among different components in a cropping system. However, complex models contain many extra model states and require more input data that may not be readily obtained. Complex models may introduce data-associated uncertainties with covariances that are difficult to define. In addition, the cost of running complex models may be prohibitive in a large-scale problem, considering the stochastic nature of Monte Carlo simulation method that is used in the ensemble Kalman filter. Simple models are easier to implement in large-scale problems, and they do not cost as much as complex models to implement in a stochastic data assimilation framework. However, due to the simplified nature of the model, updated states in the simple models may be accompanied with relatively higher estimation uncertainty.

In this dissertation, two soil carbon dynamics models with different complexities were used. Chapter 4 used a complex cropping systems model in a field-scale study, and Chapter 6 used a simple model in a regional-scale study. To handle the complexity of DSSAT-Century model in Chapter 4, a suboptimal filter was designed to update only three selected filter states (i.e. two model states, soil carbon and crop biomass, and a model parameter, soil mineralization). Although the two models were not compared side-by-side, estimates made by data assimilation in both chapters showed superior accuracy and less uncertainty, compared to estimations based

on measurements alone. Furthermore, the overall results from Chapters 4 and 6 showed that, as far as measurements may be relatively more uncertain than model predictions, a data assimilation is expected to provide more accurate soil carbon estimations by incorporating temporal and spatial correlations of soil carbon. Thus, the choice of an underlying model in the data assimilation framework may primarily depend on one's perspective of the simulated model outputs, whether one aims to analyze the overall cropping system of interest or focuses on few selected components of the system, and the size of problems (i.e., temporal and spatial scale). The extent of model errors would be another important factor. Welch and Bishop (2003) also reported that a simple model may produce acceptable results if a realistic model error is included.

Compared to previous studies (e.g., Jones et al., 2007), this dissertation was based on more complex cropping systems in a larger study area (Chapter 6) using a complex cropping systems model (Chapter 4). However, assumptions made in this theoretical study may be still idealistic compared to reality to some extent (e.g., fixed field boundary in Chapter 6). Improvements in these assumptions can be made to further improve the data assimilation method as it was tested in this dissertation.

APPENDIX
SURVEY FORMS USED IN CHAPTER 2

Table A-1 Form used to survey with farmers about their field management practices and cropping history in 2004

DATE ___ July 2004	**GPS SAMPLE ID** _____
LOCATION	On-Farm Experiment [ ] On-Station [ ] Other [ ]
DOMINANT SPECIES	Peanut [ ] Maize [ ] Sorghum [ ]
	Rice [ ] Soybean [ ] Fallow [ ] Wild [ ] Other _____
SECONDARY SPECIES	Wild Vegetation [ ] Other _____
CANOPY CLOSURE	_____% Height:_____m
STAND UNIFORMITY	Good [ ] Fair [ ] Poor [ ]
ROW SPACING	_____m
PLANTING DATE	____ / ____ / 2004
SOIL CARBON	_____% (Top 20cm, Composite of _____ points)
LAI	_____ by SunScan / _____ by LAI-2000
BIOMASS	_____ g / _____ m^2
REFLECTANCE	B _____%, G _____%, R _____%, IR _____%
LAND-USE HISTORY	

Table A-2 Form used to survey with farmers about their field management practices and cropping history in 2006

DATE _____/ _____/ 2006 **FIELD ID** W_____

VILLAGE _____

LOCATION Farmers' Field [ ] On-Farm [ ] On-Station [ ]

CROPS 1ST _____ (CV:) [%]

2ND _____ (CV:) [%]

OTHER _____ (CV:) [%]

ROW SPACING ___ m x ___ m **SOIL SAMPLE** _____ subsamples

CROP / PRODUCTION / FERTILIZER / RESIDUE / LIVESTOCK

2004 CROP SEASON

2004-2005 FALLOW

2005 CROP SEASON

2005-2006 FALLOW

2006 CROP SEASON

LIST OF REFERENCES

Amanor, K. S. and O. Pabi. 2007. Space, time, rhetoric and agricultural change in the transition zone of Ghana. *Human Ecology* 35, no. 1:51-67.

Amato, M. and J. N. Ladd. 1992. Decomposition of C-14-Labeled Glucose and Legume Material in Soils - Properties Influencing the Accumulation of Organic Residue-C and Microbial Biomass-C. *Soil Biology & Biochemistry* 24, no. 5:455-464.

Anderson, J. L. 2001. An ensemble adjustment Kalman filter for data assimilation. *Monthly Weather Review* 129, no. 12.

Annan, J. D., D. J. Lunt, J. C. Hargreaves, and P. J. Valdes. 2005. Parameter estimation in an atmospheric GCM using the Ensemble Kalman Filter. *Nonlinear Processes in Geophysics* 12, no. 3.

Antle, J. M. and G. Uehara. 2002. Creating incentives for sustainable agriculture: defining, estimating potential and verifying compliance with carbon contractors for soil carbon projects in developing countries. In *A Soil Carbon Accounting and Management System for Emission Trading*, 1-12. (Honolulu, HI: University of Hawaii).

Asiedu, E., S. Twumasi-Afriyie, P. Y. K. Sallah, J. N. Asafu-Agyei, and A. J. G. van Gastel. Maize seed production in Ghana - principles and practices. 2000. Crops Research Institute.

Atkinson, P. M. and A. R. L. Tatnall. 1997. Neural networks in remote sensing - Introduction. *International Journal of Remote Sensing* 18, no. 4:699-709.

Badu-Apraku, B., S. Twumasi-Afriyie, P. Y. K. Sallah, W. Haag, E. Asiedu, K. A. Marfo, S. Dapaah, and B. D. Dzafi. 2006. Registration of 'Obatanpa GH' maize. *Crop Science* 46, no. 3:1393-1395.

Bagan, H., Q. X. Wang, M. Watanabe, Y. H. Yang, and J. W. Ma. 2005. Land cover classification from MODIS EVI times-series data using SOM neural network. *International Journal of Remote Sensing* 26, no. 22:4999-5012.

Baldock, J. A. and J. O. Skjemstad. 2000. Role of the soil matrix and minerals in protecting natural organic materials against biological attack. *Organic Geochemistry* 31, no. 7-8:697-710.

Bationo, A. and A. Buerkert. 2001. Soil organic carbon management for sustainable land use in Sudano-Sahelian West Africa. *Nutrient Cycling in Agroecosystems* 61, no. 1-2:131-142.

Bationo, Andre, Job Kihara, Bernard Vanlauwe, Boaz Waswa, and Joseph Kimetu. 2007. Soil organic carbon dynamics, functions and management in West African agro-ecosystems. *Agricultural Systems* 94, no. 1:13-25.

Batjes, N. H. and W. G. Sombroek. 1997. Possibilities for carbon sequestration in tropical and subtropical soils. *Global Change Biology* 3, no. 2:161-173.

Bertino, L., G. Evensen, and H. Wackernagel. 2003. Sequential data assimilation techniques in oceanography. *International Statistical Review* 71, no. 2.

Bishop, Christopher M. 1995. *Neural Networks for Pattern Recognition*. Oxford: Clarendon Press.

Bostick, W. M., V. B. Bado, A. Bationo, C. T. Soler, G. Hoogenboom, and J. W. Jones. 2007. Soil carbon dynamics and crop residue yields of cropping systems in the Northern Guinea Savanna of Burkina Faso. *Soil and Tillage Research* 93:138-151.

Boucher, A., K. C. Seto, and A. G. Journel. 2006. A novel method for mapping land cover changes: Incorporating time and space with geostatistics. *Ieee Transactions on Geoscience and Remote Sensing* 44, no. 11:3427-3435.

Brady, N. C. and R. R. Weil. 2002. *The Nature and Properties of Soils*. Upper Saddle River, NJ: Prentice Hall.

Brahic, C. 2006. Greenhouse gases - Price crash rattles Europe's CO2 reduction scheme. *Science* 312, no. 5777:1123.

Braimoh, A. K. and P. L. G. Vlek. 2004. The impact of land-cover change on soil properties in northern Ghana. *Land Degradation & Development* 15, no. 1:65-74.

Broge, N. H. and J. V. Mortensen. 2002. Deriving green crop area index and canopy chlorophyll density of winter wheat from spectral reflectance data. *Remote Sensing of Environment* 81, no. 1:45-57.

Brye, K. R., D. E. Longer, and E. E. Gbur. 2006. Impact of tillage and residue burning on carbon dioxide flux in a wheat-soybean production system. *Soil Science Society of America Journal* 70, no. 4:1145-1154.

Burke, I. C., C. M. Yonker, W. J. Parton, C. V. Cole, K. Flach, and D. S. Schimel. 1989. Texture, Climate, and Cultivation Effects on Soil Organic-Matter Content in Us Grassland Soils. *Soil Science Society of America Journal* 53, no. 3:800-805.

Cherr, C. M., J. M. S. Scholberg, and R. McSorley. 2006. Green manure approaches to crop production: A synthesis. *Agronomy Journal* 98, no. 2:302-319.

Chikowo, R., P. Mapfumo, P. Nyamugafata, and K. E. Giller. 2004. Maize productivity and mineral N dynamics following different soil fertility management practices on a depleted sandy soil in Zimbabwe. *Agriculture Ecosystems & Environment* 102, no. 2:119-131.

Colombo, R., D. Bellingeri, D. Fasolini, and C. M. Marino. 2003. Retrieval of leaf area index in different vegetation types using high resolution satellite data. *Remote Sensing of Environment* 86, no. 1:120-131.

Conant, R. Global Carbon Sequestration Potential. From the Ground Up: Agronomy News 22[2], 3-4. 2002. Colorado State University Cooperative Extension. 12-30-2006.

Conant, R. T. and K. Paustian. 2002. Spatial variability of soil organic carbon in grasslands: implications for detecting change at different scales. *Environmental Pollution* 116:S127-S135.

Daley, R. 1991. *Atmospheric Data Analysis*. Cambridge, NY: Cambridge University Press.

Dankyi, A. A., P. Y. K. Sallah, A. Adu-Appiah, and Gyamera-Antwi. 2005. Determinants of the adoption of quality protein maize, Obatanpa, in southern Ghana - Logistic regression analysis. Paper presented at Fifth West and Central Africa Regional Maize Workshop, 2 2005.

Daughtry, C. S. T., C. L. Walthall, M. S. Kim, E. B. de Colstoun, and J. E. McMurtrey. 2000. Estimating corn leaf chlorophyll concentration from leaf and canopy reflectance. *Remote Sensing of Environment* 74, no. 2:229-239.

Del Frate, F., P. Ferrazzoli, and G. Schiavon. 2003. Retrieving soil moisture and agricultural variables by microwave radiometry using neural networks. *Remote Sensing of Environment* 84, no. 2:174-183.

DigitalGlobe. 2006. "QuickBird Specifications." Accessed on Mar 21, 2007. Available from http://www.digitalglobe.com/about/quickbird.html.

Duncan, D. B. 1955. Multiple Range and Multiple F Tests. *Biometrics* 11, no. 1:1-42.

Eknes, M. and G. Evensen. 2002. An Ensemble Kalman filter with a 1-D marine ecosystem model. *Journal of Marine Systems* 36, no. 1-2.

El-Swaify, S. A., T. S. Walker, and S. M. Virmani. 1984. Dryland management alternatives and research needs for alfisols in the semi-arid tropics. Paper presented at Consultants' Workshop on the State of the Art and Management Alternatives for Optimizing the Productivity of SAT Alfisols and Related Soils, 1 1983.

Evensen, G. 1994. Sequential data assimilation with a nonlinear quasi-geostrophic model using Monte-Carlo methods to forecast error statistics. *Journal of Geophysical Research-Oceans* 99, no. C5.

Falloon, P. D., P. Smith, J. U. Smith, J. Szabo, K. Coleman, and S. Marshall. 1998. Regional estimates of carbon sequestration potential: linking the Rothamsted Carbon Model to GIS databases. *Biology and Fertility of Soils* 27, no. 3:236-241.

FAO. Carbon sequestration in dryland soils. 102, 1-129. 2004. Rome, Italy, FAO. World Soil Resources Report.

Farage, P., J. Pretty, and A. Ball. Biophysical Aspects of Carbon Sequestration in Drylands. 2003. Rome, Italy, FAO.

Ferreyra, Rafael Andres. 2003. Knowledge-based techniques for parameterizing spatial biophysical models. Ph.D. Dissertation, University of Florida.

Fitzgerald, G. J., D. Rodriguez, L. K. Christensen, R. Belford, V. O. Sadras, and T. R. Clarke. 2006. Spectral and thermal sensing for nitrogen and water status in rainfed and irrigated wheat environments. *Precision Agriculture* 7, no. 4:233-248.

Franke, A. C., S. Schulz, B. D. Oyewole, and S. Bako. 2004. Incorporating short-season legumes and green manure crops into maize-based systems in the moist Guinea savannah of West Africa. *Experimental Agriculture* 40, no. 4:463-479.

Gelb, A. 1974. *Applied Optimal Estimation*. Cambridge, NY: MIT Press.

Ghosh, P. K., M. C. Manna, D. Dayal, and R. H. Wanjari. 2006. Carbon sequestration potential and sustainable yield index for groundnut- and fallow-based cropping systems. *Journal of Agricultural Science* 144:249-259.

Gijsman, A. J., G. Hoogenboom, W. J. Parton, and P. C. Kerridge. 2002. Modifying DSSAT crop models for low-input agricultural systems using a soil organic matter-residue module from CENTURY. *Agronomy Journal* 94, no. 3:462-474.

Goovaerts, P. 1999. Geostatistics in soil science: state-of-the-art and perspectives. *Geoderma* 89, no. 1-2:1-45.

Halvorson, A. D., C. A. Reule, and R. F. Follett. 1999. Nitrogen fertilization effects on soil carbon and nitrogen in a dryland cropping system. *Soil Science Society of America Journal* 63, no. 4:912-917.

Hassink, J. 1997. The capacity of soils to preserve organic C and N by their association with clay and silt particles. *Plant and Soil* 191, no. 1:77-87.

Hassink, J., A. P. Whitmore, and J. Kubat. 1997. Size and density fractionation of soil organic matter and the physical capacity of soils to protect organic matter. *European Journal of Agronomy* 7, no. 1-3:189-199.

Hauser, S., C. Nolte, and R. J. Carsky. 2006. What role can planted fallows play in the humid and sub-humid zone of West and Central Africa? *Nutrient Cycling in Agroecosystems* 76, no. 2-3:297-318.

He, Y., X. L. Guo, and J. Wilmshurst. 2006. Studying mixed grassland ecosystems I: suitable hyperspectral vegetation indices. *Canadian Journal of Remote Sensing* 32, no. 2:98-107.

Heuvelink, G. B. M. 1998. Uncertainty analysis in environmental modelling under a change of spatial scale. *Nutrient Cycling in Agroecosystems* 50, no. 1-3:255-264.

Heuvelink, G. B. M. and E. J. Pebesma. 1999. Spatial aggregation and soil process modelling. *Geoderma* 89, no. 1-2:47-65.

NCSS and PASS. Number Cruncher Statistical Systems. Kaysville, Utah.

DSSAT v4 CD-ROM and Software. Ver. 4.0.2.0. University of Hawaii, Honolulu, HI.

Hussain, I., K. R. Olson, and S. A. Ebelhar. 1999. Long-term tillage effects on soil chemical properties and organic matter fractions. *Soil Science Society of America Journal* 63, no. 5:1335-1341.

Hutchinson, J. J., C. A. Campbell, and R. L. Desjardins. 2007. Some perspectives on carbon sequestration in agriculture. *Agricultural and Forest Meteorology* 142, no. 2-4:288-302.

Inoue, Y. 2003. Synergy of remote sensing and modeling for estimating ecophysiological processes in plant production. *Plant Production Science* 6, no. 1:3-16.

IPCC. 2006 IPCC guidelines for national greenhouse gas inventories. Eggleston, S., L. Buendia, K. Miwa, T. Ngara, and K. Tanabe. 2006.

Jagtap, S. S., M. Mornu, and B. T. Kang. 1993. Simulation of growth, development and yield of maize in the transition zone of Nigeria. *Agricultural Systems* 41, no. 2.

Jensen, John R. 1996. *Introductory Digital Image Processing: A Remote Sensing Perspective*. Upper Saddle River, N.J: Prentice Hall.

Jiang, D., X. Yang, N. Clinton, and N. Wang. 2004. An artificial neural network model for estimating crop yields using remotely sensed information. *International Journal of Remote Sensing* 25, no. 9:1723-1732.

Johnson, J. M. F., R. R. Allmaras, and D. C. Reicosky. 2006. Estimating source carbon from crop residues, roots and rhizodeposits using the national grain-yield database. *Agronomy Journal* 98, no. 3:622-636.

Jones, J. W., A. J. Gijsman, W. J. Parton, K. J. Boote, and P. Doraiswamy. 2002. Predicting soil carbon accretion: The role of biophysical models in monitoring and verifying soil carbon. In *A Soil Carbon Accounting System for Emissions Trading*, 41-68. (Honolulu, HI: University of Hawaii).

Jones, J. W., W. D. Graham, D. Wallach, W. M. Bostick, and J. Koo. 2004. Estimating soil carbon levels using an Ensemble Kalman filter. *Transactions of the ASABE* 47, no. 1:331-339.

Jones, J. W., G. Hoogenboom, C. H. Porter, K. J. Boote, W. D. Batchelor, L. A. Hunt, and P. W. Wilkens. 2003. The DSSAT cropping system model. *European Journal of Agronomy* 18, no. 3-4.

Jones, J. W., J. Koo, J. B. Naab, W. M. Bostick, P. C. S. Traore, and W. D. Graham. 2007. Integrating stochastic models and *in situ* sampling for monitoring soil carbon sequestration. *Agricultural Systems* 94, no. 1:52-62.

Kalman, R. E. 1960. A new approach to linear filtering and prediction problems. *Transaction of ASME* 82.

Keppenne, C. L. 2000. Data assimilation into a primitive-equation model with a parallel ensemble Kalman filter. *Monthly Weather Review* 128, no. 6.

Kimball, J. S., K. C. McDonald, and M. Zhao. 2006. Terrestrial vegetation productivity in the western arctic observed from satellite microwave and optical remote sensing. *Earth Interactions* 10.

Kiunsi, R. B. and M. E. Meadows. 2006. Assessing land degradation in the Monduli District, northern Tanzania. *Land Degradation & Development* 17, no. 5:509-525.

Ko, J., S. J. Maas, S. Mauget, G. Piccinni, and D. Wanjura. 2006. Modeling water-stressed cotton growth using within-season remote sensing data. *Agronomy Journal* 98, no. 6:1600-1609.

Koller, M. and S. K. Upadhyaya. 2005. Relationship between modified normalized difference vegetation index and leaf area index for processing tomatoes. *Applied Engineering in Agriculture* 21, no. 5:927-933.

Kuplich, T. M. 2006. Classifying regenerating forest stages in Amazonia using remotely sensed images and a neural network. *Forest Ecology and Management* 234, no. 1-3:1-9.

Lal, R. 2002. Soil carbon dynamics in cropland and rangeland. *Environmental Pollution* 116, no. 3:353-362.

-----. 2004a. Soil carbon sequestration impacts on global climate change and food security. *Science* 304, no. 5677:1623-1627.

-----. 2006. Enhancing crop yields in the developing countries through restoration of the soil organic carbon pool in agricultural lands. *Land Degradation & Development* 17, no. 2:197-209.

-----. 1997. Residue management, conservation tillage and soil restoration for mitigating greenhouse effect by CO2-enrichment. *Soil & Tillage Research* 43, no. 1-2:81-107.

-----. 2003. Offsetting global CO2 emissions by restoration of degraded soils and intensification of world agriculture and forestry. *Land Degradation & Development* 14, no. 3:309-322.

-----. 2004b. Soil carbon sequestration to mitigate climate change. *Geoderma* 123, no. 1-2:1-22.

Lal, R., M. Griffin, J. Apt, L. Lave, and M. G. Morgan. 2004. Ecology - Managing soil carbon. *Science* 304, no. 5669:393.

Li, B., R. W. McClendon, and G. Hoogenboom. 2004. Spatial interpolation of weather variables for single locations using artificial neural networks. *Transactions of the ASABE* 47, no. 2:629-637.

Liu, J., C. E. Goering, and L. Tian. 2001. A neural network for setting target corn yields. *Transactions of the ASABE* 44, no. 3:705-713.

Liu, J. X., G. F. Shao, H. Z. Zhu, and S. G. Liu. 2005. A neural network approach for enhancing information extraction from multispectral image data. *Canadian Journal of Remote Sensing* 31, no. 6:432-438.

Locke, C. R., G. J. Carbone, A. M. Filippi, E. J. Sadler, B. K. Gerwig, and D. E. Evensen. 2002. Using remote sensing and modeling to measure crop biophysical variability. at Madison, WI.

Mackin, K. J., E. Nunohiro, M. Ohshiro, and K. Yamasaki. 2006. Land cover classification from MODIS satellite data using probabilistically optimal ensemble of artificial neural networks. *Knowledge-Based Intelligent Information and Engineering Systems, Pt 3, Proceedings* 4253:820-826.

Manlay, R. J., D. Masse, J. L. Chotte, C. Feller, M. Kaire, J. Fardoux, and R. Pontanier. 2002. Carbon, nitrogen and phosphorus allocation in agro-ecosystems of a West African savanna II. The soil component under semi-permanent cultivation. *Agriculture Ecosystems & Environment* 88, no. 3:233-248.

Margulis, S. A., D. McLaughlin, D. Entekhabi, and S. Dunne. 2002. Land data assimilation and estimation of soil moisture using measurements from the Southern Great Plains 1997 Field Experiment. *Water Resources Research* 38, no. 12.

MathWorks, Inc. 2004. "Neural Network Toolbox." Accessed on Apr 15, 2007. Available from http://www.mathworks.com/access/helpdesk/help/toolbox/nnet/nnet.shtml.

Maybeck, P. 1979. *Stochastic Models, Estimation and Control*. New York, NY: Academic Press.

Metherell, A. K., L. A. Harding, C. V. Cole, and W. J. Parton. CENTURY Soil Organic Matter Model Environment: Technical Documentation Agroecosystem Version 4.0. 4. 1993. Fort Collins, CO. Great Plains System Research Unit Technical Report.

Mooney, S., J. Antle, S. Capalbo, and K. Paustian. 2004. Design and costs of a measurement protocol for trades in soil carbon credits. *Canadian Journal of Agricultural Economics-Revue Canadienne D Agroeconomie* 52, no. 3:257-287.

Mooney, S., K. Gerow, J. Antle, S. Capalbo, and K. Paustian. 2007. Reducing standard errors by incorporating spatial autocorrelation into a measurement scheme for soil carbon credits. *Climatic Change* 80, no. 1-2:55-72.

Moradkhani, H., S. Sorooshian, H. V. Gupta, and P. R. Houser. 2005. Dual state-parameter estimation of hydrological models using ensemble Kalman filter. *Advances in Water Resources* 28, no. 2.

Moran, M. S., T. R. Clarke, Y. Inoue, and A. Vidal. 1994. Estimating Crop Water-Deficit Using the Relation Between Surface-Air Temperature and Spectral Vegetation Index. *Remote Sensing of Environment* 49, no. 3:246-263.

Moulin, S., A. Bondeau, and R. Delecolle. 1998. Combining agricultural crop models and satellite observations: from field to regional scales. *International Journal of Remote Sensing* 19, no. 6:1021-1036.

Naab, J. B., P. Singh, K. J. Boote, J. W. Jones, and K. O. Marfo. 2004. Using the CROPGRO-peanut model to quantify yield gaps of peanut in the Guinean Savanna Zone of Ghana. *Agronomy Journal* 96, no. 5:1231-1242.

Nichols, J. D. 1984. Relation of Organic-Carbon to Soil Properties and Climate in the Southern Great Plains. *Soil Science Society of America Journal* 48, no. 6:1382-1384.

Noh, H., Q. Zhang, B. Shin, S. Han, and L. Feng. 2006. A neural network model of maize crop nitrogen stress assessment for a multi-spectral imaging sensor. *Biosystems Engineering* 94, no. 4:477-485.

O'Neal, M. R., B. A. Engel, D. R. Ess, and J. R. Frankenberger. 2002. Neural network prediction of maize yield using alternative data coding algorithms. *Biosystems Engineering* 83, no. 1:31-45.

Osei, W. Y. and S. Aryeetey-Attoh. 1997. The Physical Environment. In *Geography of Sub-Saharan Africa*, ed. Aryeetey-Attoh, S., 1-34. (Upper Saddle River, New Jersey: Prentice Hall).

Özesmi, S. L., C. O. Tan, and U. Özesemi. 2006. Methodological issues in building, training, and testing artificial neural networks in ecological applications. *Ecological Modelling* 195, no. 1-2:83-93.

Parton, W. J. and P. E. Rasmussen. 1994. Long-Term Effects of Crop Management in Wheat-Fallow .2. Century Model Simulations. *Soil Science Society of America Journal* 58, no. 2.

Parton, W. J., J. W. B. Stewart, and C. V. Cole. 1988. Dynamics of C, N, P and S in Grassland Soils - a Model. *Biogeochemistry* 5, no. 1.

Pebesma, E. J. and C. G. Wesseling. 1998. Gstat: A program for geostatistical modelling, prediction and simulation. *Computers & Geosciences* 24, no. 1:17-31.

Poss, J. A., W. B. Russell, and C. M. Grieve. 2006. Estimating yields of salt- and water-stressed forages with remote sensing in the visible and near infrared. *Journal of Environmental Quality* 35, no. 4:1060-1071.

Prasad, R., B. Gangaiah, and K. C. Aipe. 1999. Effect of crop residue management in a rice-wheat cropping system on growth and yield of crops and on soil fertility. *Experimental Agriculture* 35, no. 4:427-435.

Ranson, K. J., G. Sun, J. F. Weishampel, and R. G. Knox. 1997. Forest biomass from combined ecosystem and radar backscatter modeling. *Remote Sensing of Environment* 59, no. 1:118-133.

Ray, S. S., G. Das, J. P. Singh, and S. Panigrahy. 2006. Evaluation of hyperspectral indices for LAI estimation and discrimination of potato crop under different irrigation treatments. *International Journal of Remote Sensing* 27, no. 23-24:5373-5387.

Reichle, D., B. Kane, J. Houghton, and J. Ekmann. Carbon Sequestration Research and Development. 1999. Washington, D.C., Office of Science, Office of Fossil Energy, U.S. Department of Energy.

Reichle, R. H., J. P. Walker, R. D. Koster, and P. R. Houser. 2002. Extended versus ensemble Kalman filtering for land data assimilation. *Journal of Hydrometeorology* 3, no. 6.

Reicosky, D. C. 1997. Tillage-induced CO2 emission from soil. *Nutrient Cycling in Agroecosystems* 49, no. 1-3:273-285.

Rodriguez, D., G. J. Fitzgerald, R. Belford, and L. K. Christensen. 2006. Detection of nitrogen deficiency in wheat from spectral reflectance indices and basic crop eco-physiological concepts. *Australian Journal of Agricultural Research* 57, no. 7:781-789.

Rosenzweig, R., M. Varilek, B. Feldman, R. Kuppalli, and J. Janssen. The Emerging International Greenhouse Gas Market. 2002. Pew Center. Global Climate Change.

Sahrawat, K. L., T. Bhattacharyya, S. P. Wani, P. Chandran, S. K. Ray, D. K. Pa, and K. V. Padmaja. 2005. Long-term lowland rice and arable cropping effects on carbon and nitrogen status of some semi-arid tropical soils. *Current Science* 89, no. 12:2159-2163.

Sainju, U. M., A. Lenssen, T. Caesar-Thonthat, and J. Waddell. 2006. Carbon sequestration in dryland soils and plant residue as influenced by tillage and crop rotation. *Journal of Environmental Quality* 35, no. 4:1341-1347.

Schjonning, P., I. K. Thomsen, J. P. Moberg, H. de Jonge, K. Kristensen, and B. T. Christensen. 1999. Turnover of organic matter in differently textured soils - I. Physical characteristics of structurally disturbed and intact soils. *Geoderma* 89, no. 3-4:177-198.

Schlecht, E., A. Buerkert, E. Tielkes, and A. Bationo. 2006. A critical analysis of challenges and opportunities for soil fertility restoration in Sudano-Sahelian West Africa. *Nutrient Cycling in Agroecosystems* 76, no. 2-3:109-136.

Schlegel, A. J. and J. L. Havlin. 1995. Corn Response to Long-Term Nitrogen and Phosphorus Fertilization. *Journal of Production Agriculture* 8, no. 2:181-185.

Schlesinger, W. H. 2000. Carbon sequestration in soils: some cautions amidst optimism. *Agriculture Ecosystems & Environment* 82, no. 1-3:121-127.

Scurlock, J. M. O. and D. O. Hall. 1998. The global carbon sink: a grassland perspective. *Global Change Biology* 4, no. 2:229-233.

Sharp, K., 2000. Soil management is key to fighting world hunger, reducing greenhouse gases. *Ohio State News*, 30 December.

Singer, J. W. and W. J. Cox. 1998. Agronomics of corn production under different crop rotations in New York. *Journal of Production Agriculture* 11, no. 4:462-468.

Stoorvogel, J. J. and J. M. Antle. 2001. Regional land use analysis: the development of operational tools. *Agricultural Systems* 70, no. 2-3:623-640.

Sundermeier, A., R. Reeder, and R. Lal. 2005. "Soil carbon sequestration - Fundamentals." Accessed on Apr 15, 2007. Available from http://ohioline.osu.edu/aex-fact/0510.html.

Thomas, J. R. and H. W. Gausman. 1977. Leaf Reflectance Vs Leaf Chlorophyll and Carotenoid Concentrations for 8 Crops. *Agronomy Journal* 69, no. 5:799-802.

Tschakert, P., M. Khouma, and M. Sene. 2004. Biophysical potential for soil carbon sequestration in agricultural systems of the Old Peanut Basin of Senegal. *Journal of Arid Environments* 59, no. 3:511-533.

Tsuji, G. Y., G. Uehara, and S. Balas. 1994. *DSSAT V3*. Honolulu, HI: University of Hawaii.

Tucker, C. J. 1979. Red and Photographic Infrared Linear Combinations for Monitoring Vegetation. *Remote Sensing of Environment* 8, no. 2:127-150.

Twomlow, S. and R. Tabo. 2006. "Small fertilizer doses yield big impact in sub-Saharan Africa." Accessed on Dec 28, 2006. Available from http://www.icrisat.org/New&Events/LatestNews.htm.

USGS. 2004. "Shuttle Radar Topography Mission." Accessed on Oct 12, 2006. Available from http://srtm.usgs.gov.

Walkley, A. and I. A. Black. 1934. An examination of the Degiareff method for determining SOM and a proposed modification of the chromic acid titration method. *Soil Science* 37.

Wallach, D., B. Goffinet, J. E. Bergez, P. Debaeke, D. Leenhardt, and J. N. Aubertot. 2001. Parameter estimation for crop models: A new approach and application to a corn model. *Agronomy Journal* 93, no. 4.

Walter, C., R. A. V. Rossel, and A. B. McBratney. 2003. Spatio-temporal simulation of the field-scale evolution of organic carbon over the landscape. *Soil Science Society of America Journal* 67, no. 5:1477-1486.

Walthall, C., W. Dulaney, M. Anderson, J. Norman, H. L. Fang, and S. L. Liang. 2004. A comparison of empirical and neural network approaches for estimating corn and soybean leaf area index from Landsat ETM+ imagery. *Remote Sensing of Environment* 92, no. 4:465-474.

Wang, X. B., D. X. Cai, W. B. Hoogmoed, O. Oenema, and U. D. Perdok. 2005. Scenario analysis of tillage, residue and fertilization management effects on soil organic carbon dynamics. *Pedosphere* 15, no. 4:473-483.

Weier, J. and D. Herring. 2007. "Measuring Vegetation (NDVI & EVI)." Accessed on Mar 20, 2007. Available from http://earthobservatory.nasa.gov/Library/MeasuringVegetation/printall.php.

Welch, G. and G. Bishop. An introduction to the Kalman filter. 2003. Chapel Hill, NC, University of North Carolina at Chapel Hill. 5-23-2003.

Williams, J. R., J. M. Peterson, and S. Mooney. 2005. The value of carbon credits: Is there a final answer? *Journal of soil and water conservation* 60, no. 2:36A-40A.

Xie, H., Y. Q. Tian, J. A. Granillo, and G. R. Keller. 2007. Suitable remote sensing method and data for mapping and measuring active crop fields. *International Journal of Remote Sensing* 28, no. 1-2:395-411.

Yang, C., J. H. Everitt, and J. M. Bradford. 2006. Evaluating high-resolution QuickBird satellite imagery for estimating cotton yield. *Transactions of the ASABE* 49, no. 5:1599-1606.

Ye, X. J., K. Sakai, L. O. Garciano, S. I. Asada, and A. Sasao. 2006. Estimation of citrus yield from airborne hyperspectral images using a neural network model. *Ecological Modelling* 198, no. 3-4:426-432.

Yost, R., P. Doraiswamy, and M. Doumbia. 2002. Defining the contract area: using spatial variation in land, cropping systems and soil organic carbon. In *A Soil Carbon Accounting and Management System for Emissions Trading*, 13-40. (Honolulu, HI: University of Hawaii).

Zevenbergen, L. W. and C. R. Thorne. 1987. Quantitative-Analysis of Land Surface-Topography. *Earth Surface Processes and Landforms* 12, no. 1:47-56.

BIOGRAPHICAL SKETCH

Jawoo Koo was born on February 17, 1974, in Seoul, South Korea. He grew up in mostly urban areas in South Korea, including Seoul and Ulsan. In 1992, he began an undergraduate program in the Agricultural Biology Department of Korea University. After two years of studying in the program, he enrolled in the Seoul Metropolitan Police Department from 1994 until 1996 to fulfill the mandatory army service as a South Korean citizen. After discharge, he resumed his undergraduate study and graduated in 1998. After graduation, he worked at the Forest Pathology Laboratory of the National Forestry Research Institute, Seoul, South Korea, as a research associate for about one and half years. He began his master's degree study in 1999 with Dr. James W. Jones and joined the McNair Bostick Simulation Lab in the Agricultural and Biological Engineering Department of the University of Florida, Gainesville, Florida. He studied the impacts of climate variability on the tomato production and disease epidemics in South Florida for his master thesis. He earned the Master of Science degree in spring 2002. In summer 2002, he worked at the International Livestock Research Institute, Nairobi, Kenya, as a consultant for three months. In fall 2002, he returned to Gainesville, Florida, and continued his education at the McNair Bostick Simulation Lab with Dr. James W. Jones for his Ph.D. degree program.

In August 2000, Jawoo Koo married Soonho Kim, who was his classmate in undergraduate years. His advisor, Dr. Jones, conducted their wedding ceremony, following a Korean culture that the most respected person for a couple performs their wedding ceremony. Soonho began her doctoral degree program in the same department in 2000 and earned Ph.D. degree in fall 2005. In October 2004, Jawoo became a father of a lovely girl, Bonny.